**Ministry of Higher Education and Scientific Research**
**Babylon University**
**College of Engineering**
**Department of Mechanical Engineering**

# A Mathematical Model to predict Fluid properties for a Centrifugal Pump Impeller

## A Thesis

**Submitted to the College of Engineering of the University of Babylon in Partial Fulfillment of the Requirements For the Degree of Master of Science in Mechanical Engineering**

## By

**Sahir Rakim Al-Waeely**

**B. SC. 2000**

Supervisors

**Dr.**
**Abdul Kareem A. Wahab**

**Dr.**
**Emad S. ali**

NOVEMBER 2003

# P

لا الشمس ينبغي
لها أن تدرك
القمر ولا الليل
سابق النهار
وكل في فلك
يسبحون

صدق الله العلي العظيم

سورة ياسين (٤٠)

detectorDETCATION

# gÉM

My Parents

# YÉÜ

# g{x|Ü ÄÉäx? c tà|xÇvx? V tÜx

# T Çw f âÑÑÉÜà

# ; \ Ç g{x a tÅx Éy T ÄÄt{? g{x ZÜtv|Éâá? g{x ` xÜv|yâÄ<

Praise is to "**ALLAH**", prophet **"Mohammed**" and his family. This research has been completed under their benediction.

I would like to express my thanks my supervisor, **Dr. Abdul Kareem A. Wahab** for his support, in the references of present work.

I am also indebted to the head and staff of Mechanical Engineering Department.

I record my sincere gratitude to my family and especially to my father and mother for their assistance, encouragement and support during the period of preparing this work.

Finally, I would also like to thank all my friends in Babylon University especially to (**Mr. Hussain K. Holwass**) and also to Miss**. Anaam, Mona& sahra'a** in library of Babylon University for their helpful and encouragement during the entire period of this research.

**Sahir Rakim Raheam**

2003

# Abstract

A complete procedure was developed to compute centrifugal impeller dimensions by the design factor method in which point by point method was used for developed impeller shape.

Two centrifugal pump impeller were analyzed first (Q=0.132458 $m^3$/sec, N=3600 rpm, H=137.16 m) and the second (**Q**=0.00387 $m^3$/sec, **N**=150 rpm, **H**=0.8199 m). The dimensions of two devolved pump impellers were ($r_1$=69.02 mm, $r_2$=147.71 mm, $b_1$=21°, $b_2$=25°), ($r_1$=107.9 mm, r2=241.3 mm, $b_1$=16°, $b_2$=23° for the second Impeller).

The flow was analyzed by using a FORTRAN program language, which is modified to make it run with rotating condition.

Study of velocity, pressure, kinetic energy of turbulence ($k$), dissipation rate of kinetic energy of turbulence ($\varepsilon$) were done for distribution from blade to blade, the SIMPLE algorithm is used for solving steady 2-D, viscous turbulent fluid flow adopting finite volume applied on colocated body fitted grid.

A uniform distribution of pressure and velocity was shown in the first impeller and a relative circulation was shown in the second impeller.

# Nomenclature

| Symbol | Description | Unit |
|---|---|---|
| A | Matrix coefficient | ___ |
| a | Area | $m^2$ |
| b | Impeller breadth | m |
| d | Impeller diameter | m |
| F | Flux | $Kg_*m/sec^2$ |
| g | Gravity acceleration | $m/sec^2$ |
| H | Head | m |
| k | Kinetic energy of turbulence | $m^2/sec^2$ |
| L | Length | m |
| $\dot{m}$ | Mass flow rate | Kg/sec |
| N | Speed | rpm |
| Ns | Specific speed. | $rpm_*m^{1/6}/sec^{1/2}$ |
| n | Normal vector | ___ |
| PP | Power | Watt |
| p | Static pressure | $N/m^2$ |
| Q | Volume flow rate | $m^3/sec$ |
| r | Radius of impeller | m |

| T | Torque | N.m |
|---|---|---|
| U | Peripheral velocity | m/sec |
| $u_\tau$ | Shear velocity | m/sec |
| $u_p^+$ | Dimensionless velocity | ___ |
| V | Absolute velocity | m/sec |
| W | Relative velocity | m/sec |
| w | Relative mean velocity | m/sec |
| X | Cartesian coordinate axis. | m |
| Y | Cartesian coordinate axis. | m |
| $y_p^+$ | Dimensionless distance from wall | ___ |
| Z | Number of blade | ___ |

## Greek symbols

| Symbol | Description | Unit |
|---|---|---|
| $\alpha$ | Flow angle | rad |
| $\beta$ | Blade angle | rad |
| $\delta$ | Discretized form | ___ |
| $\Delta$ | Change in value | ___ |
| $\varepsilon$ | Dissipation rate of Kinetic energy of turbulence | $m^2/sec^2$ |
| $\Phi$ | Conservative quantity | ___ |

| | | |
|---|---|---|
| $\lambda$ | Linear interpolation factor | ___ |
| $\mu_e$ | Effective viscosity | kg/m.sec |
| $\mu$ | Laminar viscosity | kg/m.sec |
| $\theta$ | Tangential position | rad |
| $\rho$ | Density | $kg/m^3$ |
| $\sigma$ | Slip factor | ___ |
| $\tau$ | Shear stress | $N/m^2$ |
| $\Omega$ | Volume | $m^3$ |
| $\omega$ | Rotational speed | rad/sec |

**Superscripts**

| Symbol | Description |
|---|---|
| c | convective term |
| CDS | Central difference scheme |
| d | Diffusive term |
| deff | Differed correction interpolation |
| E | Explicit |
| H | Higher order |
| impl | Implicit |
| L | Lower order |
| m | Current iteration |
| UDS | Up Wind Scheme |
| - | Mean value |
| ′ | Fluctuated component |

| | |
|---|---|
| ″ | Corrected value |
| * | The value of Variable during iteration |

## Subscripts

| Symbol | Description |
|---|---|
| e | East face |
| i | Index of sides (e,n,w.s) |
| E | East node |
| I | Index of coordinate (X,Y) |
| n | North face |
| N | North node |
| ne | North east corner of control volume |
| NE | North east node |
| nw | North east corner of control volume |
| NW | North west corner of control volume |
| P | Control volume center |
| r | Radial direction |
| se | south east corner of control volume |
| SE | south east node |
| sw | south west corner of control volume |
| SW | south west node |
| t | Tangential direction |
| w | west face |

| | |
|---|---|
| **X** | **Component of coordinate** |
| **Y** | **Component of coordinate** |

## Abbreviation

| | |
|---|---|
| **BB** | **Blade to blade** |
| **CDS** | **Central difference scheme.** |
| **CFD** | **Computational fluid dynamics.** |
| **CV** | **Control volume.** |
| **FE** | **Finite element.** |
| **FV** | **Finite volume.** |
| **LU** | **Lower upper.** |
| **PS** | **Pressure side.** |
| **QUICK** | **Quadratic upwind Interpolation.** |
| **RNS** | **Reynolds average Navier-Stockes.** |
| **SS** | **Suction side.** |
| **SIMPLE** | **Simi implicit method for pressure linked equation.** |
| **UDS** | **Up wind scheme.** |

# List of Content


| Subject. | | Page |
|---|---|---|
| Acknowledgement. | | I |
| Abstract. | | II |
| Nomenclature. | | III |
| List of Content. | | V |
| Nomenclature | | VII |
| Chapter One: - Introduction. | | |
| 1.1 | General Introduction. | 1 |
| 1.2 | Flow Analysis Problem. | 3 |
| 1.3 | Objective of The Present Work. | 5 |
| Chapter Two: - Literature Review. | | |
| 2.1 | Introduction. | 7 |
| 2.2 | Design Factor Method. | 7 |
| 2.3 | Through Flow Analysis. | 9 |
| 2.4 | Control Volume Approach. | 12 |
| Chapter Three: - Theoretical Background. | | |
| 3.1 | Introduction. | 15 |
| 3.2 | Input Variable. | 16 |
| 3.3 | Calculation of Impeller Dimension. | 17 |
| 3.3.1 | Geometry of Flow Through Impeller. | 17 |
| 3.3.2 | The Euler Head Theory. | 19 |
| 3.3.3 | Calculation of the Impeller dimension By Design Factor. | 19 |
| 3.3.4 | Developing of Impeller Shape. | 25 |

| | | |
|---|---|---|
| 3.4 | Grid Generation | 27 |
| 3.5 | | 29 |
| 3.5.1 | Equation of Motion. | 29 |
| 3.5.2 | $\mathbf{k-\varepsilon}$ **Model** . | 29 |
| 3.6 | Approximation of Integral. | 30 |
| 3.6.1 | Convective And Diffusive Term. | 30 |
| 3.6.2 | Approximation of Volume Integral. | 31 |
| 3.6.3 | Interpolation Practice. | 32 |
| 3.6.4 | Pressure Correction Equation. | 34 |
| 3.5.5 | Implementation of Boundary Condition. | 37 |
| 3.6.5 | The Algebraic Equation System. | 38 |
| 3.6.6 | Solution of Algebraic Equation. | 40 |
| 3.6.6 | SIMPLE Algorithm For A Colocated Variable Arrangement. | 42 |
| 3.6.7 | Computer Program. | 43 |
| Chapter Four: - Results And Discussion. | | |
| 4.1 | Introduction. | ٤٦ |
| 4.2 | Results And Discussion. | 46 |
| Chapter five: - Conclusions And Recommendation. | | |
| 5.1 | Conclusions. | ٦٨ |
| 5.2 | Recommendation. | ٦٩ |
| Appendix | | |
| Appendix [A] | Point By Point Method. | 73 |

| | | |
|---|---|---|
| Appendix [B] | Equation of Motion | 75 |
| Appendix [C] | The Divergence Theorem | 83 |

**الخلاصة.**

**طريقة تامة لحساب أبعاد دافعة مظخة مركزية بواسطة معاملات التصميم التي أستخدم فيها طريقة النقطة بعد نقطة لشكل ريشة الدافعة.**

**دافعتين تم تحليلهما ظروف الأولى ($Q=0.132458\ m^3/sec, N=3600\ rpm, H=137.1m$) ظروف الثانية ($Q=0.00387\ m^3/sec, N=150\ rpm, H=0.8199\ m$). أبعاد دافعتي المضختين الناتجتين كانت ($r_1=69.02\ mm$ , $r_2=147.71\ mm$ , $b_1=21°$ , $b_2=25°$) للدافعة الأولى ($r_1=107.9mm$, $r_2=241.3\ mm$, $b_1=16°$, $b_2=23°$) للدافعَة الثانية**

**طور نموذج رياضي لتحليل الجريان أخذا بنظر الأعتبار قوة الطرد المركزي وقوة Coriloes المؤثرة بالسائل داخل البشارة.**

**حلل الجريان بأستخدام برنامج بلغة فورتران حيث حور البرنامج لكي يعمل في ظرووف تدوير. تم دراسة لتوزيع السرع ،الضغط ،الطاقة الحركية للأظطراب (k) ومعدل تبدد الطاقة الحركية للأظطراب ( ε ) بين الريشتين، تم الحل بواسطة أستخدام خوارزمية (SIMPLE) لحل الجريان الأضطرابي ببعدين بواسطة طريقة الحجوم المحددة المطبقة على شبكة موازية للحدود المتمركزة المتغيرات. تم تقريب االكميات المحفوضة بواسطة ثلاثة مخططات الأول(Upwind) ،الثاني(Central difference) والثالث (differed correction). توزيع منتظم للضغط والسرعة لوحظ في الدافعة الأولى ودوارة نسبية في الدافعة الثانية.**

وزارة التعليم العالي والبحث العلمي
جامعة بابل
كلية الهندسة
قسم الهندسة الميكانيكية

# الموديل الرياضي لتنبؤ خواص المائع خلال دافعة مضخة نابذة

**أطروحة**

**مقدمة إلى كلية الهندسة في جامعة بابل**

**كجزء من متطلبات نيل درجة الماجستير علوم**

**في الهندسة الميكانيكية**

**أعدت من قبل**

ساهر راقم رحيم الوائلي
**بكالوريوس ٢٠٠٠**

**المشرفون**

**د.عبد الكريم عبد الوهاب**

**د. عماد شكري علي**

**تشرين الثاني ٢٠٠٣**

# Chapter One

# Introduction

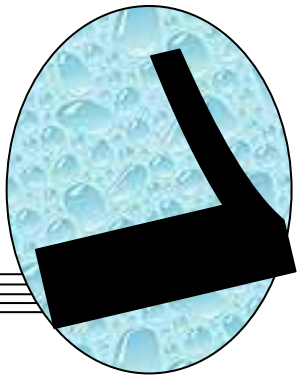

## 1.1 General introduction.

A Centrifugal pump is defined as a machine that increases the pressure energy of fluid with help of centrifugal action. Whirling motion is imparted to the fluid by means of blades mounted on the disc known as impeller. Centrifugal pump consists essentially of one or more impellers equipped with vanes, mounted on a rotating shaft and enclosed by casing. Liquid enters near the axis of a high speed impeller and thrown radially outward. As the fluid leaves the impeller at relatively high velocity, it's collected in a volute which transforms the kinetic energy in to pressure. After the conversion is accomplished, the fluid is discharged from machine [1].

The most common type of centrifugal pump is the volute pump. This type has single stage (single-Impeller pump), radial flow, single entry and horizontal position in volute pump Fig (1.1).

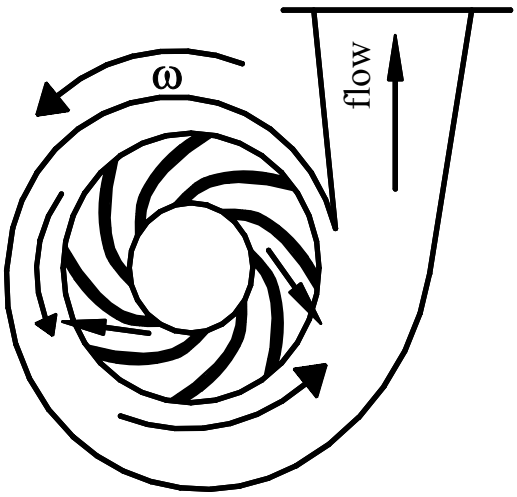


**Fig.(1.1) volute centrifugal pump casing design .**

During steady flow through the impeller, the stream surfaces cannot take random shapes, it mostly forms a common system of stream surface with the faces of the blades and it regarded the surfaces of blades as stream surfaces bounding the flowing liquid.

Fig.(1.2) is diagrammatic representation of the stream surfaces in the impellers:-

- Centrifugal pump (radial flow) Fig. (1.2a).
- Diagonal pump (mixed flow) Fig. (1.2b).
- Propeller pumps (axial flow) Fig. (1.2c).

As shown in Fig.(1.2a) the stream surface perpendicular to the Impeller axis [2].

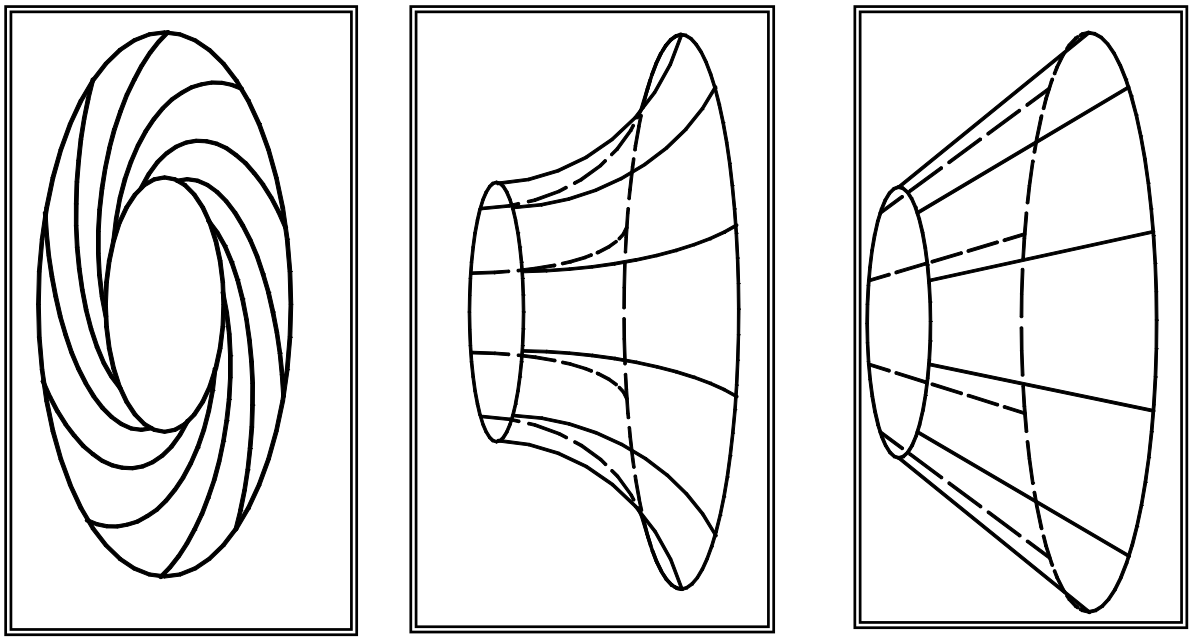

(a) (b) (c)

**Fig.(1.2) diagrammatic representation of the shapes of stream surfaces[2].**

## 1.2 Flow Analysis Problem: -

The real flows in centrifugal pump are complex, and not yet completely understood. It occurs in rotating curvature passages which has significant viscous and secondary flow. Moreover it is unsteady and includes region of separation. There are known mechanisms by which the structure of turbulence can be affected by both rotating and curvature of the passage. Finally there is the jet-wake flow, which exists down stream.

According to the complexity of the flow no single analysis can be found to model the entire flow phenomenon. Therefore simplified flow models are used which divide the over all problem in to two major groups; invicid and viscous models, which can be divided in to further groups. The analysis of the flow through the impeller of the rotodynmic pump is based on the experimentally established fact, that the path of streamline in turbulent flow of real liquid through the passage is similar to the path of a stream line determined for flow of perfect liquid through passages of the same shape; deviation only occurs near the walls.

Simplification is considered that the absolute velocity is resultant of relative and peripheral velocity [**2**].

The flow is complex Hence the computation fluid dynamic (**CFD**) is used for flow calculations [**3**].

In **CFD** more types of method are employed.

**1)** Finite-element method (**FE**) can be easily used to predict the flow on irregular geometries, but the equations are more complex and it is often more difficult to explain them physically. In this method a simple piece wise function (linear, quadratic….etc) is used to describe local variations of the unknowns flow.

**2)** Finite-difference method (**FD**) is the easiest method to use for simple geometries, the **FD** method can be applied to any grid type that

has structure grid, the grid lines serve as a local coordinate line, Taylor series expansion or polynomial fitting is used to obtain approximation to the first and second derivatives of the variables with respect to the coordinates; On structured grids, the **FD** is very simple and effective, it is especially easy to use higher–order schemes on regular grids; the disadvantage of **FD** method is that the conservation is not enforced unless special care is taken, also, the restriction to simple geometries is a significant disadvantage in complex flows.

**3)** Finite-volume method **(FV)**: - The finite volume method is similar to **FE** method in many ways, the **FV** method uses the integral form of the conservation equations as it's starting point, the solution domain is subdivided into a finite number of contiguous control volumes **(CVs)** and conservation equations are applied to each control volume, interpolation is used to express variable values at the **CV** surface in terms of nodal **CV**-center values. Surface and volume integrals are approximated by using suitable quadratic formula as a result one obtains an algebraic equation for each **CV**, in which number of neighbor nodal values appears [**4**].

The **FV** method can accommodate any type of grid, so it is suitable for complex geometries; the grid defines only the control volume boundaries and need not to be related to the coordinate system; the method is conservative by construction, so long as surface integral are the same for the **CVs** sharing the boundary; the finite volume approach is perhaps the simplest to understand and to program; all that need be approximated have physical meaning which is why it is popular with engineers; the disadvantage of **FV** method comparing to **FD** schemes is that method of order is higher than second are more difficult; this is due to fact that the **FV** approach requires two levels of approximation: interpolation & integration .

Other methods, like spectral schemes, boundary element methods, and cellular anotomata are used in **CFD** but their use is limited to special problems [**5]**.

## 1.3 Objective of the Present Work: -

The flow through centrifugal pump impeller is analyzed by using a numerical solution to the equation of motion. The stream surface in the radial impeller is normal to the axis of rotation, hence stream line is drawn between blades by dividing the angle between any two blades in to a number of division, and then curves are extended between these points parallel to the boundary Fig. (1.3).

In this work the analysis is of **2D** taken from blade to blade with slip losses by using finite volume method using **SIMPLE** algorithm on colocated body fitted grids.

The solution is of **2D** viscous and turbulent flow, and the geometry is devloped from experimental and theoretical chart that is used by Lobanof & Stepanoff.

And the impeller shape is to be developed by Point by point method and variable thickness from inlet to outlet.

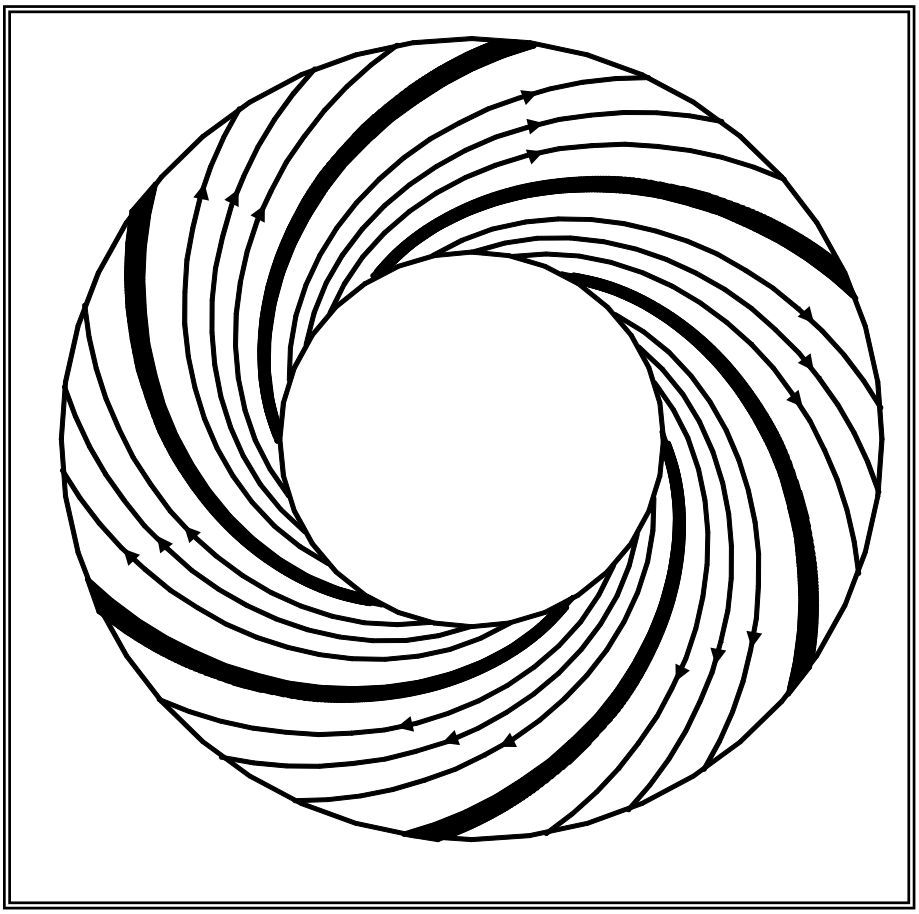

**Fig. (1.3) Figure shows Blade to Blade stream line.**

# Chapter Two

# Literature Review

## 2.1 Introduction.

There were a set of experimental and theoretical methods in approaches can be summarized as follows.

## 2.2 Design factor method.

It was an experimental method based on the different factors (experimental factors), from one model to another, the factors are plotted against specific speed, and all of them depend on Euler's equation .Most of these methods were old, and there is only one acceptable design for a certain specific speed.

The first authorities' reference on the complete hydraulic design of pump was produced by stepanoff [**6**] and then followed by many workers as follows.

**Stepanoff (1967), [6],** Stepanoff's design method based on the velocity and geometry analysis chart plotted against specific speed, the principles variable were head and flow coefficients.

The chart assumes consistency of design so that only data in pumps of similar type, a number of vanes, etc., should be plotted in one chart.

If stepanoff's own data was used, there is a little design flexibility in that, superficially at least; only one acceptable design can be produced for each specific speed.

**Stephen&Ademt's (1967), [2]** produced a method for the design the impeller with blade angle of single , double arc curvature and point by point method.

The method was based on the Euler's equation that helps in solving the necessary values of variable (peripheral velocity, meridonal velocity at the out let, the outlet blade angle, the number of blades, and the ratio of inlet radius).

Optimum results were mostly likely to be obtained for a given operating condition when the variables chosen on the basis of experimental test carried out on existing pumps that have efficiencies.

The results give the main dimensions of inlet and outlet diameters of the impeller. The impeller shape has been suggested by the research engineers of the hydro mechanical institute of polytechnic.

The comparison of six impellers with same the number of blade and inlet and outlet of the angle with varying lengths forming passages at various divergences.

**Lobanoff &Ross (1985),[7],** presents a method of designing **2D** ,invicid and steady, the method is based on the Euler's head equation ,the experimental performance test in various specific speeds.

Design factors that where taken from the experimental tests have been used, these factors are: - head, speed, capacity constant and diameter ratio.

**Reddy &Car ,(1971),[8]** ,Developed the theoretical and experimental method to calculate the number of blades and out let of blade angle , the method investigation, Stodola's effect for logarithmic shapes vanes and theoretical equations have been obtained to estimate the vane number for optimum efficiency of the unit, the experiments were conducted on the six impeller whose blade number from 2-10. Results show a maximum efficiency of 62.4 percent of impeller having seven blades at angle of 30 deg.

The theoretical analysis derived from Euler's equation of head developed and takes the loss, due to the channel circulation secondary flow loss, slip flow loss and loss due to friction.

## 2.3 Through Flow Analysis.

More and more sophisticated numerical codes were finding application of fluid dynamic analysis of turbomachinery. This was because growing a number of applications involves extremely high & low specific speed, tighter cavitations restriction using fluid, and similar requirements, there by necessitating for more accuracy in fluid dynamic design such as: -

**Pollad (1982), [9],** developed the method of **2D**, steady flow and assumed that the fluid to be non-viscous but losses arising from viscosity in particular boundary layers can be accounted for by inclusion of viscous of a large force and appropriate other terms in the equation of motion .The equation can be solved on the meridonal flow through pump.

The method was described as follows: -

- Determine the basic size and shape by hydraulic criterion.
- Flow analysis & modify passage and blade to remove separated and high velocity regions.
- Determine the losses that carry out off design check cavitations performance.

**Salsibury, (1982), [10],** reviewed method of designing the impeller in many approaches, the first approach was based on Euler equation and free vortex and takes in to account the hydraulic losses and slip factor and found that the good result at out flow angle and the second deal with design coefficient and design parameter.

**Nubert, Stokman & Kramer, (1963), [11],** derived a method of analysis pump impelle from the equations of motion, continuity & momentum for

incompressible non-viscous fluid, relative flow is assumed to follow along stream surface.

**Martelli & Michelssi, (1991), [12],** presented a viscous computer code for designing the meridonal channels of high performance pump.

An average technique is used to reduce the three dimensional flow to **2D** incompressible flow, was validated in complex flow geometries prior to application in the design analysis of an actual pump, viscous effect are taken into account by two different turbulence model, the **Navier–Stocks** equations solver was used in conjunction with a standard **BB** calculation by means of automatic graphic procedure that exchanges geometries and flow field data, various meridonal shape solution are presented and discussed in relation to physical evidence .

**J,Tuzson, (1991), [13],** a new way of plotting the computer output was proposed which illustrates the energy distribution through the flow.

The consequence deviating from optimal flow pattern was discussed and specific causes were reviewed. A criterion was derived for the existence of a jet-wake flow pattern and for the minimum wake loss.

**S. M. Miner & R. D. Flack, (1992), [14],** two dimensional potential flow was used to determine the flow velocity field within a laboratory centrifugal pump.

The finite element technique was used to model the impeller and volute was simulated by using steady-state solution with the impeller in ten different angular orientations.

This allowed the interaction between the impeller and the volute to develop naturally as a result of solution the result of a complete pump model showed that there were circumferential a symmetric in the velocity field even at design flow rates

**Blanco & Fernandez, (2000), [15],** showed a numerical simulation of three dimensional fluid flows inside a centrifugal pump. The pump was a

commercial centrifugal water pump with (190 mm) outlet impeller pump, backward curved blades, nominal flow of (0.013 m3/sec) and (11 m) of head .

This simulation has been made with an unsteady calculation and using the sliding mesh technique to make into account the impeller volute interaction .with them, it was possible to simulate correctly the blade passage in the front of the tongue and the flow and the pressure fluctuation measured in the volute.

The data obtained allowed the analysis of the main phenomenon existent in these pumps, such as: pressure changes in the volute for different flow rates, the incidence at the leading edge of the blade with different flow condition, and the secondary flow generated in the volute due to the width change between the impeller and the volute.

**Bart van Esch, (1997), [16],** showed the numerical method developed for solving unsteady potential flow was based on a fully three-dimensional, **FE** method. The computational mesh was divided into two parts, one for the rotor and other is for the pump casing, and connected by a sliding interface. In this way the impeller rotating motion with respect to the pump casing can be simulated efficiently. Some special numerical techniques were employed in order to reduce computing time. These were based on the substructuring method combined with the implicit imposition of the Kutta conditions at the trailing edges of the impeller and diffuser blades.

The losses which occur in pumps were quantified using additional models for energy dissipation in boundary layers, in mixing areas and at sudden expansions and contractions in through flow area, as well as models for disc friction and leakage flow. Based on the velocity distribution along the rotating and stationary surfaces, as obtained from a three-dimensional potential flow computation, the state of boundary layers was determined by using a one-dimensional boundary layer method.

**T. Alberto & L. Gerhard, (2001), [17],** quantified and compare the different individual efficiencies which comprise the total efficiency of a

centrifugal pump. A combination of experimental data, theoretical analysis and numerical simulation is used for this study. A special test rig and a single stage volute casing pump of specific speed (**Ns** = 12) was used for the experimental investigations, the test rig is shown in Fig.(2.1).

This test rig permitted the hydraulic and mechanical data to be acquired with high precision. The theoretical approach was based on different loss-models and assumptions. A software code developed at our institute was used to determine the different losses and efficiencies. The test pump was simulated 3-dimensionally first without the side spaces (i.e. only impeller and spiral casing) to obtain **H** and **Q** characteristic curves for different relative impeller-spiral casing positions and rotational speeds. Finally, the entire pump was modeled to study the disc friction and leakage losses at the best efficiency point of operation for different radial gap widths of clearance seals. The **CFD** results show the applicability of a quasi-steady formulation where higher discrepancies with the measurements occur. These discrepancies were related to strongly unequal mass flow rates through each impeller channel.

## 3.4 Control volume approach.

Finite volume approach has become popular in **CFD** as a result, primarily, of two advantages .First, they ensure that the discretizatioin was conserved, i.e. mass, momentum and energy were conserved in discrete sense. Second, finite volume method does not require a coordinate transformation in order to be applied on irregular meshes **[18]**. As a result they can be applied on unstructured meshes consisting of arbitrary polygon in two dimension or arbitrary polyhedral in three dimensions. This increased flexibility can be used to great advantage in generating grid about arbitrary geometries.

The important research covering this field will be reviewed bellow:

**Atta, (2000), [19],** developed a computational and experimental investigation for flow through cascade of twisted compressor blade, the analysis

was carried out using **SIMPLE** algorithm for Quasi–Three dimensional flow between axial compressor blade. The flow field was discritized using **Navier-stoke** equations, continuity & momentum equations and $\mathbf{k-\varepsilon}$ turbulent model in orthogonal curve linear coordinate system and then they were solved by using control volume based on finite difference method with staggered grid arrangement. The numerical results obtained were fairly accurate for a high angle of attack and with a large deviation near the leading and trailing edges of the blade. It should be mentioned that the physical region was poorly described in the blade surface

And near the leading and trailing edge where the grid lines lack the clustering in this regions which was unacceptable case for viscous flow (i.e., high gradients near the wall boundary), however this reason may lead to the poor prediction at the leading and trailing edges where it could be reduced by adding controlling function to the Laplace equation and solving Poisson's equation instead of Laplace equation to generate computational grid.

**Ghozeh, (2000), [20],** developed a general procedure (algorithm) for numerical solution of the steady incompressible **Navier-Stokes** equation in a body fitted non-orthogonal coordinate system. A theoretical and experimental investigation for the three dimensional flow between twist axial compressor blades was conducted. The solution algorithm was based on a technique of automatic numerical generation of curvilinear coordinate system having coordinate lines coincident with the body contour regardless of it's shape. The general numerical solution scheme was based on the control volume formulation. A staggered grid technique was employed, which uses Cartesian velocity components and pressure as the main variable. Continuity was coupled with momentum through the **SIMPLE** algorithm. Turbulence modeled by three different models, $\mathbf{k-\varepsilon}$ &**RANS** and $\mathbf{k-\omega}$ models. The numerical results obtained agree with the experimental work except for the region of a high twist. However the disagreement in his work especially at the region of high twist was

attributed to the use of Cartesian velocity components as the main variables for the momentum equations with staggered grid technique which does no longer valid to avoid oscillation of pressure instead, should use velocity components direction along the grid lines curves in tangential manner (i.e. covariant velocity components) so that the staggering was done along the truth direction of velocity components another reason for the disagreement was attributed to the severe skewness of the grid lines at a certain points along the boundary however the computational grit was not very clear and have some discrepancies at the boundaries.

## 3.5 Scope of the present work.

As compared with previous published; the present work was carried out to add to the existing knowledge merge between the recent method by design factor and flow calculation by numerical solution to the equation of motion with finite volume method.

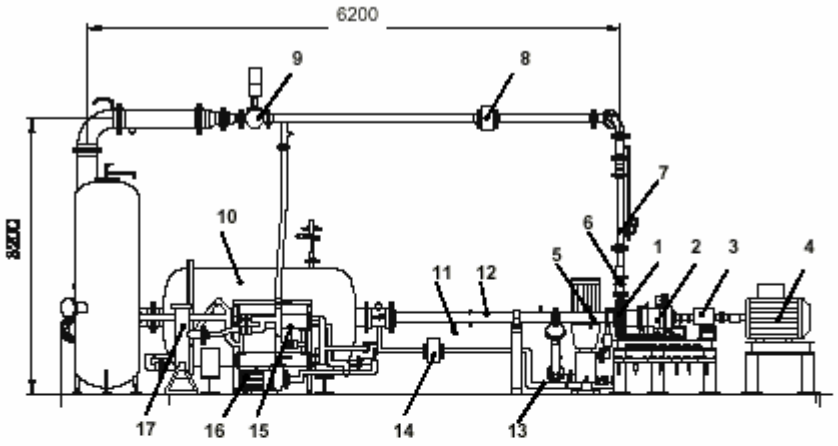


1. test pump
2. hydrostatic-journal-bearing
3. torque meter
4. AC motor
5. inlet pressure sensor
6. exit pressure sensor
7. discharge line
8. MID (DN 80)
9. electro-hydraulic-valve
10. tank
11. resistance thermometer
12. suction pipe
13. bypass pipe
14. MID (DN 40)
15. heat exchanger
16. heat exchanger pump
17. water filter

**Fig(2.1)Scheme of the test-rig**

# Chapter Three

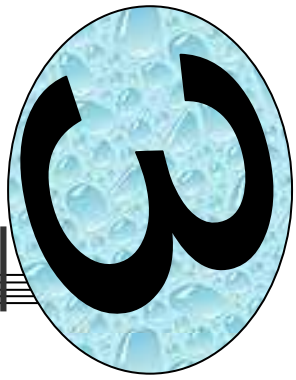


# Theoretical Analysis and Mathematical Model

## 3.1 Introduction.

In order to analyze the flow through impeller it must be found a model to investigation the flow. In this search the geometry was developed by the recent method (Stepanoff, Stephen, Lobanof), then generating **2D** profile and study it from blade- blade with calculation of viscous and turbulent parameters along stream line, this chart represents the main steps in the flow analysis Fig.(3.1).

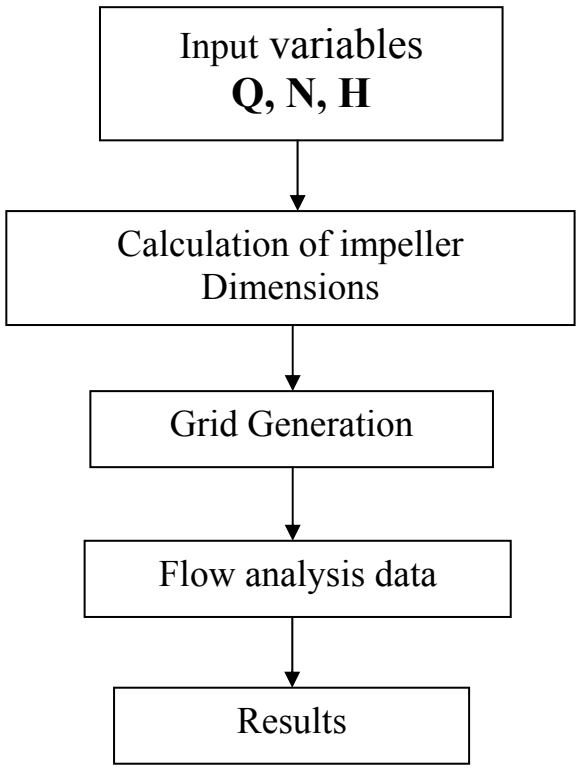


**Fig. (3.1) main steps in the flow analysis.**

## 3.2 Input variables.

Input variables were enforced by the type of pump; hence the pump must be classified before selection and given input variables.

The prime parameter for evaluating, pump selection and prediction possible field problem was specific speed [7], its also a reference number that describes the hydraulic features of a pump whether radial ,axial ,mixed or semi axial as shown in Fig.(3.2), this figure shows the value of specific speed of different pump types, the input variables are head (m), volume flow rate ($m^3$/sec) and speed (rpm), the three main input variables are gathered in the relation of specific speed this relation is.

$$N_S = \frac{N\sqrt{Q}}{H^{3/4}} \qquad \ldots(3.1)$$

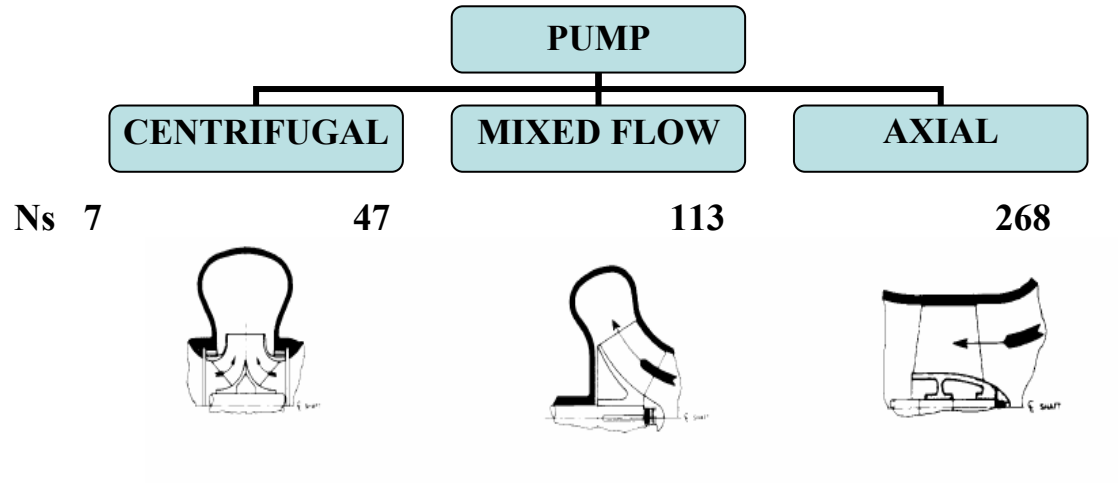


**Fig.(3.2) specific speed of difference types of pumps [21].**

## 3.3 Calculation of Impeller Dimension.

In order to calculate impeller dimensions. The theoretical back ground had been studied as follows: -

### 3.3.1 Geometry of Flow through Impeller.

The liquid particles flow into the impeller through a cylindrical surface of radius $\mathbf{r_1}$ with an absolute velocity $\mathbf{V_1}$ inclined at angle $\alpha_1$ to the peripheral velocity $\mathbf{U_1}$ at the impeller inlet and it flows out of the impeller through a cylindrical surface of radius $\mathbf{r_2}$ with an absolute velocity of $\mathbf{V_2}$ and inclined at angle $\alpha_2$ to the peripheral velocity $\mathbf{U_2}$ Fig. (3.3).

The flow patterns at the inlet and outlet of an impeller, rotating with a constant angular velocity $\omega$, were defined by the velocity triangle Fig. (3.4), the absolute velocity $\mathbf{V_1}$ at the inlet edge of the blade was resolved in to the peripheral velocity $\mathbf{U_1 = r_1.\omega}$ and the relative velocity $\mathbf{W_1}$.The symbol $\mathbf{V_{r1}}$ and circumferential components denote the meridonal component of the absolute velocity by $\mathbf{V_{u1}}$. Similarly the velocity $\mathbf{V_2}$ at the outlet edge is resolved the velocities: $\mathbf{U_2 = r_2 . \omega}$ and relative velocity $\mathbf{W_2}$ .

If the direction of the relative velocity coincide with the tangent to the first element of the blade entry to the impeller is shock less, and the angle of relative inlet velocity $\beta_1$ same as the angle of the inclination of the first element of the blade to the tangent to the circumstances of circle of radius $\mathbf{r_1}$. If the flow through impeller passage takes place without losses the relative outlet velocity vector $\mathbf{W_2}$ is tangential to the last element of blade.

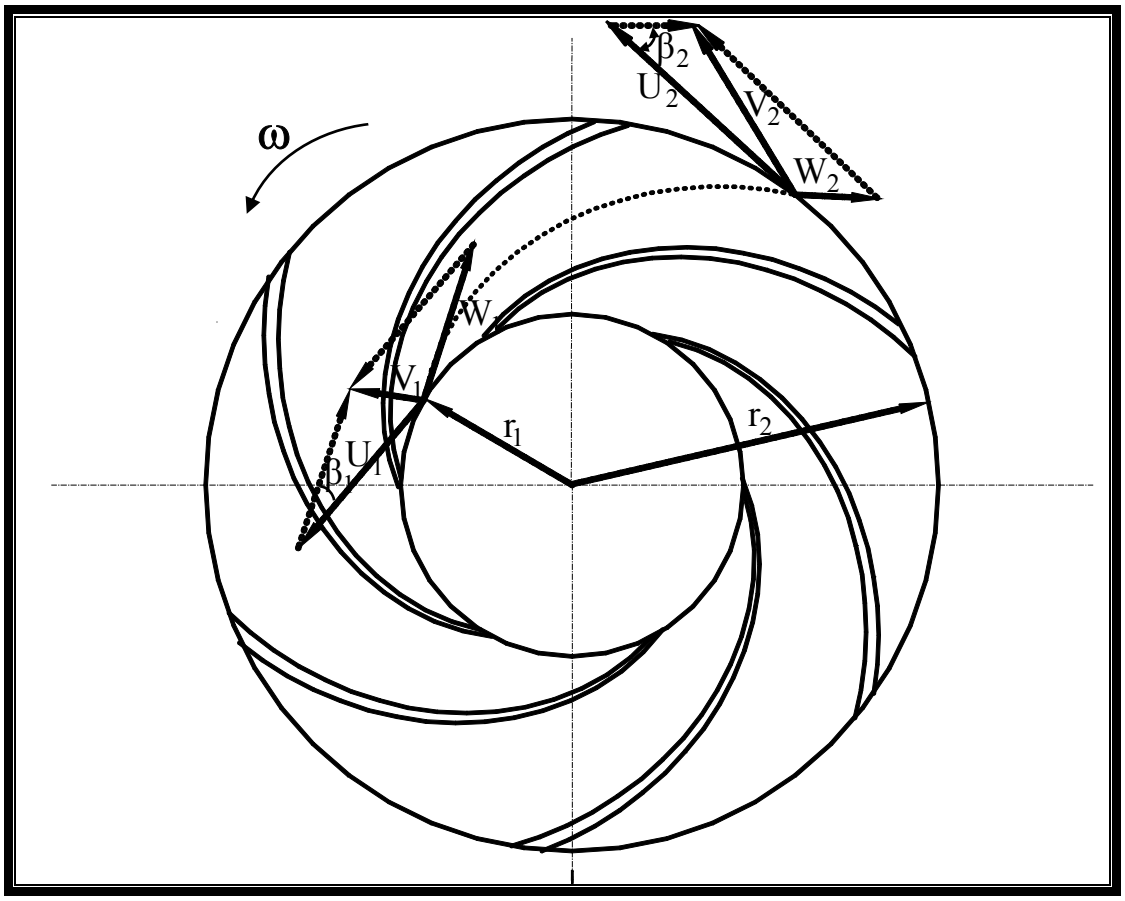


**Fig. (3.3) Geometry of flow through centrifugal pump.**

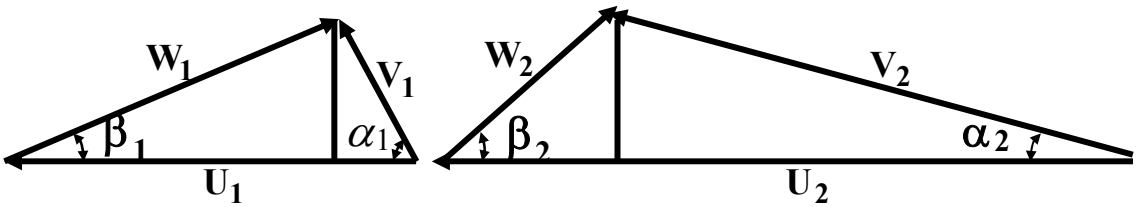


**W1 > W2**

**V1 < V2**

**U1 < U2**

**Inlet velocity triangle** **Out let velocity triangle**

**Fig.(3.4) velocity triangles.**

## 3.3.2 The Euler Head Theory.

The basic relationship for centrifugal pump is simple and is derived from Newtonian's law of motion applied to a fluid transferring a rotor assuming a steady flow , the change of torque exerted by an impeller on the flowing fluid is.

$$dT = \rho Q d(rV_t) \quad \text{...(3.2)}$$

Integrating the above equation between $r_1$ and $r_2$ for constant density and volume flow rate gives:-

$$T = \rho Q(V_{t2}r_2 - V_{t1}r_1) \quad \text{...(3.3)}$$

The rate of energy transfer is the product of torque and angular velocity, so:-

$$T\omega = \rho Q \omega(V_{t2}r_2 - V_{t1}r_1) \quad \text{...(3.4)}$$

Hence $\omega.r=U$, Where **U** is peripheral speed of the impeller at radius.

$$PP=T.\omega=\gamma.Q.H$$

by dividing Eq (3.4) by $\gamma.Q$ yield

$$H = \frac{(U_2.V_{t2} - U_1.V_{t1})}{g} \quad \text{...(3.5)}$$

Where **H**: total head (**m**).

Eq(3.5) is known as Euler's head equation. This equation based on the follqwing assumptions[**6**]:

1. The fluid leaves the impeller passages tangential to the vane surfaces or there is completely guidance of the fluid at the outlet.
2. The impeller passages are completely filled with actively flowing fluid at all times.
3. The velocities of the fluid at similar points on all the flow lines are the same.

The flow of liquid through an impeller passage may be regarded as a flow of liquid particles only the center line of the passage the theory flow based on this assumption is called the one dimensional theory of (rotodynmic) machine.

### 3.3.3 Calculation of the Impeller dimension By Design Factor.

The first authorities on the complete hydraulic design of a pump were produced by a Stepanoff. The design procedures suggested were still valid so long as up to date [**22**]. Stepanoff's design method was based on velocity and geometry analysis chart plotted against specific speed. The principles variables are head and flow coefficients

Speed constant

$$K_t = \frac{U_2}{\sqrt{2gH}} \qquad \ldots(3.6)$$

Capacity constant

$$K_{r2} = \frac{V_{r2}}{\sqrt{2gH}} \quad \text{(outlet)} \qquad \ldots(3.7)$$

$$K_{r1} = \frac{V_{r1}}{\sqrt{2gH}} \quad \text{(inlet)} \qquad \ldots(3.8)$$

Where

$U_2$ … Impeller peripheral velocity (m/sec)
$g$ … Gravitational constant (9.81 m/sec$^2$)
$H$ … Impeller head (m)
$V_{r1}$ … Radial velocity at impeller inlet (m/sec)
$V_{r2}$ … Radial velocity at impeller discharge (m/sec)

The design factor gives direct relationship between the impeller total head and a capacity at the design point and several elements of Euler's velocity triangle [**7**]. These factor are entirely experimental and don't lend them to theoretical treatment [**21**]. Design parameters (geometric and velocity ratio) of existing designs are plotted in chart against specific speed **Ns**. Each pump is identified by, type, size, number impeller vanes, etc. to enable consistent data to be used in subsequent new design parameter selection.

To produce a preliminary design layout the following data were needed:-

**A.** Vane inlet and outlet angles and vane number.

**B.** Meridonal velocities at inlet and out let.

**C.** Impeller out let diameter.

By adopting the following procedure.

1. Given $\mathbf{Q, H}$
2. select $\mathbf{N}$
3. select $\beta_2, Z$ from Fig.(3.6)
4. read $\mathbf{K_{t2}}$ from Fig.(3.7)and calculate $\mathbf{U_2}$
5. calculate $D_2$
6. read $\frac{\mathbf{D_1}}{\mathbf{D_2}}$ from Fig.(3.8)& calculate $\mathbf{D_1}$
7. Read $\mathbf{K_{r1}}$ **&** $\mathbf{K_{r2}}$ from Fig.(3.9) & Fig.(3.10) then calculate $\mathbf{V_{r1}}$ **&** $\mathbf{V_{r2}}$.

   Inlet angles are calculated by using the inlet velocity triangle, in practice $\beta_1$ limit 50 –15 degrees. Outlet angle $\beta_2$ practically vary between 35 and 15 and the normal range between (20-25), number of vanes[6].

   $\mathbf{Z = \frac{\beta_2}{3}}$ Approximately.

   $\mathbf{Z = 6}$ Minimum for low $\beta_2$.

   $\mathbf{Z = 8}$ Normal**[6].** .

We can say that the number of blade is a function of blade angle this relation can be shown in Fig. (3.6). When select $\beta_2$ the number of blade is known and vise versa .From Fig.(3.7) diameter ratio from this figure we compute inlet diameter $\mathbf{D_1}$ eye diameter ($\mathbf{D_1}$ some times it's equal to the diameter at inlet edge and some times it's larger than it, finally reading $\mathbf{K_{r1}}$ Fig (3-8) and compute $\mathbf{V_{r1}}$ .

$$K_{r1} = \frac{V_{r2}}{\sqrt{2gH}} \qquad \ldots(3.9)$$

$$V_{r1} = K_{r1} \sqrt{2gH} \qquad \ldots(3.10)$$

For calculating of Stepanoff make the following recommendation

$\frac{P_{1s}}{U_1}$ = 1.15 to 1.25 for single entry, end suction see Fig. (3.5):-

where $\frac{P_{1s}}{U_1}$ prerotaion factor.

$$\beta_1 = \tan^{-1} \frac{P_{1s}}{U_1} \qquad \ldots(3.11)$$

$$b_1 = \frac{Q}{V_{r1} (\pi \cdot D_1 - Z.Su)} \qquad \ldots(3.12)$$

**Su** is blade thickness

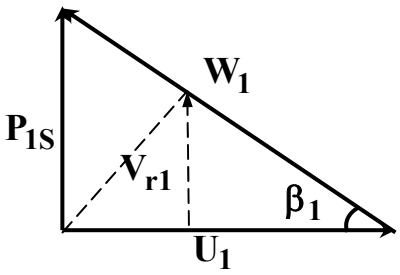


**Fig. (3.5) Inlet velocity triangle.**

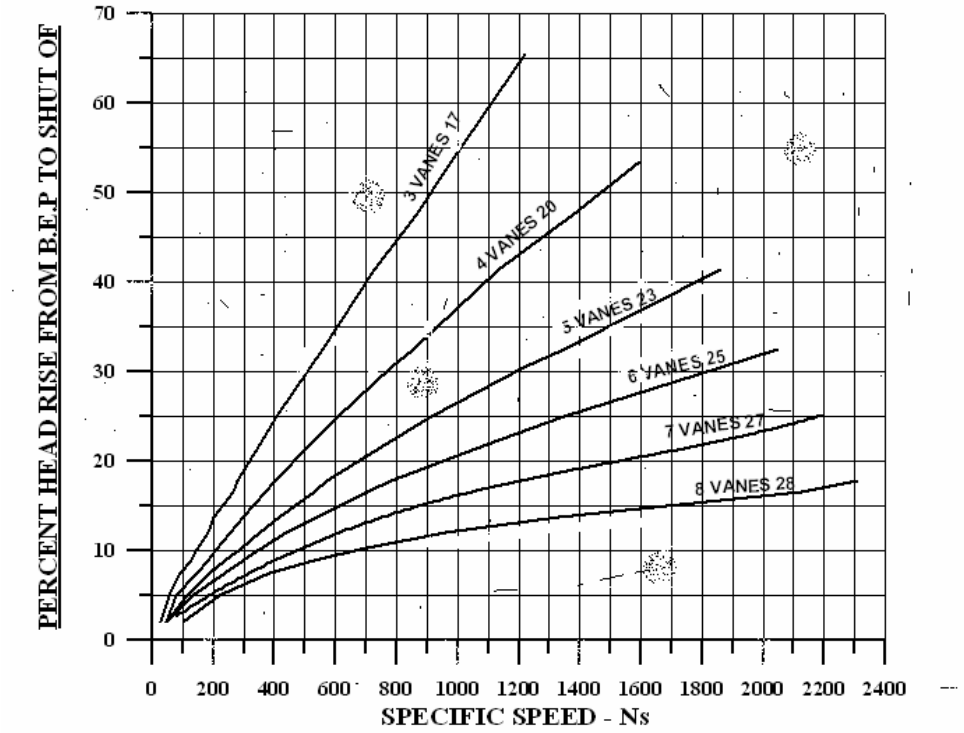


**Fig.(3.7) Speed Constant [7].**

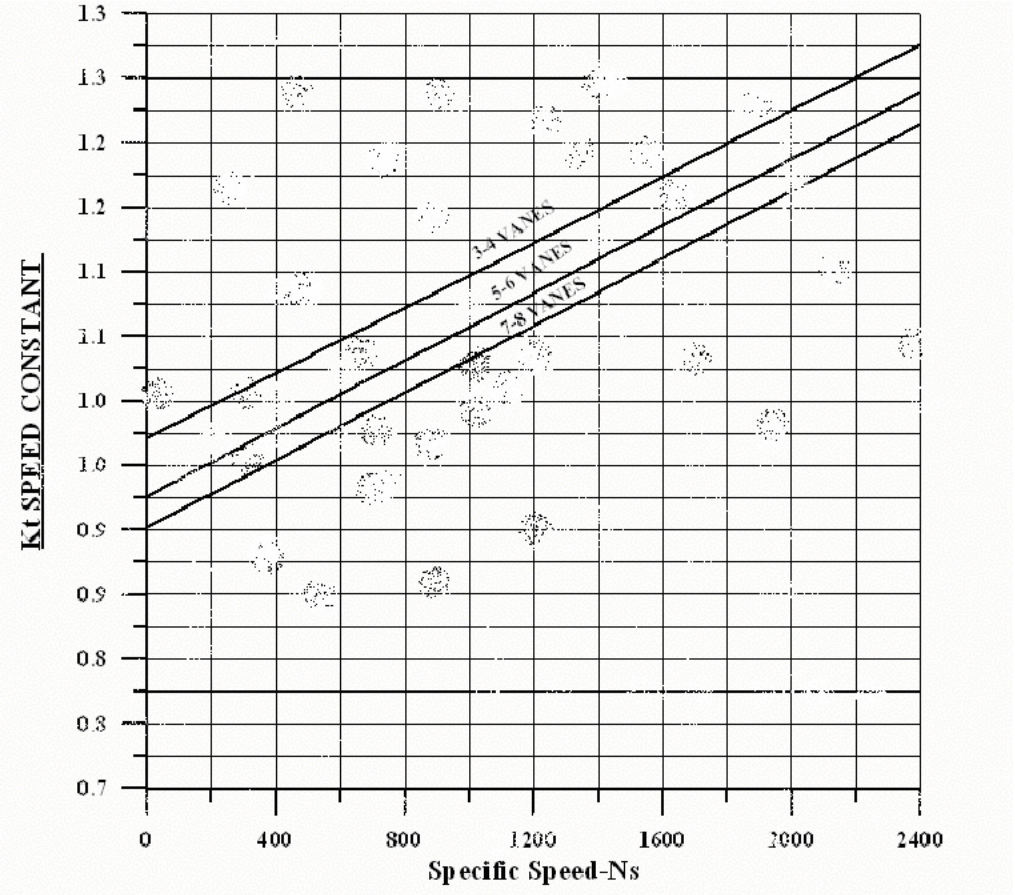


**Fig.(3.7) Speed Constant [7].**

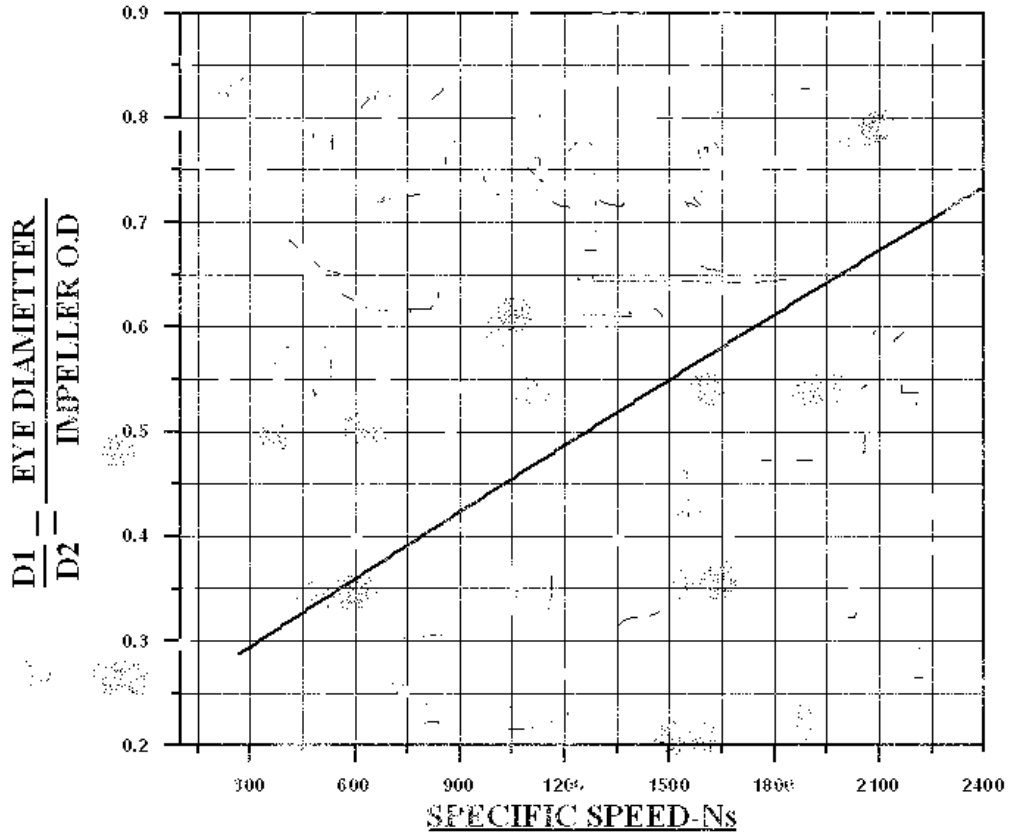


Fig.(3.8) Diameter ratio with radial distance [7].

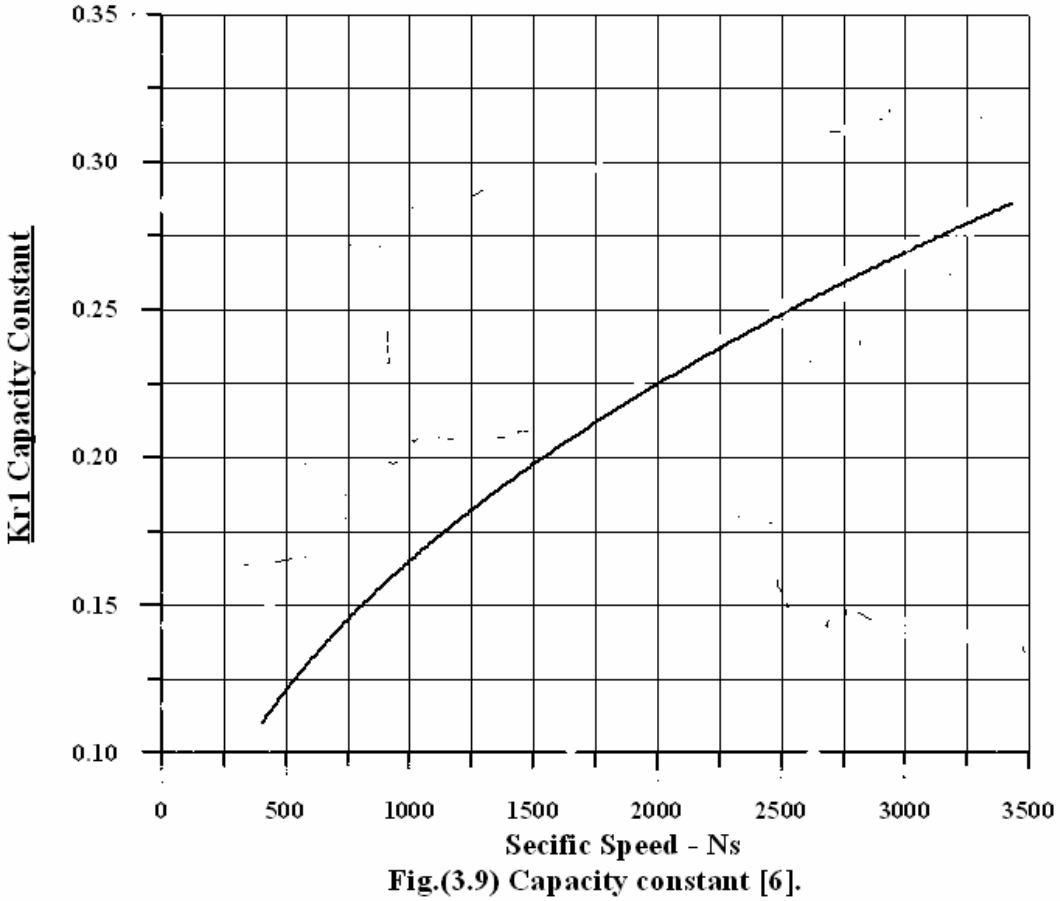


Fig.(3.9) Capacity constant [6].

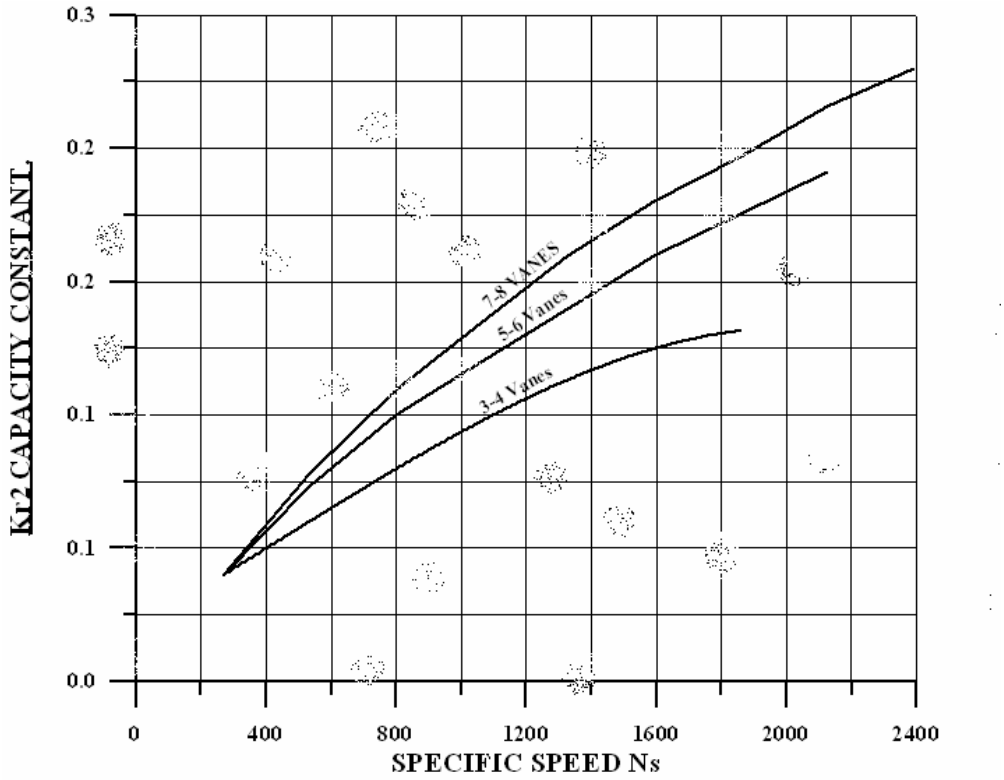


FIG.(3.10) Capacity Constant [7].

## 3.3.4 Developing Of Impeller Shape.

From the calculations obtained in the previous section the impeller blade shape can be developed.

There are three principles methods for determine the shape of blade [2]:-

**a-** Single arc method.

**b-** Point by point method.

**c-** The conformal representations method.

In order to chose the best method a comparison should be taken between these methods.

The single arc method is very simple ,it does not allow any alteration in the blade length for given values of $\mathbf{r_1}$, $\mathbf{r_2}$ and $\beta_1, \beta_2$ and it is difficult to shape the impeller passage correctly , the angle of inclination of the blade changes greatly along the blade and intermediate values of $\beta$ may be longer than $\beta_2$ , For this reason this method is seldom used .

The point by point method and conformal representation method give the designer the greatest freedom in shaping the blades, the angle of inclination of the blade changes gradually along the blade, and give highest total head than the single arc method [23].

In the present work, follow the point by point method, in this method points in the surface of vane are found numerically by solving the integral of the following equation:-

$$\theta = \frac{180}{\Pi}\int_{r1}^{r}\frac{dr}{r\ \tan\beta} \approx \frac{180}{\Pi}\sum_{r1}^{r}\frac{\Delta r}{r\tan\beta} \qquad ..(3.13)$$

The method and its derivation are explained in appendix **[A]** and the developed impeller shape is shown in Fig. (3.11)**.**

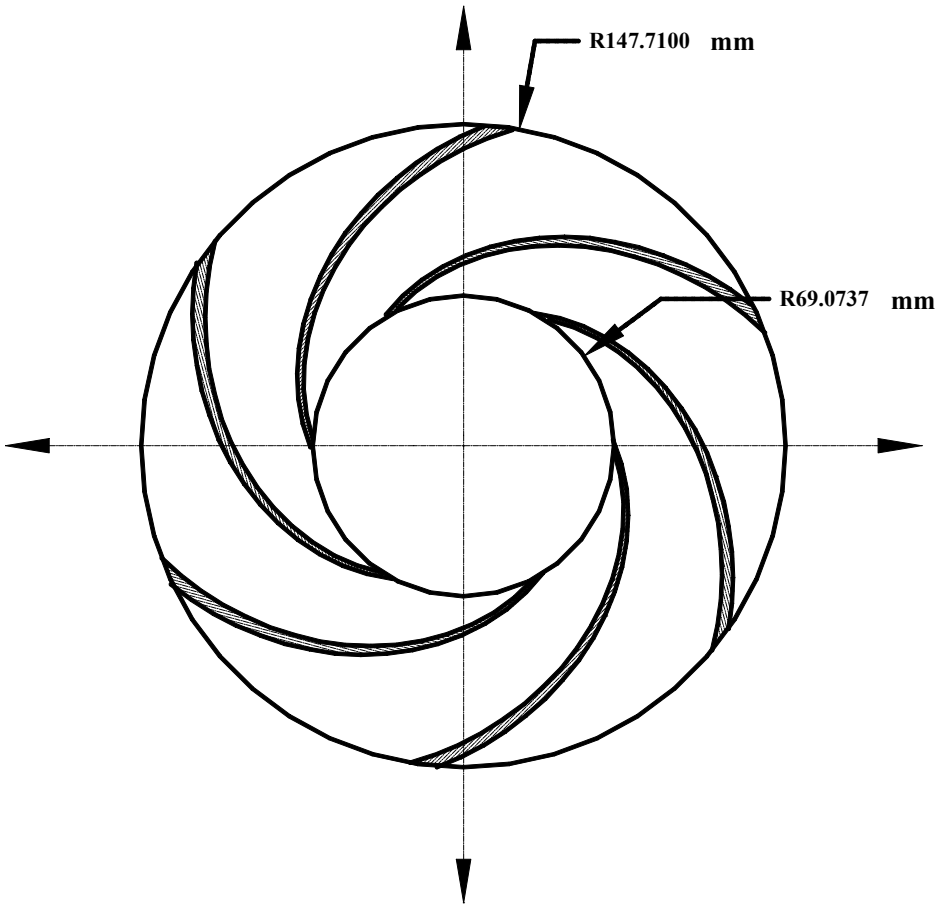


**Fig.(3.11) Figure shows the developed impeller .**

## 3-4 Grid Generations.

One of the central problems in computing numerical solutions to partial differentials equations is that grid generation technique improper choice of grid point locations lead to an apparent instability or lack of convergence [24].

The problem of grid generation is that determine the mapping which takes the grid points from the physical domain to computational domain several requirements must be placed on such mapping.

Grid generation techniques can be roughly classified in to three categories :-

**a-** Complex variable methods.

**b-** Algebraic method (boundary –fitted grid).

**c-** Differential equation method.

Complex variable method has an advantage that the transformation used are analytically or partially analytic as apposed to those methods which entirely numerical, algebraic method is used to cluster grid points near solid boundaries to provide adequate resolution of the viscous boundary layer.

Transformation from physical coordinate to computational coordinate in finite difference (**FD**) by finding metrics of transformation and evaluating the Jacobin, but in finite volume (**FV**) methods there is no need for coordinate transformation [**25**].

When the gradient normal to the control volume **CV** surface is approximated, one can use local coordinate transformation, as will be shown in the appendix **[B]**.

The advantage of the algebraic method that can be adapted to any geometry, and that optimum properties are easier to achieve than with orthogonal curve linear grids, since the grid lines follow the boundaries ,the boundary conditions are more easily implemented than with step wise approximation of curved boundaries then this method is easy to program. The grid can also adapted to the flow ,i.e. one set of grid lines can be chosen to follow the streamlines (which enhanced accuracy ) and the spacing can be made smaller in regions of

strong variables change especially if block-structured or unstructured are used .Non orthogonal grids have also several advantages .The transformed equation contained more variable by increasing both the difficulty to programming and the cost of solving the equation ,the non orthogonal grid may causes unphysical solution and the arrangement of variables on the affects the accuracy and efficiency of algorithm.

In the present work the procedure of generation the grid was summarized as follows: -

**1)** From Eq.(3.13) the numerical integration gives the relation between $\mathbf{r}$ and $\theta$ of the surface points of blade (**PS**).

**2)** Rotating the curve of **PS** by the angle between two blades in order to estimate the points of **SS**.

**3)** Generate number of curves between **PS** and **SS** with same procedure by number of division.

**4)** Generate number of arcs between $\mathbf{r_1}$ and $\mathbf{r_2}$ by the points of the curves.

The variables arrangement on the grid may be staggered or colocated. Colocated arrangement is the simplest one, since all variable shares to the same **CV** but it requires more interpolation. The generation of grid and the arrangement of variables are shown in Fig. (3.12) and Fig.(3.13).

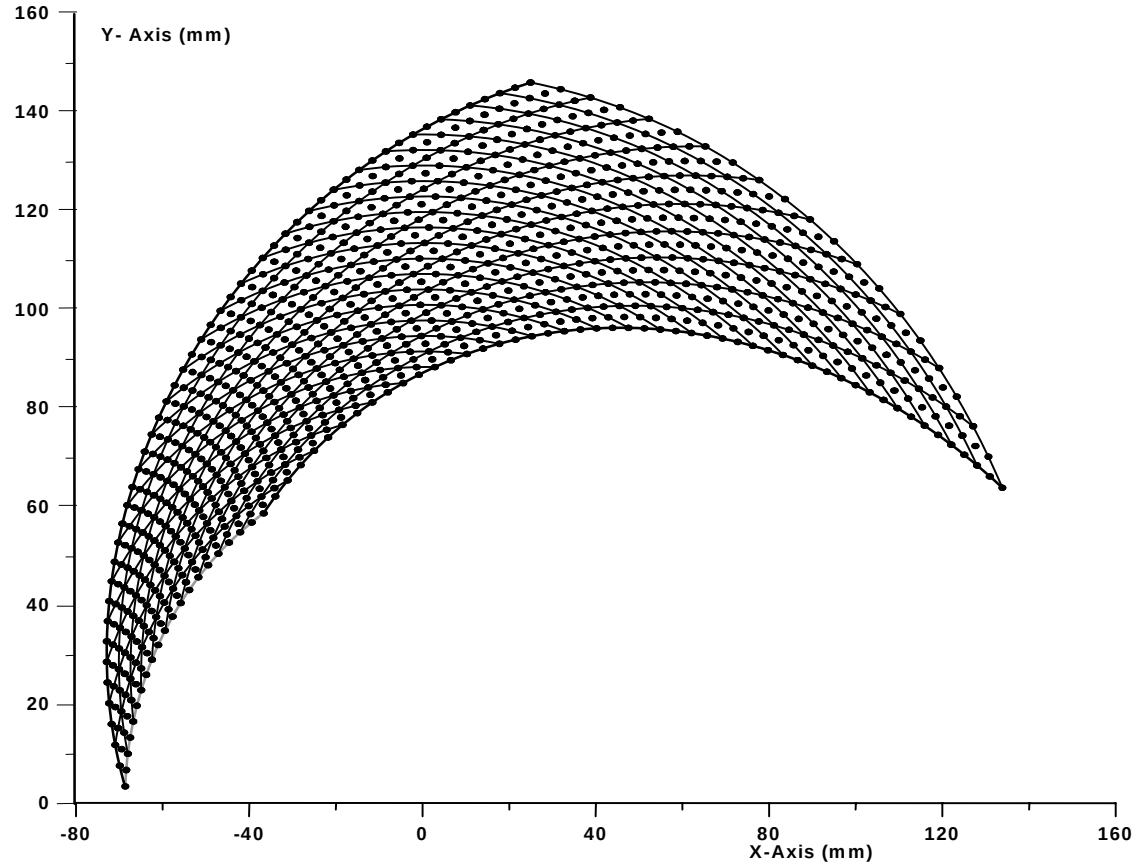


**Fig.(3.12) 2D grid generation between two blades (body fitted grid).**

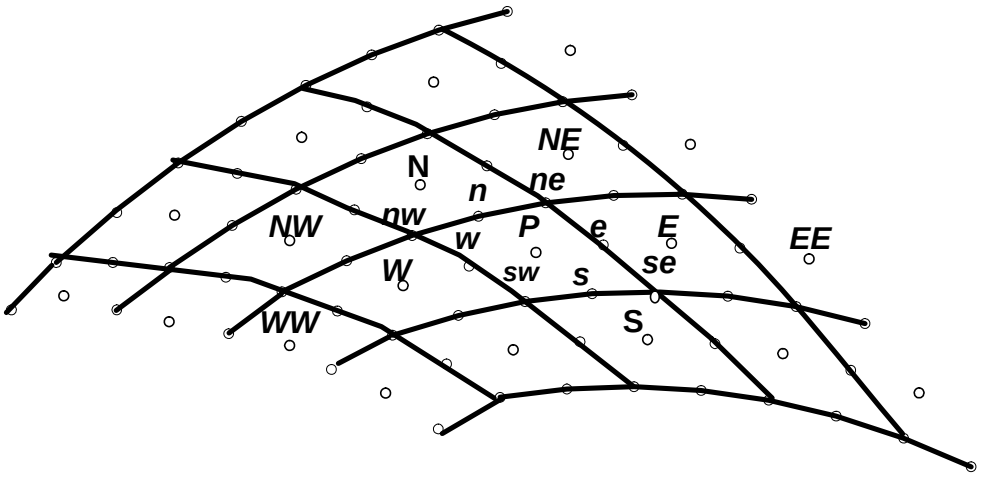


**Fig (3-13) 2D control volume for non-orthogonal grid.**

## 3.5 flow analysis.

### 3.5.1 Equation of motion.

The equation of relative system is derived by Vavra [**26**] and produce the relative system in vector form, the derivation of equation for viscous incompressible &turbulent fluid flow with details in the appendix [B] :-

Continuity equation:-

$$\rho \nabla \cdot \vec{w} = 0 \qquad \ldots(3.14)$$

Momentum equation:-

$$\rho \vec{w} \cdot \nabla \vec{w} = 2\rho \vec{w} \times \vec{\omega} + \rho \vec{\omega} \times (\vec{r} \times \vec{\omega}) - \nabla p + \nabla \mu_e \nabla \vec{w} \qquad \ldots(3.15)$$

The two terms in the right hand side represents carioles and centrifugal acceleration.

To solve the above equations the mathematical expression of effective viscosity $\mu_e$ will be required.

### 3.5.2 $k-\varepsilon$ Model .

In a recirculation flow a two–equation (Eq(3.18)&Eq(3.19)) turbulence model which describes the turbulence velocity by transport equation will be more appropriate .This model uses the turbulence kinetic energy $k$ and kinetic energy dissipation $\varepsilon$ . This is usually know as $k-\varepsilon$ turbulence model and currently it is the most widely used because of it's applicability to wide ranging flow problem and it's lower computational demand than more complex model which are available [28].

The values of $k$ , $\varepsilon$ and its differential equations are written in the following.

$$\varepsilon = \frac{c_\mu k^{1.5}}{L_m} \quad \text{Where } L_m \text{ is mixing length.} \qquad \ldots(3.16)$$

$$\mu_t = \frac{c_\mu \rho k^2}{\varepsilon} \qquad \ldots(3.17)$$

k − eq

$$\nabla\cdot(\rho w k) = \nabla\left(\frac{\mu_e}{\sigma_k}\nabla k\right) + \mu_t\left[2\left[\left(\frac{\partial w_x}{\partial x}\right)^2 + \left(\frac{\partial w_y}{\partial y}\right)^2\right] + \left[\frac{\partial w_x}{\partial y} + \frac{\partial w_y}{\partial x}\right]^2\right]$$

$$-\rho\varepsilon \qquad \ldots(3.18)$$

ε − equation

$$\nabla\cdot(\rho w \varepsilon) = \nabla\left(\frac{\mu_e}{\sigma_\varepsilon}\nabla \varepsilon\right) + \frac{C_1 \varepsilon \mu_t}{k}\left[2\left[\left(\frac{\partial w_x}{\partial x}\right)^2 + \left(\frac{\partial w_y}{\partial y}\right)^2\right] + \left[\frac{\partial w_x}{\partial y} + \frac{\partial w_y}{\partial x}\right]^2\right]$$

$$-C_2\rho\frac{\varepsilon^2}{k} \qquad \ldots(3.19)$$

The model contains empirical constants, which are assigned the value in table (3.1)

| $C_1$ | $\sigma_k$ | $C_2$ | $C_\mu$ | $\sigma_\varepsilon$ |
|---|---|---|---|---|
| 1.44 | 1.0 | 1.92 | 0.09 | 1.3 |

Table (3.1) empirical constants in high Reynolds's number(Re>2300).

## 3.6 Approximation of Integral.

### 3.6.1 Convective and diffusive term.

According to Fig. (3.13) a typical two dimension **CV** are shown together. The **CV** surface can be subdivided into four plane faces denoted by lower case later corresponding to their direction (**e**, **w**, **n**, and **s**) with respect to the central node **(P)**.

The net flux (Convective and diffusive) through the **CV** boundary is the surface integrals over the four faces:-

$$\iint_{s} F^{c,d} ds = \sum_{k} \iint_{s_i} F^{c,d} ds \qquad \text{...(3.20)}$$

where $i = e, w, n \,\&\, s$ direction.

To calculate the surface integral in equation above one would need to know the integrand $F$ every where on surface $S$ .

The cell face values are approximated in terms of nodal (**CV** center) values, the simplest approximation to the integral is the mid point rule.

$$\sum_{k} \iint_{s_i} F^{c,d} ds = F_e s_e + F_w s_w + F_n s_n + F_s s_s \qquad \text{...(3.21)}$$

### 3.6.2 Approximation of Volume Integral.

The simplest second order accurate approximation is to replace the volume integral by the product of the mean value and the **CV** volume the former is approximated as follows[3]: -

$$Q_p = \iiint_{\Omega} q d\Omega = \bar{q} \Delta\Omega = q_p \Delta\Omega \qquad \text{...(3.22)}$$

$q_p$ is the value of variable at **CV** center. This quantity is easy to calculated since all variables are available at node **P**, no interpolation in necessary.

The above approximation becomes exact if **q** is either constant or varies linearly within **CV**; other wise, it contains a second order error.

### 3.6.3 Interpolation Practice.

The approximation to integrals required the values of variables at locations other than computational nodes (**CV** center).The integrand denoted in the previous sections, involves the product of several variables and or variable gradients at those locations $F^c = W_x \vec{W}.\vec{n}$ for connective flux and $F^d = \mu \nabla W_x.\vec{n}$ for diffusive flux . We assume that velocity field and fluid properties $\rho$ & $\mu$ are known at all locations, to calculate the connective and diffusive fluxes. The value of $W_x$ and its gradients normal to the cell face at one or more locations on the **CV** surface are needed. They have to be expressed in terms of the nodal values by interpolation the following interpolation are used in the present work are[3].

**a- Up Wind (UDS).**

Approximation of conserved quantity or property by its value at the node upstream of the variable locations. It's equivalents to using backward or forward difference approximation for the first derivatives depending on the flow directions.

Hence, the upwind difference scheme (**UDS**), $\Phi_e$ is approximation as:-

$$\phi_e = \begin{cases} \phi_E (\vec{W}.\vec{n}) > 0 \\ \phi_P (\vec{W}.\vec{n}) < 0 \end{cases} \qquad \text{...(3.23)}$$

This is the only approximation that satisfies the boundness criteria unconditionally i.e. it will never yield oscillatory solutions.

**b- Linear Interpolation (CDS).**

Another straight forward approximation for the value of **CV** face center is linear interpolation between the two nearest nodes. At locations **e, w, n, s** on Cartesian grid have (see Fig.(3.13))

$$\phi_e = \phi_E \cdot \lambda_e + \phi_p (1 - \lambda_e) \qquad \text{...(3.24)}$$

Where the linear interpolation factor $\lambda_e$ is defined as[3]

$$\lambda_e = \frac{|r_e - r_p|}{|r_E - r_p|} \qquad \text{...(3.25)}$$

**c- Deferred correction.**

Other schemes can be used in order to obtain higher order interpolation such as (**QUICK**) or use polynomial of three degree. Use of higher-order interpolation leads to large compositional molecules. (such as in fourth order polynomials each flux depend on the 15 nodal values.Its simple to calculate higher order flux approximation explicitly using values from previous iteration.

This approximation can be combined with an Implicit lower-order approximation, which uses only values at nearest neighbors, in the following way (first suggested by Khosla and Rubin 1974)

$$F_e = F_e^L + \left(F_e^H - F_e^L\right)^{old} \qquad \text{...(3.26)}$$

$F_e^L$ Stands for approximations by some lower-order scheme (**UDS**) and $F_e^H$ is the higher order approximation (**CDS**). The term in brackets evaluated using values from the previous iteration. It's indicated by superscript 'old'.

## 3.7 Pressure Correction Equation.

The linearized momentum Equations are solved with sequential solution method using the old mass fluxes and the pressure from previous iteration. This produces new velocity **Wx*** and **Wy*** which don't necessarily satisfy the continuity equations.

The descretization equation in the X-component has the following form.

$$A_P W_{X,P} + \sum_L A_L W_{X,L} = Q_{X,P} \quad L = E, W, N, S \qquad \ldots(3.27)$$

**P**: is the index of an arbitrary velocity node.

L: index denote of the neighbor points that appear in the discretized momentum equation.

The source term $Q_{X,P}$ contains the discretized pressure gradient term . Irrespective of how this term is approximated, one can write:-

$$Q_{X,P} = Q^*_{X,P} + Q^p_{X,P} = Q^*_{X,P} - \frac{\delta p}{\delta x} \qquad \ldots(3.28)$$

Due to the non-linearity and coupling of the underlying differential equation Eq(3.27) cannot be solved directly as the coefficients **A** and, possibly, the source term , depend on the unknown solution $W_{x,m+1}$ . Iterative is the only choice.

The iteration with one step , in which the coefficient and source matrices is updated is called outer iteration to distinguished them from the inner iteration performed on linear system with fixed coefficient on each outer iteration the equation solved is :-

$$A_P W^{m*}_{X,P} + \sum_L A_L W^{m*}_{X,L} = Q^{m-1}_{X,P} - \left(\frac{\delta p}{\delta x}\right)^{m-1}_p \Delta\Omega \qquad \ldots(3.29)$$

Where $W^m_x$ represents the current estimate of the solution and the term on the right side of Eq (3.29) are evaluated using the variable at the proceeding outer iteration .

The momentum equation is usually solved sequentially. i.e., the set of algebraic equation for each component of the momentum is solved in turn, treating the grid point's values of its dominant velocity component as the sole set of unknowns.

Since the pressure used in this iteration was obtained from the previous outer iteration, the velocities computed from Eq (3.27) don't normally satisfy the discretized continuity Equation. To enforce the continuity condition the velocities need to be corrected; this requires modification of the pressure field, the manner of doing this is described next.

The velocity at nod **P**, obtained by solving the linerized momentum Eq(3.27) can be formally expressed: -

$$W_{X,P}^{m*} = \frac{Q_{X,P}^{m-1} - \sum_{L} A_L W_{X,L}^{m*}}{A_P} - \frac{1}{A_P}\left(\frac{\delta p}{\delta x}\right)_p^{m-1} \qquad \text{...(3.30)}$$

As already stated, these velocities do not satisfy the continuity equation, so, $W_{X,P}^{m*}$ is not the final value of velocity for the iteration **m**; it is predicted value, which is why it carries on asterisk (*). The corrected final values should satisfy the continuity equation. For connivance the first term on the right hand side of Eq (3.30) $\tilde{W}_{X,P}^{m*}$ :-

$$W_{X,P}^{m*} = \tilde{W}_{X,P}^{m*} - \frac{1}{A_P}\left(\frac{\delta p}{\delta x}\right)_p^{m-1} \qquad \text{...(3.31)}$$

The velocity field $\tilde{W}_{X,P}^{m*}$ can be thought of as one from which the contribution of the pressure gradient has been removed. Because the method is implicitly. This is not the velocity that would be obtained by dropping the pressure gradient entirely from Eq (3.27).

The next task is to correct the velocities so that they satisfy the continuity equation.

$$\frac{\delta\left(\rho W_i^m\right)}{\delta X_i} = 0, \text{where } i = x, y \qquad \ldots(3.32)$$

This can be achieved by correcting the pressure field. The corrected velocity and pressure are linked by the equation.

$$W_{i,P}^{m*} = \tilde{W}_{i,P}^{m*} - \frac{1}{A_P}\left(\frac{\delta p}{\delta x_i}\right)_p^{m-1} \qquad \ldots(3.33)$$

Continuity is now enforced by inserting this expression for $W_{i,m}$ in to the continuity Eq (3.32) to yield a discrete Poisson equation for the pressure.

$$\frac{\delta}{\delta X_i}\left[\frac{\rho}{A_p^{Wi}}\left(\frac{\delta p}{\delta x_i}\right)_p^m\right] = \left[\frac{\delta\left(\rho \tilde{W}_i^{m*}\right)}{\delta X_i}\right], \text{where } i = x, y \qquad \ldots(3.34)$$

After solving the Poisson equation for pressure Eq (3.34) the final velocity field at a new iteration $W_i^m$ is calculated from Eq (3.33). At this point we have a velocity field which satisfies the continuity condition, but the velocity and pressure field do not satisfy the momentum Eq (3.29), we begin another outer iteration and the process is continued until a velocity field which satisfies both the momentum and continuity equation is obtained.

One of the most common methods of this type is a pressure – correcting method which is used instead of the actual pressure. The velocities computed from the linearized momentum equations and the pressure $P^{m-1}$ is taken as provisional values to which a small correction must be added[3].

$$W_i^m = W_i^{m*} + W' \qquad \ldots(3.35)$$

$$p^m = p^{m*} + p' \qquad \ldots(3.36)$$

## 3.8 Implementation of Boundary Condition.

Each **CV** provides one algebraic equation .Volume integrals are calculated in the same way for every **CV**, but fluxes through **CV** faces coinciding with the domain boundary require special treatment, these boundary fluxes must either be known or be expressed as a combination of interior values and boundary data, the following boundary condition is used in the present work.

**a. Inlet Boundary**: -

The values of pressure and velocity aren't constant in the inlet boundary because of complexity in the flow hence it's required an experimental data for velocity and pressure, but this data isn't gain therefore prescribed velocity & pressure in the inlet.

**b. Wall Boundary: -**

Because of the damping effect of the wall the transport equation for the turbulence quantities ($\mathbf{k-\varepsilon}$ ) does not apply closed to the wall one way of dealing with this with this problem is to add extra source term to the transport equations for ($\mathbf{k-\varepsilon}$), constant shear wall be assumed through that wall region, i.e. $\tau_p \approx \tau_w$ within the laminar sub layer region i.e. $y^+_p \leq 11.63$

$$y_p^+ = \frac{u_\tau\, y_p}{\nu}\ , \qquad \text{…(3.37)}$$

$$u_\tau = \sqrt{\frac{\tau_w}{\rho}} \qquad \text{…(3.38)}$$

at a grid point when $y^+_p \geq 11.63$ turbulent shear become significant and where the generation and dissipation of kinetic energy of turbulence are in balance then

$$\tau_p = C_\mu\, k^{0.5} \qquad \text{…(3.39)}$$

and the following boundary condition layer expansion for momentum fluxes may be used

$$u_p^+ = \frac{1}{K} LN(E y_p^+) \quad \text{...(3.40)}$$

**K** = Karman's constant equal 0.418

### c. Out Let Boundary: -

Actually the value of pressure is not constant in the exit, but there is no experimental data therefore a prescribed pressure in the exit is assumed.

## 3.9 The Algebraic Equation System.

The summing of all the flux approximation's and source term produce an algebraic equation which relates the variable value at the center of that **CV** to the values of at several neighbor (**CVs**).

The number of equations and unknowns must be equal i.e. there has to be one equation for each **CV** thus, have a large set of linear equation which must be solved numerically. This system is sparse (meaning that each equation only contains a few unknowns) the system can be written in a matrix notation as follows: -

$$A\Phi = Q \quad \text{...(3.41)}$$

Where $A$ is square sparse coefficient matrix, $\Phi$ is a vector (or column matrix) containing the variables at the **CV** nodes and $Q$ is the vector containing the source term in the linearized equation.

The linearized algebraic equation in two dimensions is written in the form.

$$A_{L,L-N_J}\Phi_{L-N_J} + A_{L,L-1}\Phi_{L-1} + A_{L,L}\Phi_L + A_{L,L+1}\Phi_{L+1} + A_{L,L+N_J}\Phi_{L+N_J} = Q_L \quad \text{...(3.42)}$$

For two dimensions the equation has five-point computation molecules, the variables are normally stored in computers in one dimensional array .The conversion between nodal locations compass notation, and storage location, the following table shows how convert the nodal storage Fig.(3.14).

| Node location | Compass notation | Storage location |
|---|---|---|
| i,j | P | L=( i -1) $N_J$ +J |
| i-1,j | W | L- $N_J$ |
| i,j-1 | S | L-1 |
| i,j+1 | N | L+1 |
| i+1,j | E | L+ $N_J$ |

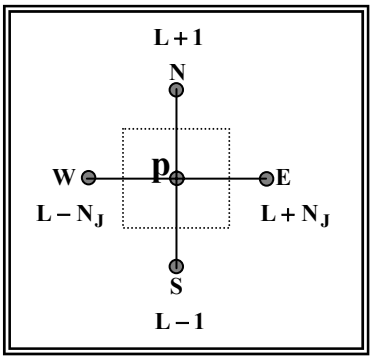


**Fig.(3.14) figure shows conversion between nodal locations compass notation ,and storage location .**

With this ordering points each node is identified with an index **L** ,which is also the relative storage location ,in this notation the equation above can be written in matrix form (if $(5\times5)$ nodal point) .

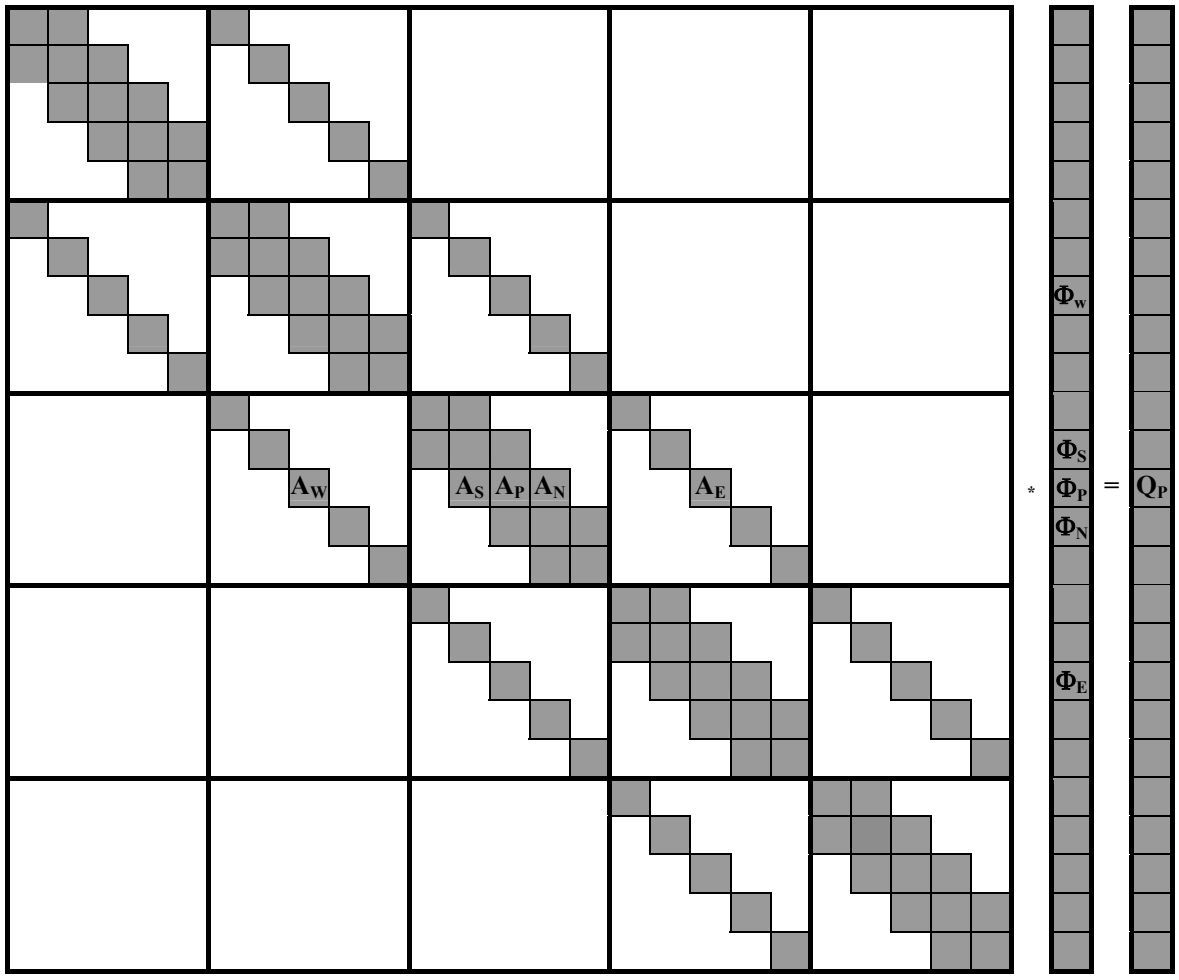


**Fig.(3.15) Figure shows the arrangement of coefficient in the matrix**

$$A_W \Phi_W + A_S \Phi_S + A_P \Phi_P + A_N \Phi_N + A_E \Phi_E = Q_P \quad \text{...(3.43)}$$

Where the index **L**, which indicated rows in Eq. (3.42) is understood, and the index indicating column or location in the vector has been replaced by the corresponding letter [**5**].

## 3.10 Solution of Algebraic Equation.

The method used for solving algebraic equation is called **LU** decomposition techniques [**28**]. The primary appeal of **LU** decomposition is that the time consuming elimination step can be formulated so that it involves only operation on the matrix of coefficient, **[A]**. In this situation where right hand side vector **{B}** is evaluated for single value of **[A]**. In this way focus on the Gauss elimination method to implement as **LU** decomposition.

The Gauss elimination involves two steps: forward elimination and back–substitution. **LU** decomposition method separates the time consuming elimination of the matrix **[A]**from the manipulation of right hand **{B}**. Thus, once **[A]** has been "decomposed "multiple right hand side vectors can be evaluated in an efficient manner.

Interestingly, Gauss elimination itself can be expressed as **LU** decomposition before showing how this can be done, let's first provides another overview of the decomposed strategy.

Algebraic equation (3.29) can be rearranged to give:

$$[A]\{\Phi\} - \{Q_p\} = 0 \quad \text{...(3.44)}$$

Suppose that Eq. (3.44) could be expressed as an upper triangular system.

$$\begin{bmatrix} u_{11} & u_{12} & u_{13} \\ 0 & u_{22} & u_{23} \\ 0 & 0 & u_{33} \end{bmatrix} \begin{Bmatrix} \Phi_1 \\ \Phi_2 \\ \Phi_3 \end{Bmatrix} = \begin{Bmatrix} d_1 \\ d_2 \\ d_3 \end{Bmatrix} \quad \text{...(3.40)}$$

Recognize that this is similar, the manipulation that occurs in the first step of Gauss elimination, that is, elimination is used to reduce the system to upper triangular form Eq(3.45) can be also expressed in matrix notation and rearranged to give: -

$$[U]\{\Phi\} - \{D\} = 0 \qquad \text{…(3.46)}$$

Now assume that there is a lower diagonal matrix with 1's on the diagonal.

$$[L] = \begin{bmatrix} 1 & & \\ L_{21} & 1 & \\ L_{31} & L_{32} & 1 \end{bmatrix} \qquad \text{…(3.47)}$$

That has a property when Eq (3.46) is pre multiplied by Eq (3.47) is the result.

$$[L]\{[U]\{\phi\} - \{D\}\} = [A]\{\phi\} - \{Q_p\}$$

If this equation holed, it follows from the rules for matrix multiplication

$$[L][U] = [A] \qquad \text{…(3.48)}$$

And

$$[L][D] = \{Q_p\} \qquad \text{…(3.49)}$$

At two steps strategy (see Fig. (3.16)) for obtaining solution can be used an Eq. (3.51)

- **LU** decomposition step: **[A]** is factored or decomposed into lower **[L]**and upper **[U]** triangular matrix.
- Substitution step: **[L]** and **[U]** are used to determine a solution of a vector $\{\Phi\}$ for right hand side $\{\mathbf{Q_P}\}$. This step itself consists of two steps: first Eq. (3.49) is used to generate an intermediate vector {D} forward substitution. Then the results are substitute in Eq. (3.46) which can be solved by back substitution for $\{\Phi\}$.

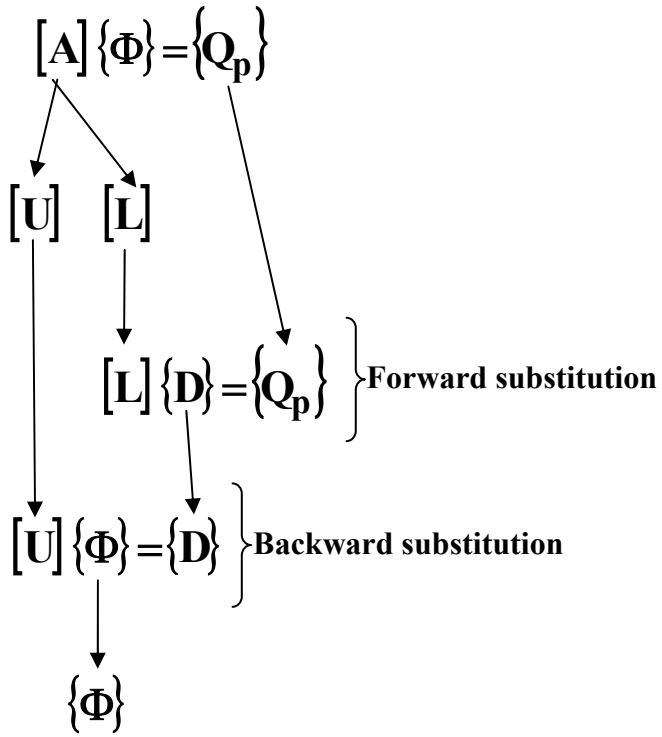


**Fig. (3.14) Figure shows the steps of solution of algebraic equation.**

## 3.11 SIMPLE algorithm for a colocated variable arrangement.

The solution algorithm for this class of method can be summarized as follows[7]:-

1. Start calculation field with guess values of pressure and velocity at all nodes .
2. Assemble and solve the linearized algebraic equation system for velocity components (momentum equations) to obtain $\mathbf{W_i}^*$.
3. Assemble and solve the pressure-correction equation to obtain $\mathbf{p'}$.
4. Correct the velocities and pressure to obtain the velocity field $\mathbf{W_i}^{\mathbf{m}}$ which is satisfies continuity equation and the new pressure.
5. Return step 2 and repeat, using $\mathbf{W_i}^{\mathbf{m}}$ and $\mathbf{p}^{\mathbf{m}}$ as improved estimates for $\mathbf{W_i}^{\mathbf{m+1}}$ and $\mathbf{p}^{\mathbf{m+1}}$, until all correction is negligible small.

## 3.12 Computer program:-

### a. First program (Calculation of Impeller dimension and grid generation).

The input parameter of the first program (**Q, N, H**) from these values we compute the value of blade angle in the outlet and the number of impeller and the value of the design factor (speed constant, capacity constant, and diameter ratio) (Fig.(3.6),Fig.(3.7), Fig.(3.8), Fig.(3.9), Fig.(3.10)). From these figures the dimensions of impeller were computed and then apply point by point method for developing of impeller shape and the mesh is generated between two blades (boundary fitted mesh), boundary condition and slip losses and pressure in the inlet and the outlet are specified. These results are printed in the output file in order to read these results from the second program. The flow chart explained the previous procedure Fig. (3.15).

### b. Second program(solve the equation of motion).

This program incorporates the **FV** method using **SIMPLE** algorithm on colocated body fitted grids **[7]**, the procedure of solution is shown in Fig.(3.16).

Firstly read data from first program and compute coordinate of **CV** center, components of normal vector, indices of boundary condition and all sides of **CV**.

After reading the data from previous program guess the initial values of velocity component and pressure for all **CV** center and specify boundary condition, then starting with iteration cycle.

Firstly, assemble and solve (**Wx,Wy**,p) equations with **LU** decomposition ,then assemble and solve **(k,ε)** equations with **LU** decomposition ,if the errors don't reach to acceptable value the velocity and pressure are corrected and restart the iteration until reach to acceptable value(1.0e-3).

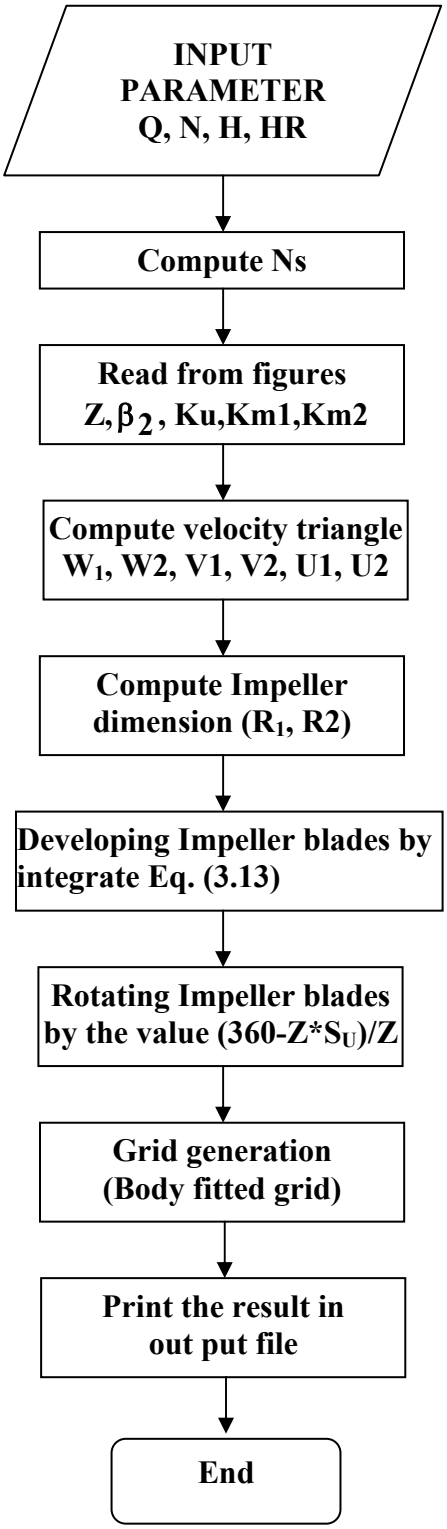


**Fig.(3.15) flow chart of first program**

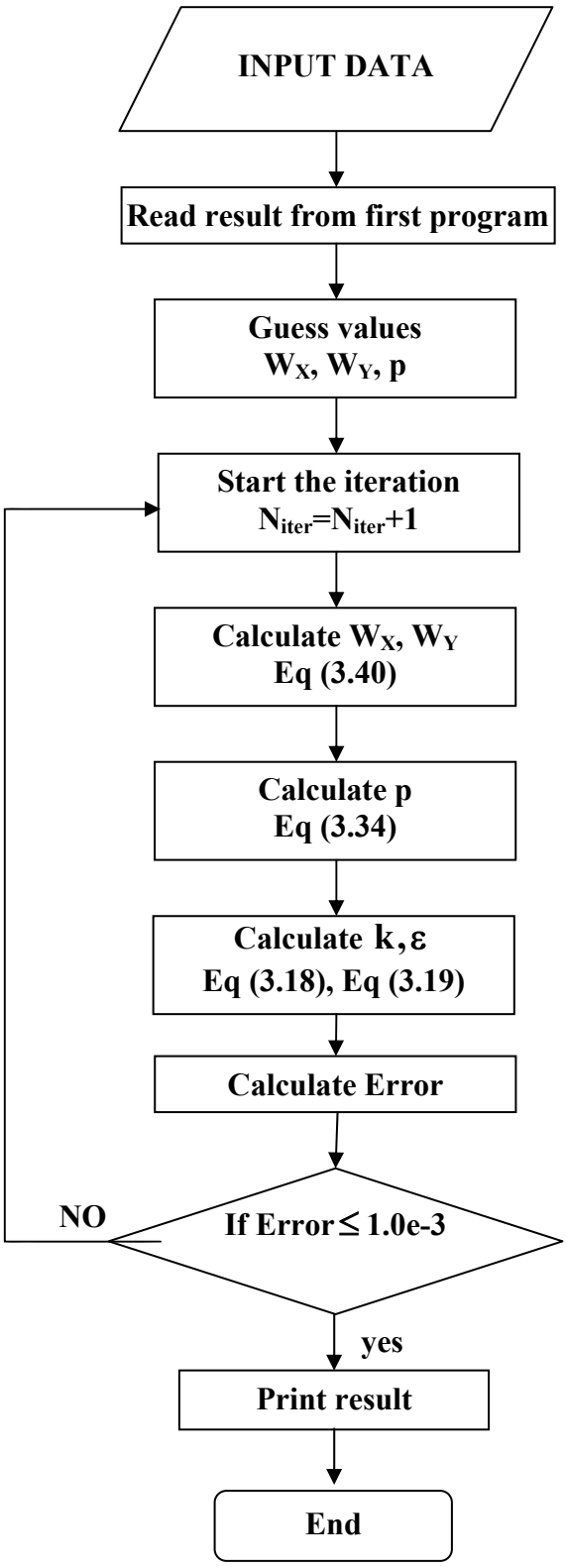


**Fig.(3.١٦) Flow chart of second program.**

# Chapter Four

# Results and Discussion

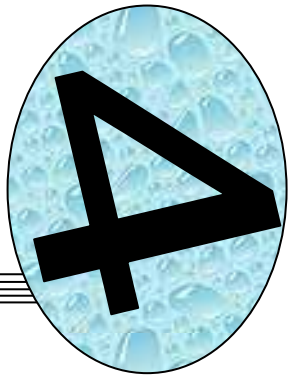


## 4.1 **Introduction:** -

The results in the figures were analyzed for two centrifugal pump impellers, the first one is developed by design factor and the second is taken from the reference [29].

The input variables are for first pump (Q=0.132458 $m^3$/sec, N=3600 rpm, H=137.16 m), second pump (**Q**=0.00387 $m^3$/sec, **N**=150 rpm, **H**=0.8199 m). These values were taken in order to show the reliability of program to solve the equations for different size and shape of the impeller.

## 4.2 Result and discussion: -

Tables (4.1) and (4.2) show the values of relative, radial (meridonal) velocity and points on the blade surface. These results represent the analysis of one dimensional theory of centrifugal pump with aid of experimental and theoretical chart (Fig.(3.6),(3.7),(3.8),(3.9) and (3.10)). The values of inlet and outlet diameter and blade angle ($r_1$=69.02 mm, $r_2$=147.71 mm, $b_1$=21°, $b_2$=25°), ($r_1$=107.9 mm, r2=241.3 mm, $b_1$=16°, $b_2$=23° for the second Impeller). The points on the blade surface were obtained by numerical solution to the integral equation (eq (3.13)).

There was an assumption that the change of relative radial velocity linearly.

The Figs.(4.1) and (4.2) were the plot of the change of radial velocity, blade angle and relative velocity, the curve of radial velocity is linear for the first impeller, this assumption is important to make the length of impeller as small as possible (decrease the area of friction), the relative velocity decreases parabolic

and it's values depend on the blade angle and radial velocity. in Fig.(4.2) the behavior of the radial velocity approximately linear (parabolic) that is mean the length of blade higher than the first impeller.

Fig (4.3) and (4.4) generated a **2D** grid, this type of grid is body fitted grid (21 × 51) lines, the lines spacing are decreased near the wall boundary in order to treatment of sudden change in properties.

In the Fig (4.5) , Fig (4.6) , Fig (4.7) and Fig (4.8) results of flow analysis, shows the percentage of error and the number of Iteration. the percentage of error is decrease until reach $10^{-3}$ and the number of outer iteration in to impeller(1) is 75, and for the second impeller is 83, we show that the behavior of the curves **($W_x$ , $W_y$ , k , ε )** is smooth but the curve of pressure is not smooth and irregular until reach the acceptable value, this irregular shape occur because of higher value of pressure reaches.

Fig (4.9) and (4.10) show the values of relative radial velocity near the **PS** and **SS,** these values decrease near the wall boundary because of laminar boundary layer effect, the relative radial velocity in **SS** is higher than the relative radial velocity in **PS** and for the values of radial velocity decrease with radial direction. In **SS** the relative radial velocity increases firstly then decreases, this is due to uniform velocity assumption in the inlet and due to curvature of the blades that reduce the centrifugal action on the absolute radial velocity (as the absolute velocity increases the relative velocity decrease).

In the Impeller(2) the relative radial velocity increases with radial direction, The value of relative radial velocity in **PS** decreases then increases that means flow reverse in this direction that means a relative circulation may be occur in this region, the effect of this reverse flow is considered as a stagnation point (contraction in flow) hence, this lead to make the relative velocity increases in **SS**.

Fig.(4.11) and (4.12) a relative tangential velocity with respect to radial direction in which the absolute value of relative tangential velocity in **SS** higher

than the absolute values of relate tangential velocity at **PS** because the minus sign refers to the direction of the flow. Hence, the absolute values of relative tangential velocity decreases with radial direction and for second impeller we see that the values of relative tangential velocity decreases until approaches to zero then a positive value, this occur because of reverse flow.

Figs.(4.13) and (4.14) presents the values of static pressure in **PS** less than the pressure in **SS** near the inlet and some values close to zero in **PS** ,these values are not expected ,This occurs because of uniform velocity assumption in the inlet boundary and due to incompressibility (single phase), and it is seen that the pressure difference between two sides in Impeller (1) is higher than the second impeller because of high head delivered , and the value of pressure at the exit close to same value because of the pressure is constant in the exit (outlet boundary condition).

Fig.(4.15) and (4.16) show that the relative radial velocity between two blades at different diameter ratio(68%, 83%,98%)it is seen that the values of radial velocity are increased in the **SS** and decreases in the **PS** and the value of radial velocity decreases in radial direction because of the increases of the absolute velocity ,but in Impeller (2) (Fig.(4.16)) the behavior of the second and third diameter ratio (83%, 98%) differ from the behavior of the first impeller this occurs because of the reveres flow.

Figs.(4.17) and (4.18) obtained the absolute values of relative tangential velocity values at **SS** higher than the absolute values of relative tangential velocity at **PS** , the negative values refer to the direction of flow. But Fig.(4.18) at ($\mathbf{r/r_2 = 0.68}$) show that the absolute values of relative tangential velocity decreases until reach to zero then this phenomenon (relative circulation) cause the small change in relative tangential velocity in third position ($\mathbf{r/r_2 = 0.98}$).

Figs.(4.19) and (4.20) show the values of pressure at constant radius for different positions in which the values of pressure in **PS** higher than the pressure in **SS** and the relation is approximately linear and it's confirm the invicid

solution of radial bladed in which the relation between pressure gradient and coriolis force $-\frac{1}{\rho r}\frac{\partial p}{\partial \theta} = 2\omega W$ [**21**]. The value of pressure increases in radial direction, the different of pressure between two sides in the first impeller higher than the second impeller, because of higher Angular velocity of a first impeller.

Figs.(4.21) and (4.22) show a couture plot of relative velocity in the impellers in which a dark position is seen , the values of relative velocity decreases until reach to zero(impeller (2)), zero velocity position represents stagnation point that is make a contract into flow and causes increasing of relative velocity in the other side, and there is white region near the inlet in **SS** the values of relative flow velocity are high this occur because of there is a two force exerted in side the impeller the first is centrifugal force and the second is the coriolis force the direction of two forces are approximately normal to the wall (at **SS**) this mean that the value of absolute velocity is very low (the relative velocity is high).

Figs.(4.23) and (4.24) shown pressure surface between two blades, there is dark lines represent lines of equal pressure, and a smooth increment with radial direction.

Figs.(4.25) and (4.26) presented vector plot of the impellers all the previous results can be concluded from them, and it is seen a relative circulation near the exit in **PS** and stagnation region before it in impeller (2).

Figs.(4.27) and (4.28) it is shown slip along radial direction, slip factor is tangential components of absolute velocity corresponding to the out let angle without slip to the same velocity with slip, slip factor is computed at the mid tangential position in the impeller ,it is a measure of deviation from blade angle, the value of slip firstly more than **1** then decreases until reach **0.85** in the exit . But in the second impeller the shape of curve is deformed this occur because of existence of stagnation region and relative circulation.

Fig. (4.29) and (4.30) it is shown the values of turbulent kinetic energy (**k**),the values of **k** proportional with the fluctuated component of velocity in the

inlet the values of relative velocity is very high (high Reynolds number) and the boundary condition is constant in the inlet that is make the value of **k** is high then decreases through radial direction and increase in the exit because of uniform pressure, in the second impeller it is seen that the value of **k** decreases in the **PS** and decreases in the **SS** because of velocity difference **.**

Fig. (4.31) and (4.32) it is shown a couture plot of the kinetic energy dissipation ( $\varepsilon$ ) the value of $\varepsilon$ depend on the value of **k** and mixing length $\mathbf{L_m}$ Eq(3.16) ,the mixing length proportional with distance from wall hence it was seen that the value of $\varepsilon$ is very high in the inlet at **PS** (higher value of **k** ) and near the exit and near the wall boundary (small distance ).

**Table (4-1) The values of relative, meridonal velocity and coordinate of blade IMPELLER (1)).**

| POINT | R (mm) | Vr(m/sec) | W(m/sec) | $\theta$ (deg) | X(mm) | Y(mm) |
|---|---|---|---|---|---|---|
| 1 | 69.198 | 8.632 | 24.18 | 120 | -34.599 | 59.928 |
| 2 | 73.331 | 8.526 | 23.306 | 111.417 | -26.777 | 68.267 |
| 3 | 77.463 | 8.42 | 22.479 | 103.527 | -18.118 | 75.314 |
| 4 | 81.595 | 8.313 | 21.699 | 96.246 | -8.877 | 81.111 |
| 5 | 85.727 | 8.207 | 20.967 | 89.501 | 0.746 | 85.724 |
| 6 | 89.86 | 8.101 | 20.282 | 83.232 | 10.591 | 89.233 |
| 7 | 93.992 | 7.995 | 19.644 | 77.381 | 20.534 | 91.721 |
| 8 | 98.124 | 7.889 | 19.054 | 71.902 | 30.482 | 93.269 |
| 9 | 102.256 | 7.783 | 18.51 | 66.751 | 40.363 | 93.953 |
| 10 | 106.388 | 7.676 | 18.014 | 61.891 | 50.125 | 93.84 |
| 11 | 110.521 | 7.57 | 17.565 | 57.286 | 59.731 | 92.99 |
| 12 | 114.653 | 7.464 | 17.164 | 52.905 | 69.151 | 91.452 |
| 13 | 118.785 | 7.358 | 16.81 | 48.72 | 78.367 | 89.267 |
| 14 | 122.917 | 7.252 | 16.503 | 44.704 | 87.363 | 86.466 |
| 15 | 127.05 | 7.146 | 16.243 | 40.834 | 96.127 | 83.074 |
| 16 | 131.182 | 7.04 | 16.03 | 37.086 | 104.648 | 79.104 |
| 17 | 135.314 | 6.933 | 15.865 | 33.439 | 112.916 | 74.564 |
| 18 | 139.446 | 6.827 | 15.747 | 29.874 | 120.917 | 69.457 |
| 19 | 143.578 | 6.721 | 15.676 | 26.372 | 128.636 | 63.778 |
| 20 | 147.711 | 6.615 | 15.652 | 22.916 | 136.053 | 57.517 |

| Table (4-2) The values of relative , meridonal velocity and coordinate of blade (IMPELLER (2)) | | | | | | |
|---|---|---|---|---|---|---|
| No | R(mm) | Vr(m/sec) | W(m/sec) | θ (deg) | X(mm) | Y(mm) |
| 1 | 107.9 | ١,٠٦٢٢٥٧ | ٤,١٠٤٢٤ | 139.6236 | -8.21988 | 6.98983 |
| 2 | 112.5 | ١,٠١٨٨٢٢ | ٣,٩٣٦٤٢ | 131.534 | -7.45948 | 8.42133 |
| 3 | 117.1 | ٠,٩٧٨٨٠٢ | ٣,٧٨١٧٩ | 123.7033 | -6.49779 | 9.74181 |
| 4 | 121.7 | ٠,٩٤١٨٠٣ | ٣,٦٣٨٨٥ | 116.1459 | -5.36281 | 10.92471 |
| 5 | 126.3 | ٠,٩٠٧٥٠٢ | ٣,٥٠٦٣١ | 108.8739 | -4.08563 | 11.95092 |
| 6 | 130.9 | ٠,٨٧٥٦١١ | ٣,٣٨٣١٠ | 101.8975 | -2.69864 | 12.8088 |
| 7 | 135.5 | ٠,٨٤٥٨٨٥ | ٣,٢٦٨٢٥ | 95.22442 | -1.23382 | 13.49371 |
| 8 | 140.1 | ٠,٨١٨١١٢ | ٣,١٦٠٩٤ | 88.86056 | 0.2786 | 14.00723 |
| 9 | 144.7 | ٠,٧٩٢١٠٤ | ٣,٠٦٠٤٥ | 82.80943 | 1.81121 | 14.3562 |
| 10 | 149.3 | ٠,٧٦٧٦٩٩ | ٢,٩٦٦١٦ | 77.07246 | 3.34012 | 14.55158 |
| 11 | 153.9 | ٠,٧٤٤٧٥٣ | ٢,٨٧٧٥٠ | 71.64889 | 4.84538 | 14.60734 |
| 12 | 158.5 | ٠,٧٢٣١٣٨ | ٢,٧٩٣٩٩ | 66.53582 | 6.31108 | 14.53935 |
| 13 | 163.1 | ٠,٧٠٢٧٤٣ | ٢,٧١٥١٩ | 61.72821 | 7.72531 | 14.36439 |
| 14 | 167.7 | ٠,٦٨٣٤٦٧ | ٢,٦٤٠٧١ | 57.2188 | 9.07982 | 14.09928 |
| 15 | 172.3 | ٠,٦٦٥٢٢٠ | ٢,٥٧٠٢١ | 52.99827 | 10.36969 | 13.76018 |
| 16 | 176.9 | ٠,٦٤٧٩٢٢ | ٢,٥٠٣٣٨ | 49.05502 | 11.59286 | 13.36195 |
| 17 | 181.5 | ٠,٦٣١٥٠١ | ٢,٤٣٩٩٣ | 45.37539 | 12.74963 | 12.9178 |
| 18 | 186.1 | ٠,٦١٥٨٩٢ | ٢,٣٧٩٦٢ | 41.9435 | 13.8422 | 12.43888 |
| 19 | 190.7 | ٠,٦٠١٠٣٥ | ٢,٣٢٢٢٢ | 38.74132 | 14.8742 | 11.93411 |
| 20 | 195.3 | ٠,٥٨٦٨٧٩ | ٢,٢٦٧٥٢ | 35.74871 | 15.8503 | 11.41004 |
| 21 | 199.9 | ٠,٥٧٣٣٧٤ | ٢,٢١٥٣٤ | 32.94329 | 16.77579 | 10.87073 |
| 22 | 204.5 | ٠,٥٦٠٤٧٦ | ٢,١٦٥٥١ | 30.30059 | 17.65633 | 10.31777 |
| 23 | 209.1 | ٠,٥٤٨١٤٦ | ٢,١١٧٨٧ | 27.79394 | 18.49762 | 9.75019 |
| 24 | 213.7 | ٠,٥٣٦٣٤٧ | ٢,٠٧٢٢٨ | 25.39453 | 19.30515 | 9.1645 |
| 25 | 218.3 | ٠,٥٢٥٠٤٥ | ٢,٠٢٨٦٢ | 23.07137 | 20.08398 | 8.55469 |
| 26 | 222.9 | ٠,٥١٤٢١٠ | ١,٩٨٦٧٥ | 20.79135 | 20.83846 | 7.91219 |
| 27 | 227.5 | ٠,٥٠٣٨١٣ | ١,٩٤٦٥٨ | 18.51915 | 21.57195 | 7.22589 |
| 28 | 232.1 | ٠,٤٩٣٨٢٨ | ١,٩٠٨٠٠ | 16.21733 | 22.28646 | 6.48212 |
| 29 | 236.7 | ٠,٤٨٤٢٣١ | ١,٨٧٠٩٢ | 13.84626 | 22.98218 | 5.66464 |
| 30 | 241.3 | ٠,٤٧٥ | ١,٨٣٥٢٥ | 11.36418 | 23.65692 | 4.75468 |

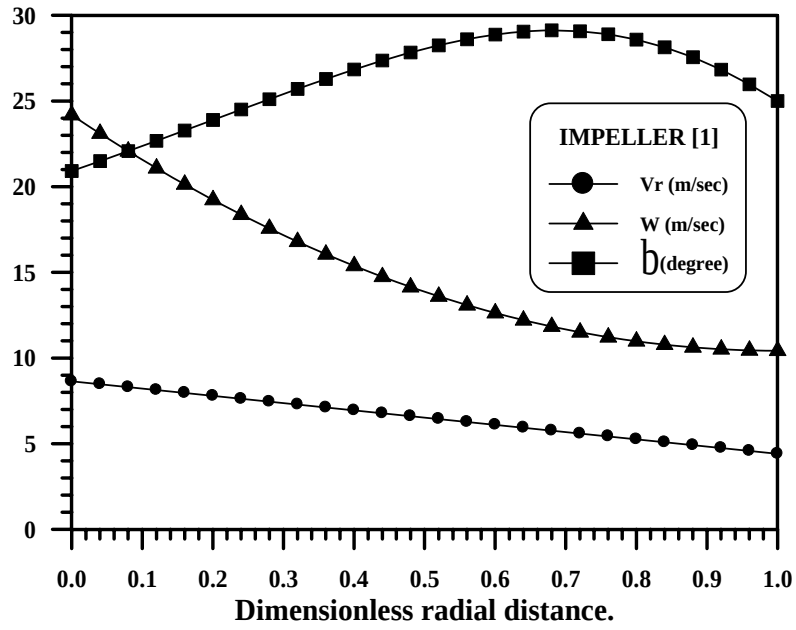


**Fig. (4.1)The variation of relative, meridonal velocity and blade angle with radial distance.**

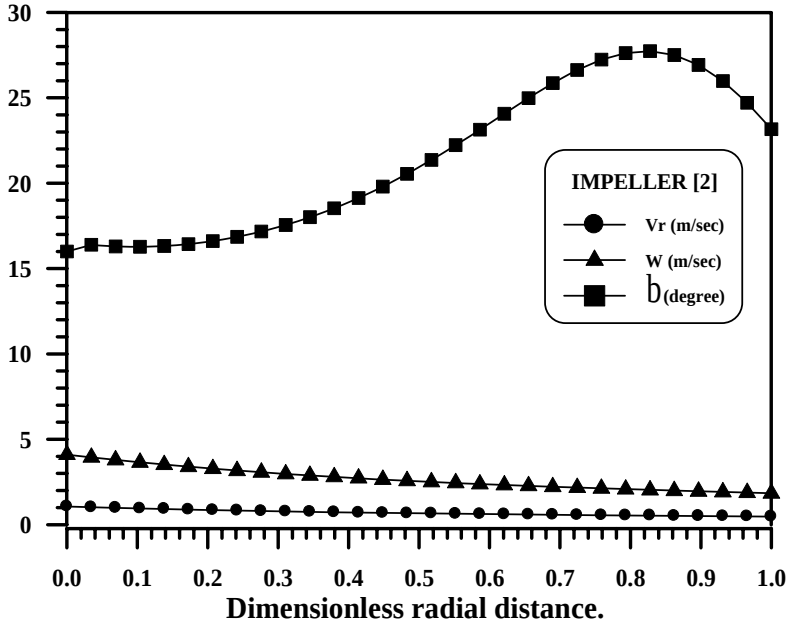


**Fig. (4.٣) The variation of relative, meridonal velocity and blade angle with radial distance.**

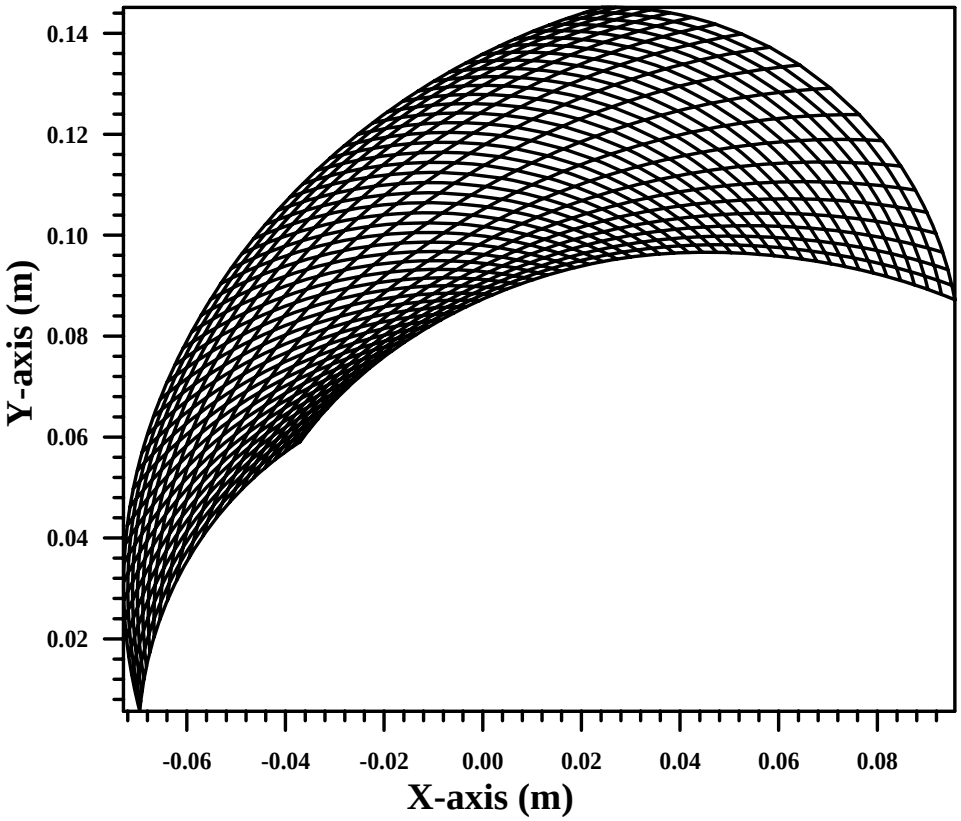


**Fig. (4.3) 2D body fitted grid generation (IMPELLER[1]).**

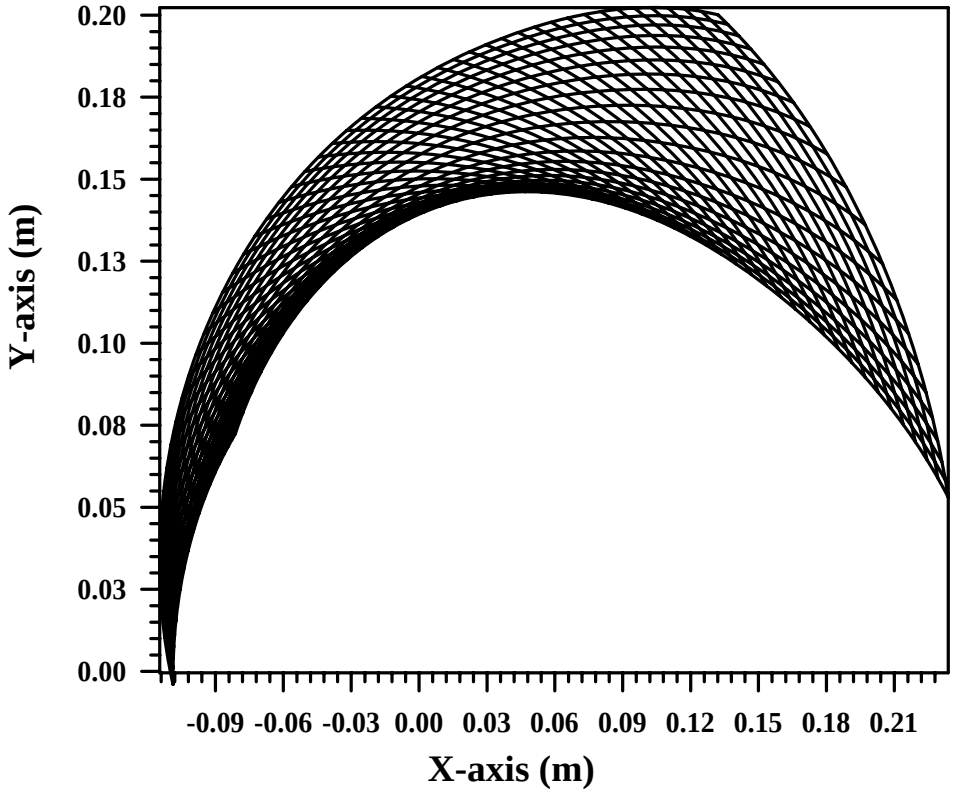


**Fig. (4.4) 2D body fitted grid generation (IMPELLER [2]).**

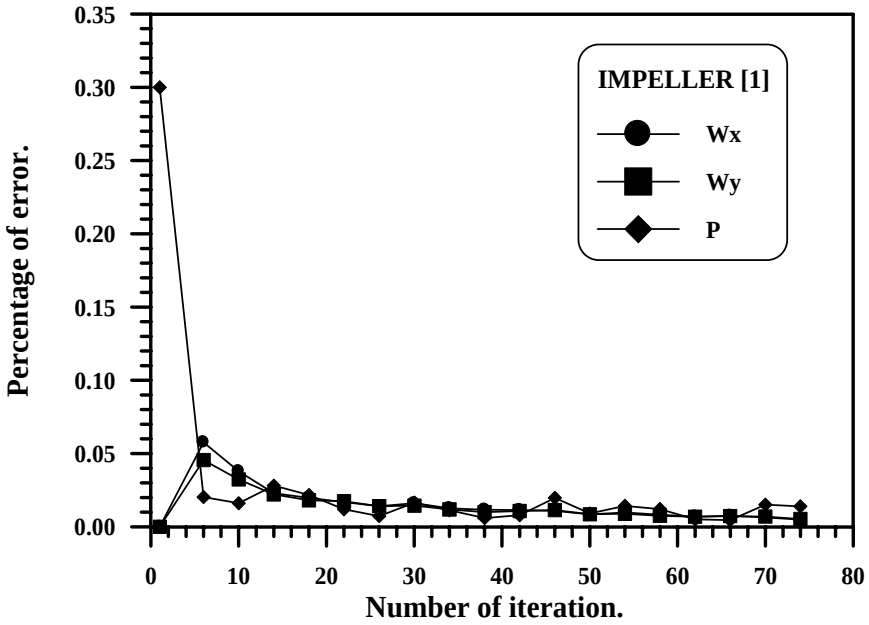


Fig.(4.5) The variation of percentage of error with number of iteration.

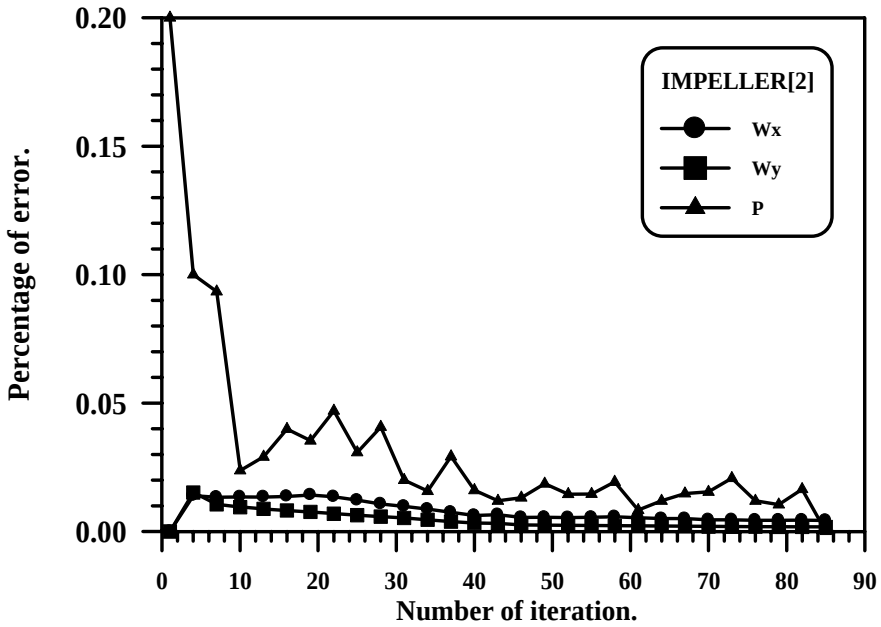


Fig.(4.6) The variation of percentage of error with number of iteration.

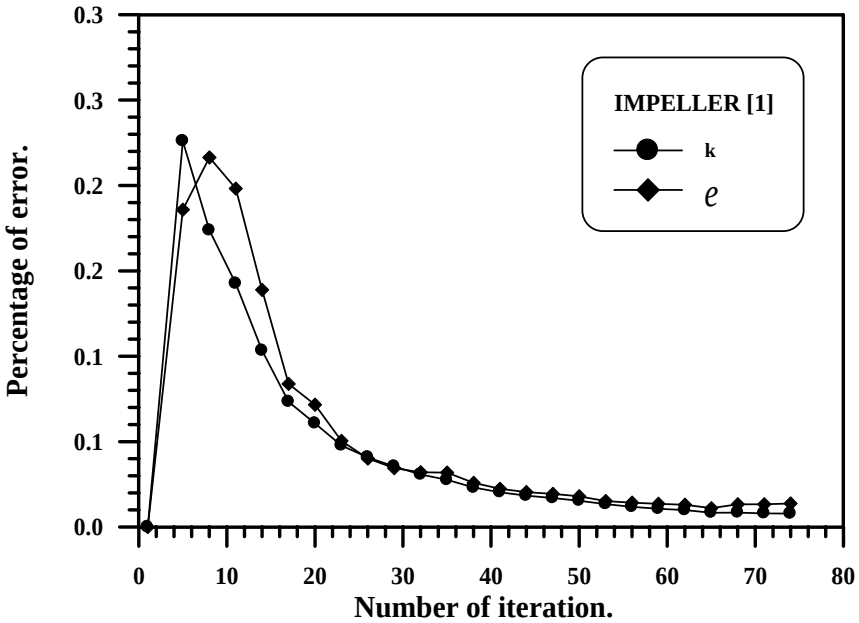


Fig.(4.7) The variation of percentage of error with number of iteration.

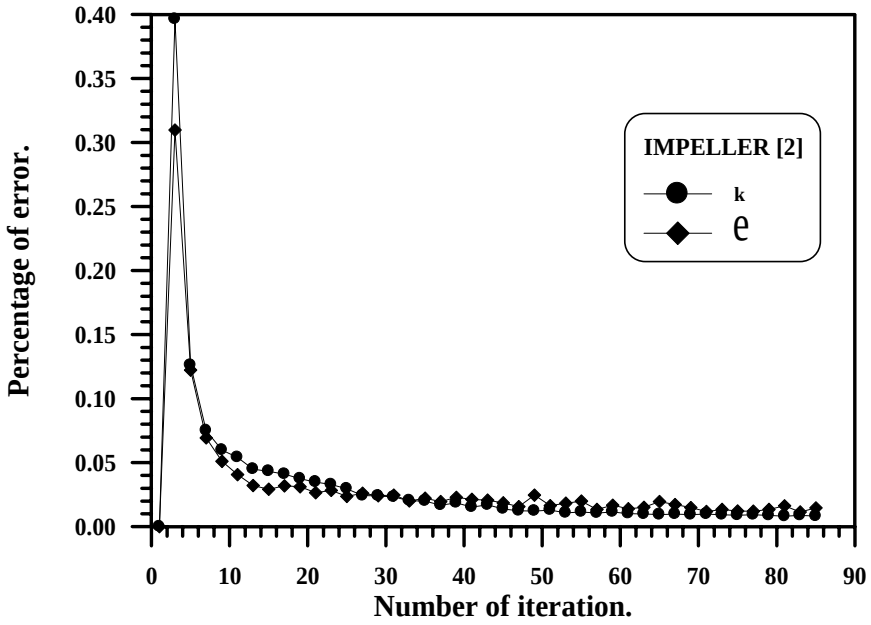


Fig.(4.8) The variation of percentage of error with number of iteration.

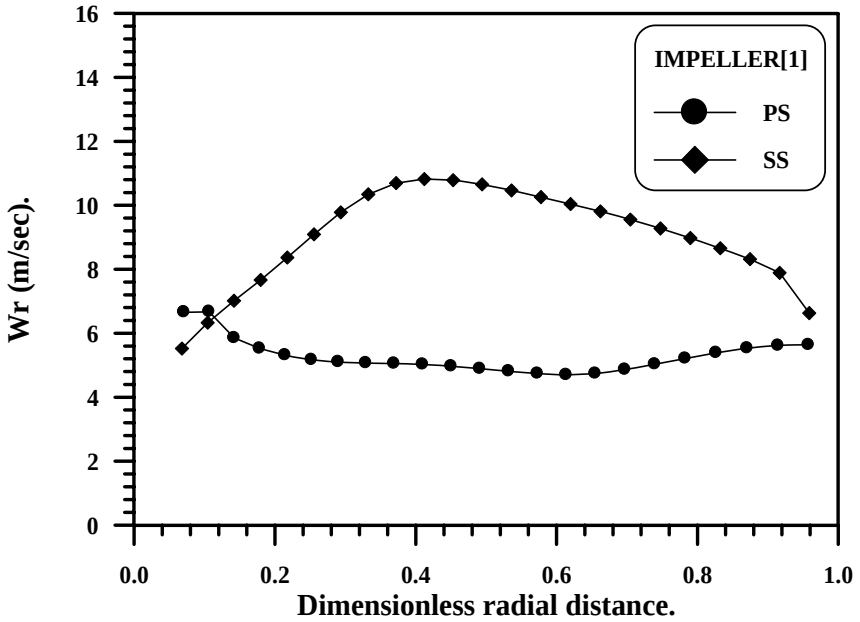


**Fig.(4.9) The variation of radial relative velocity with radial distance.**

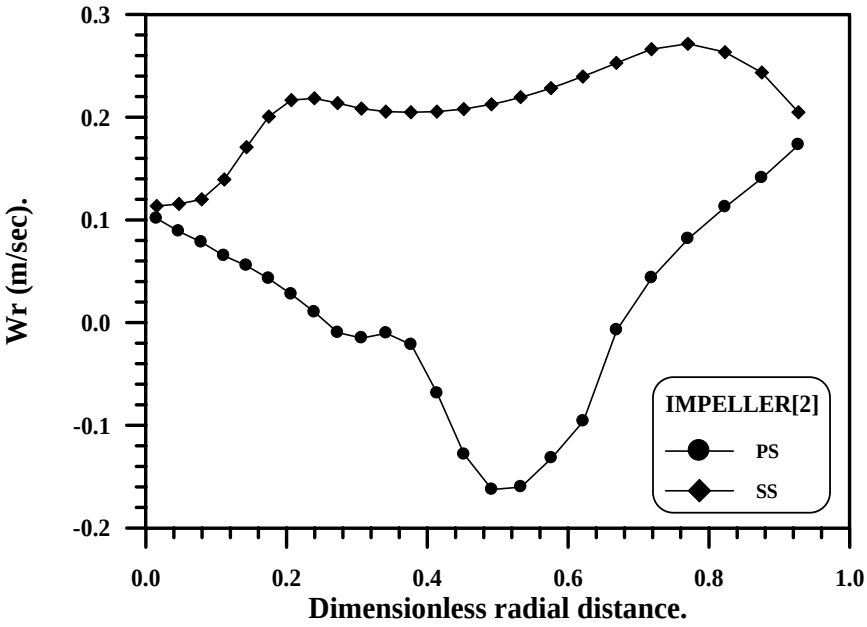


**Fig.(4.10) The variation of radial relative velocity with radial distance.**

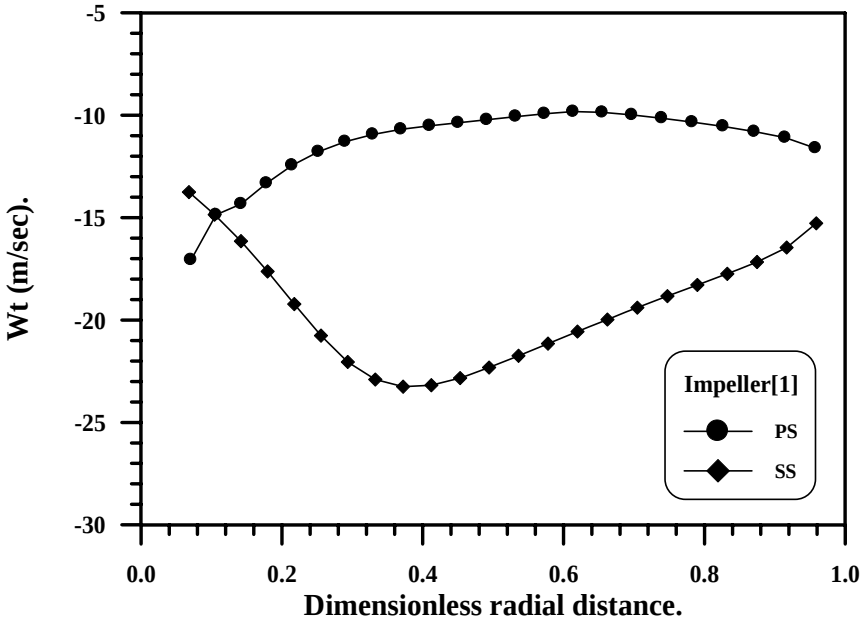


**Fig. (4.11) The variation of tangential relative velocity with radial distance.**

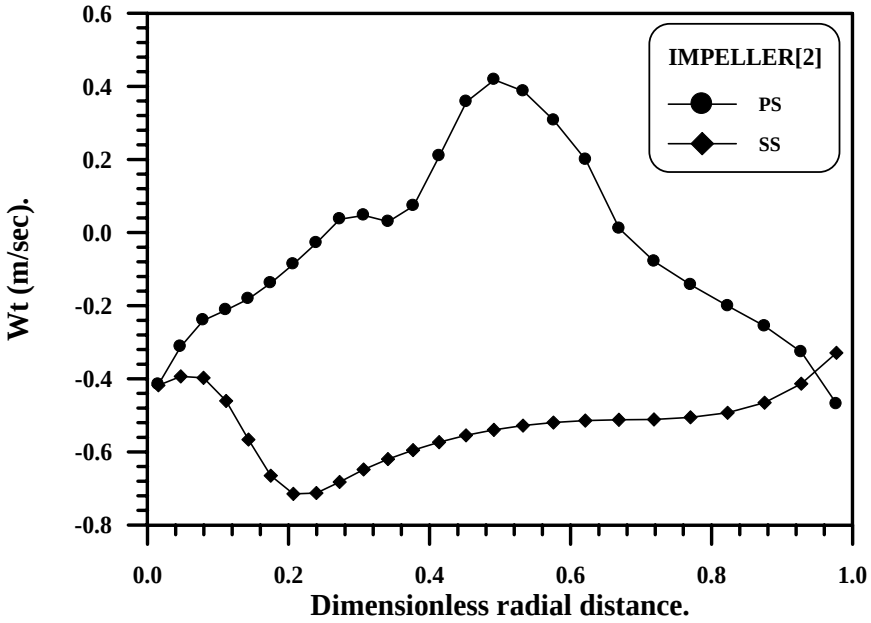


**Fig. (4.12) The variation of tangential relative velocity with radial distance.**

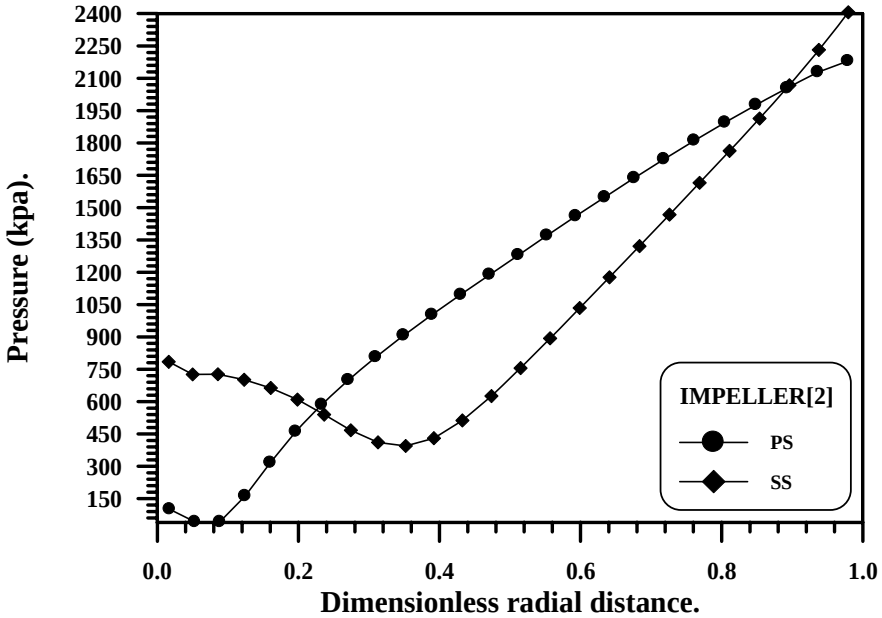


**Fig. (4.13)The variation of static pressure with radial distance.**

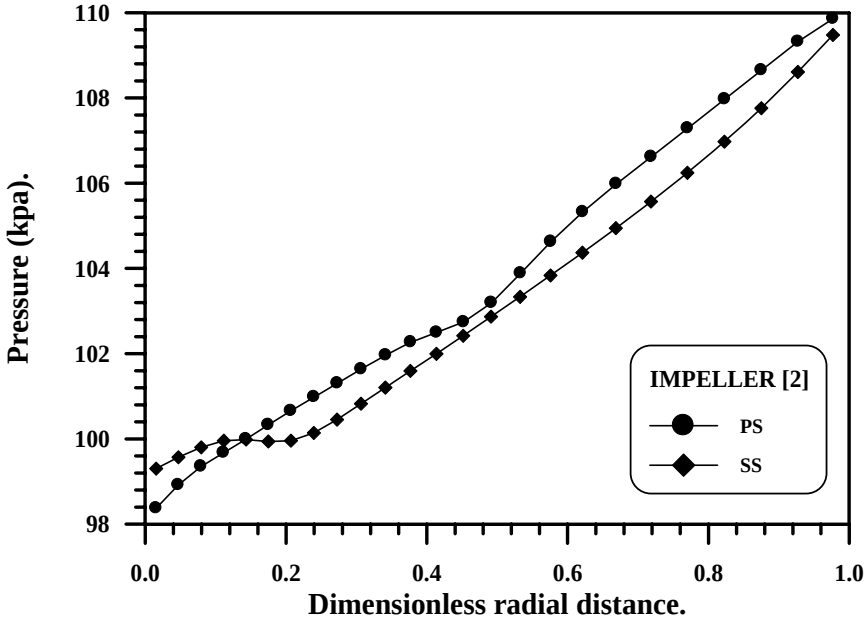


**Fig.(4.14) The variation of static pressure with radial distance.**

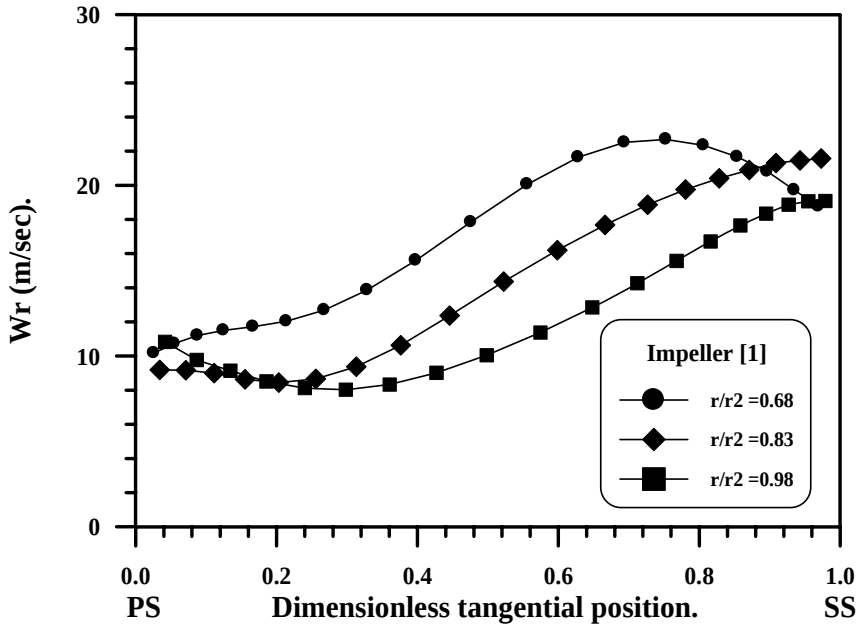


**Fig. (4.15) The variation of relative radial velocity between two blade.**

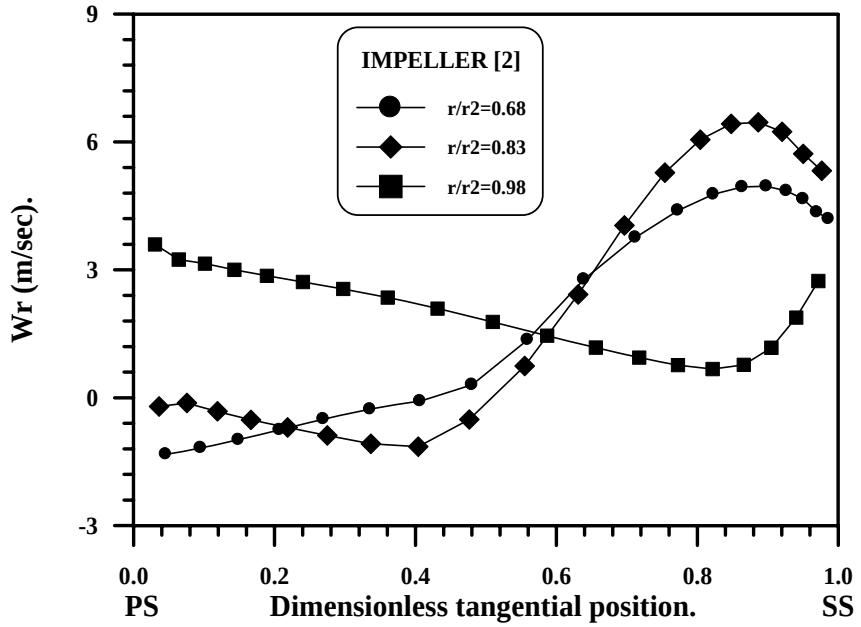


**Fig.(4.16) The variation of relative radial velocity between two blade.**

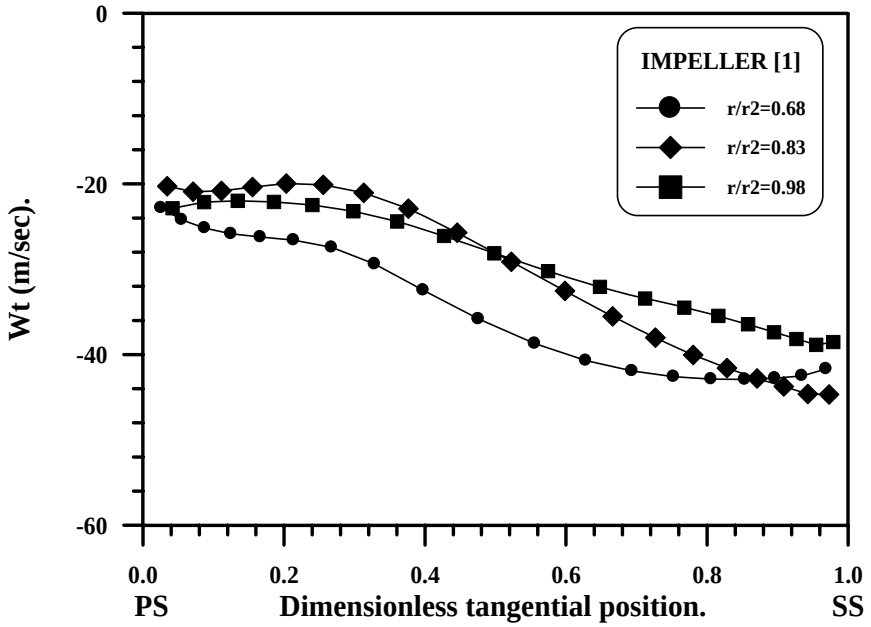


**Fig.(4.17) The variation of relative tangential velocity between two blade.**

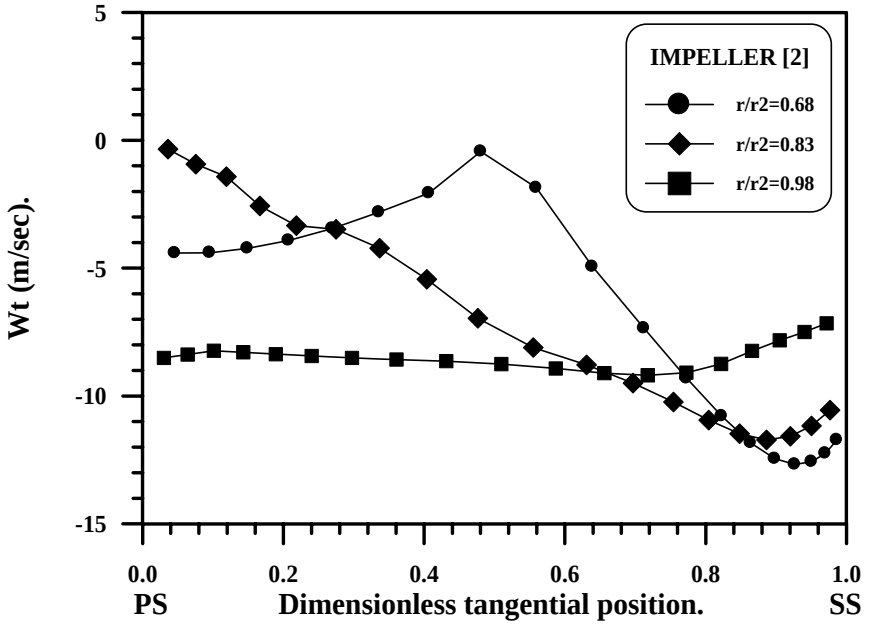


**Fig. (4.18) The variation of relative tangential velocity between two blade.**

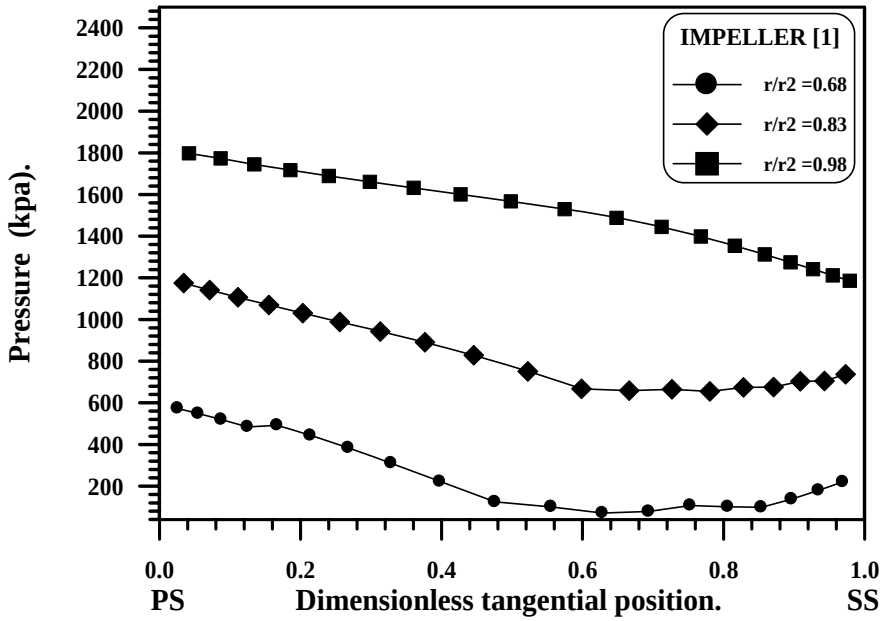


**Fig. (4.19) The variation of pressure between two blade.**

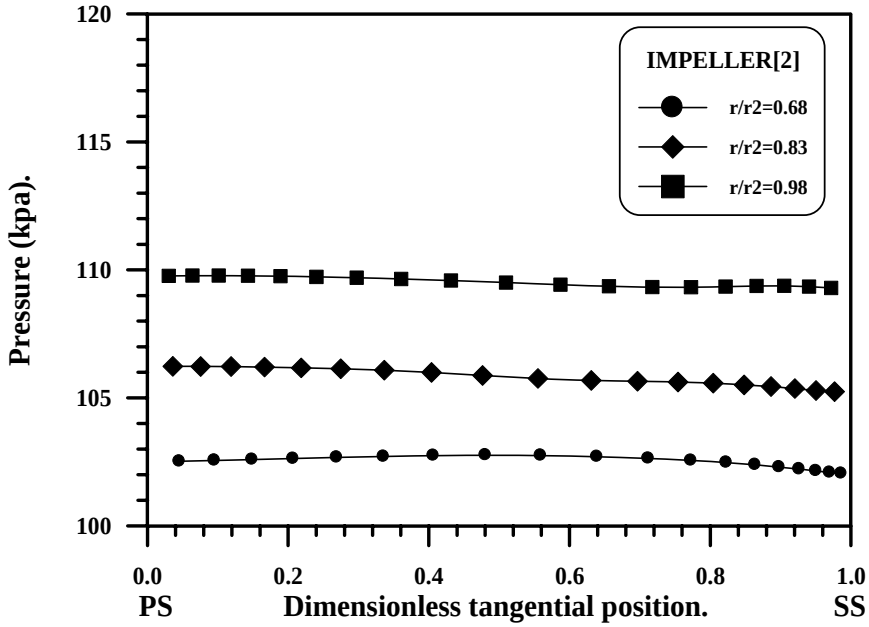


**Fig. (4.20) The variation of pressure between two blade.**

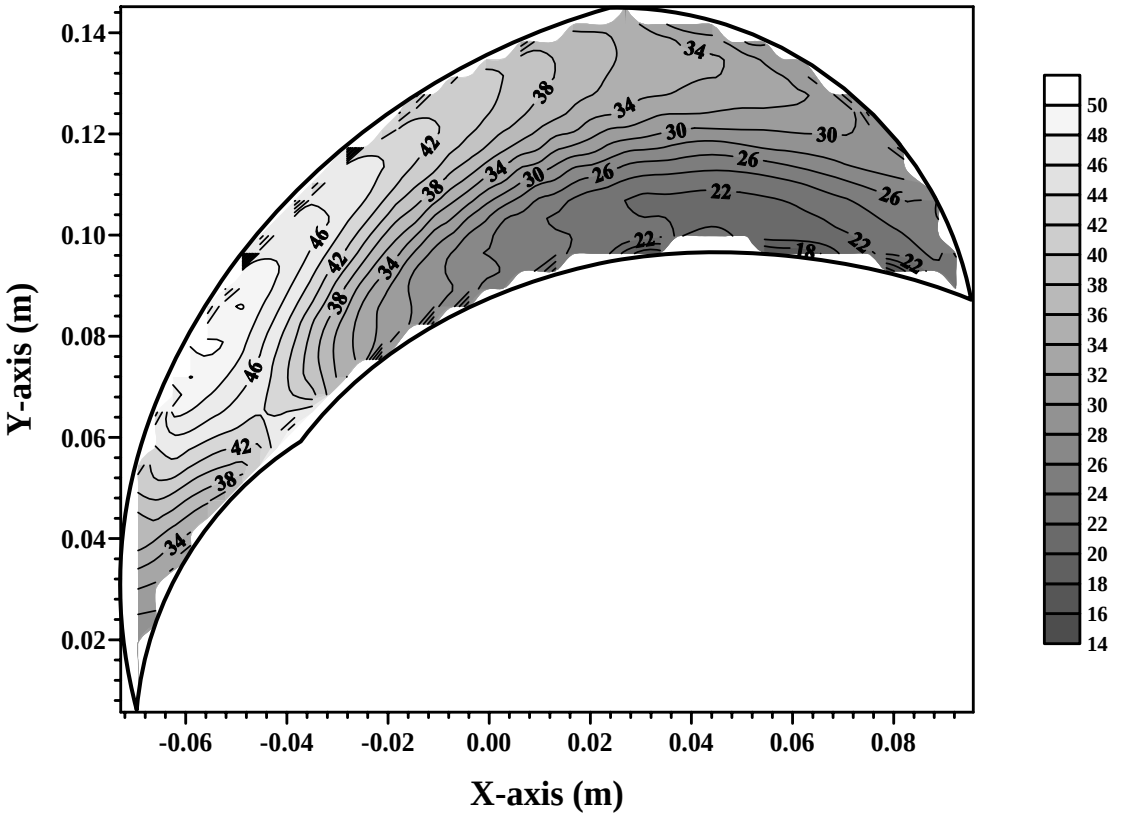


**Fig.(4.21) 2D contour plot of relative velocity (IMPELLER(1)).**

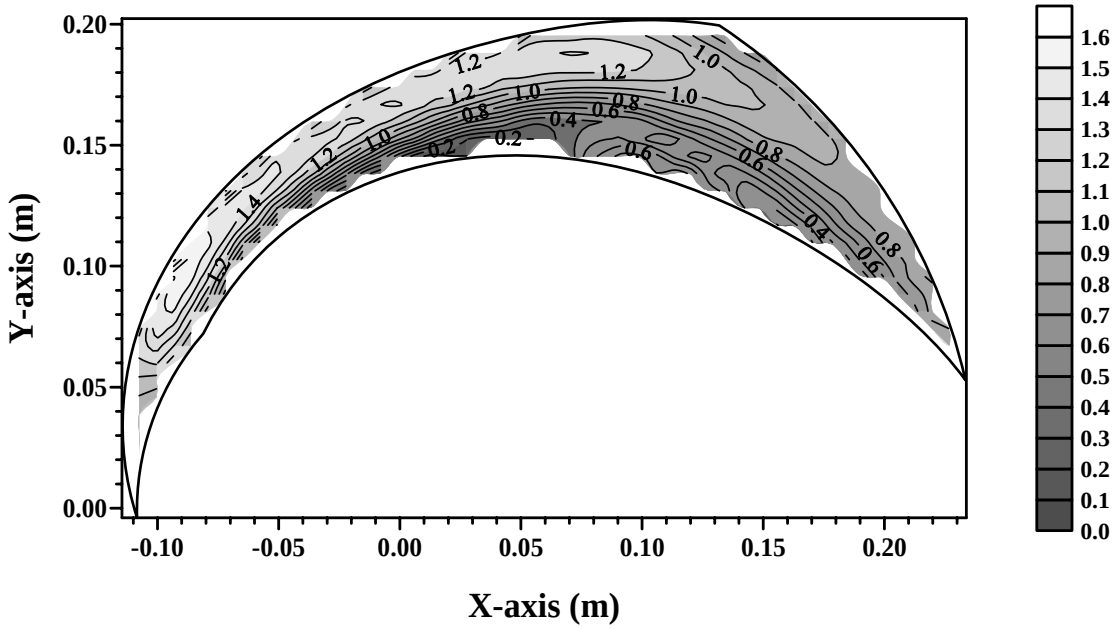


**Fig.(4.22) 2D contour plot of relative velocity (IMPELLER (2)).**

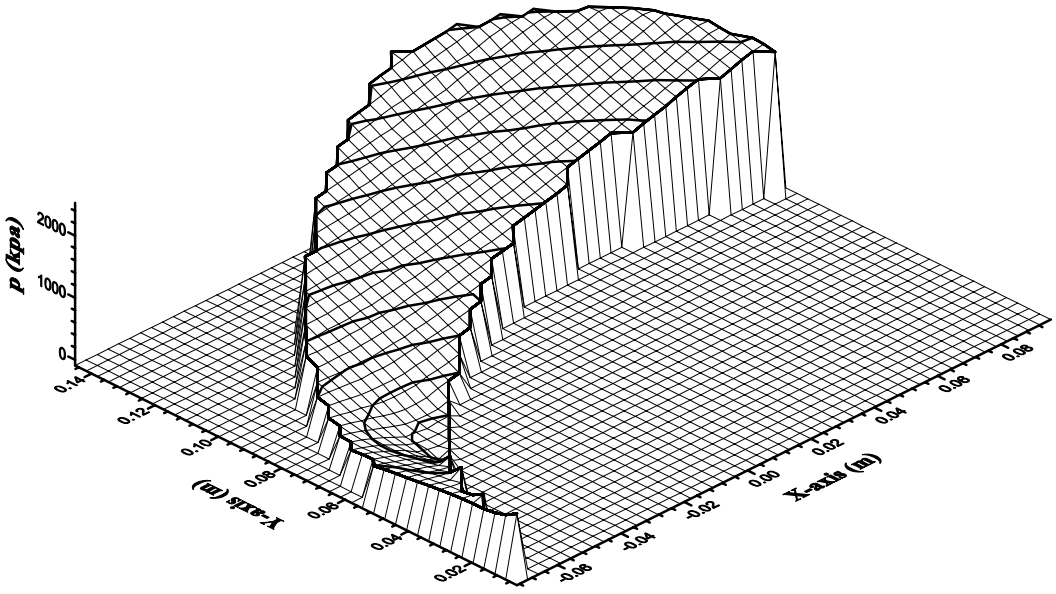


**Fig. (4.23)2D pressure surface (IMPELLER (1)).**

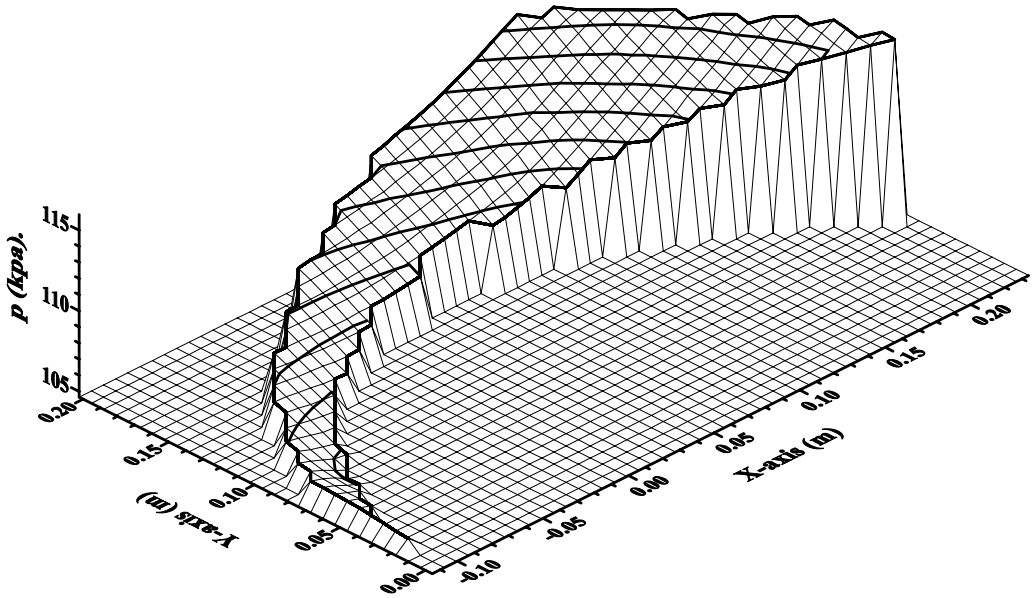


**Fig. (4.24)2D pressure surface (IMPELLER (2)).**

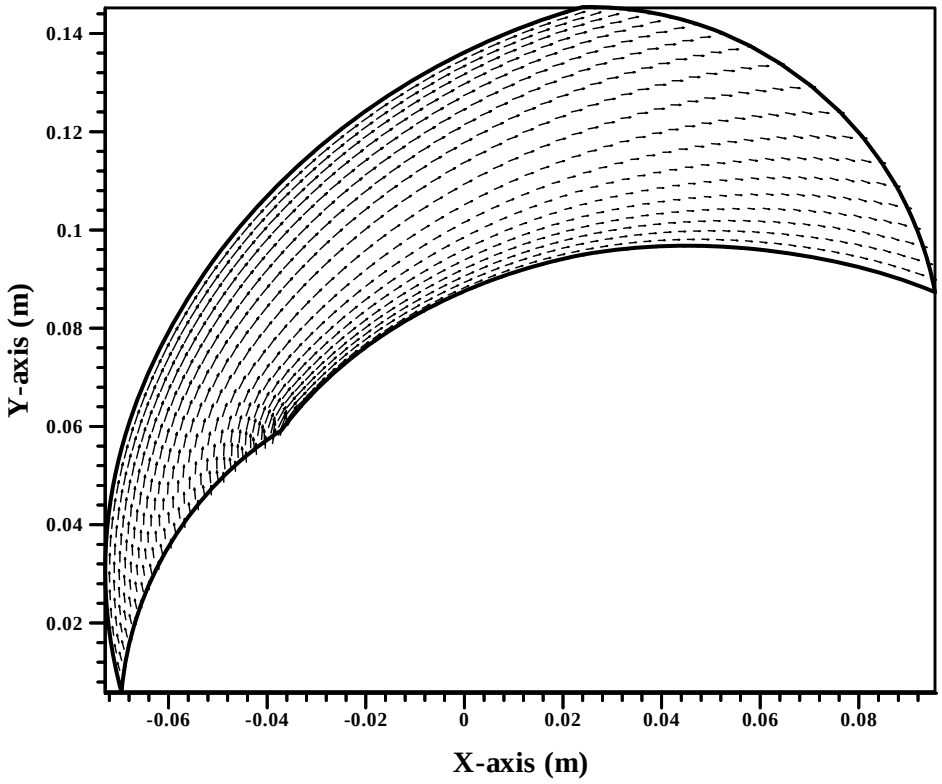


**Fig. (4.25) 2D vector plot of relative velocity (IMPELLER (1)).**

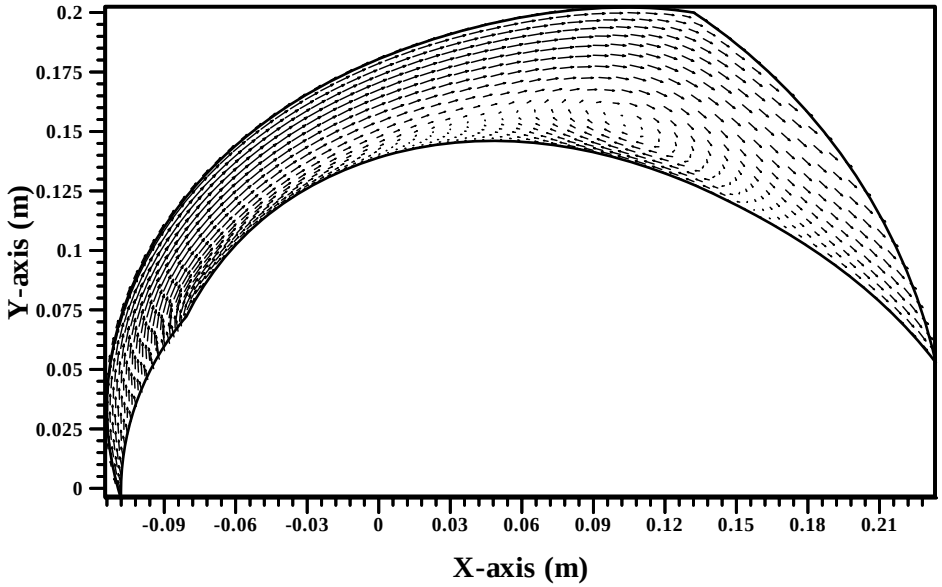


**Fig. (4.26)2D vector plot of relative velocity IMPELLER (2)).**

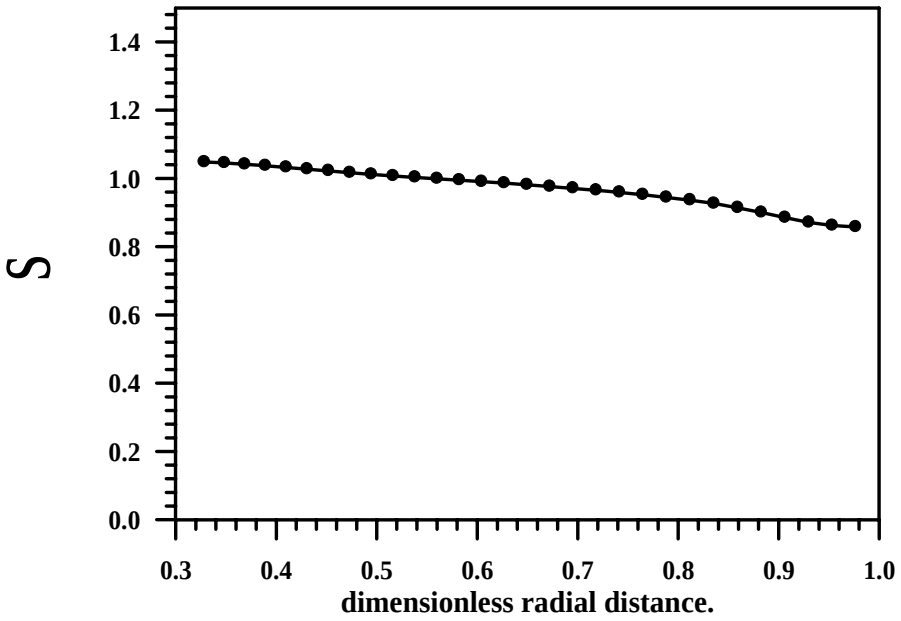


**Fig. (4.27) Slip factor with dimensionless radial distance(IMPELLER(1)).**

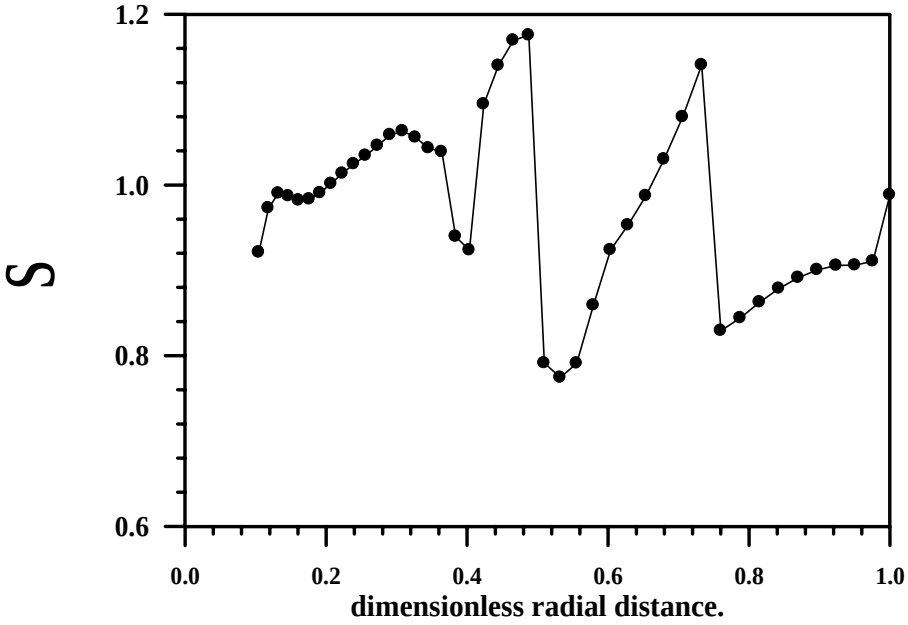


**Fig. (4.28)Slip factor with dimensionless radial distance (IMPELLER(2)).**

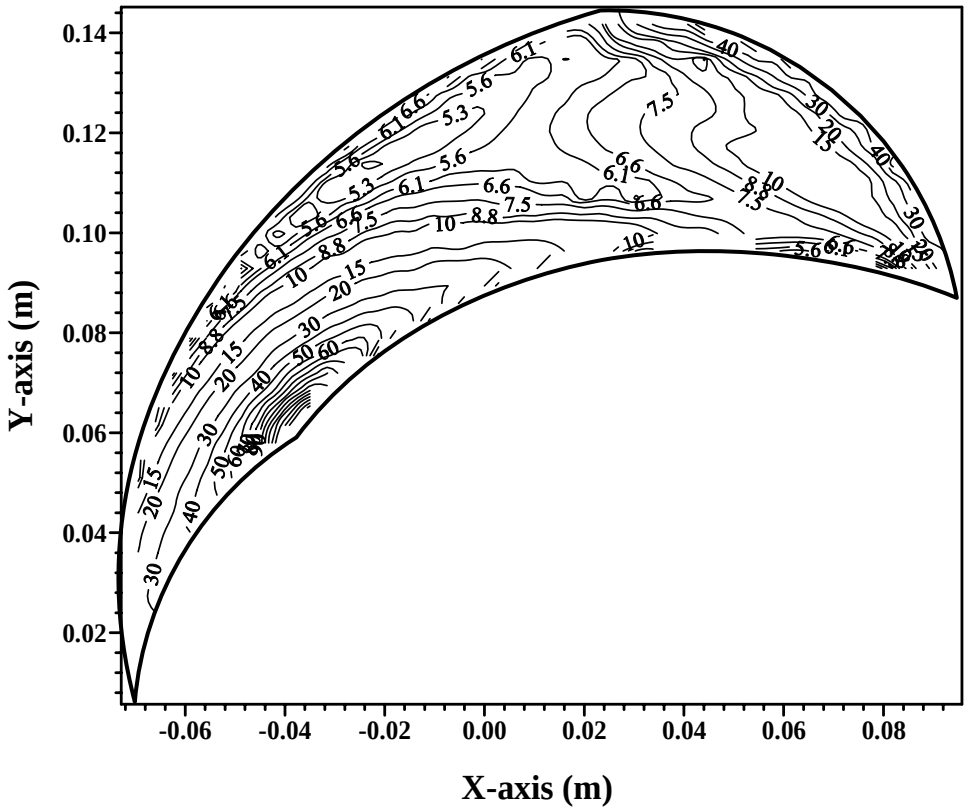


**Fig.(4.29) 2D contour plot of kinetic energy of turbulence (IMPELLER(1)).**

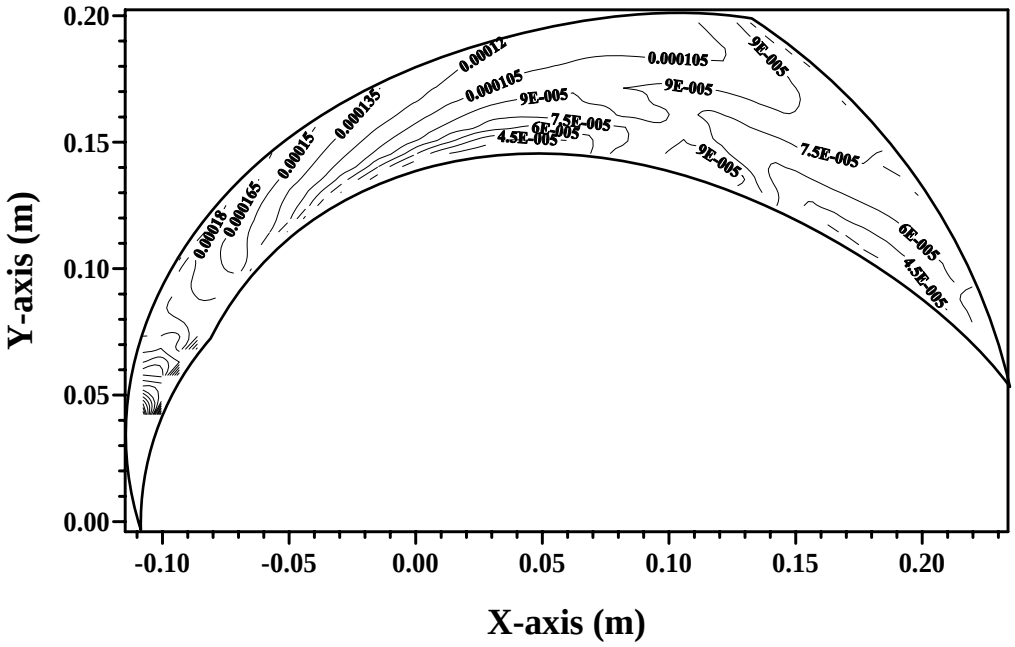


**Fig.(4.30) 2D contour plot of kinetic energy of turbulence (IMPELLER (2)).**

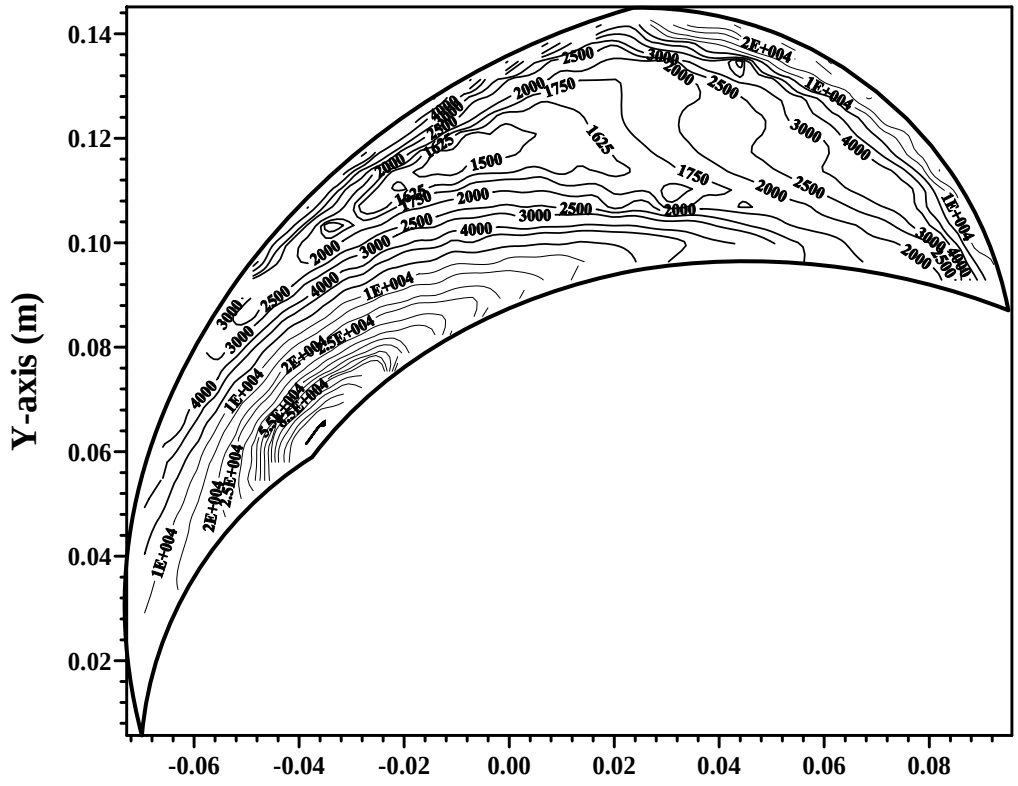


**Fig.(4.31) Two dimension couture plot of dissipation rate of turbulent kinetic energy (IMPELLER (1)).**

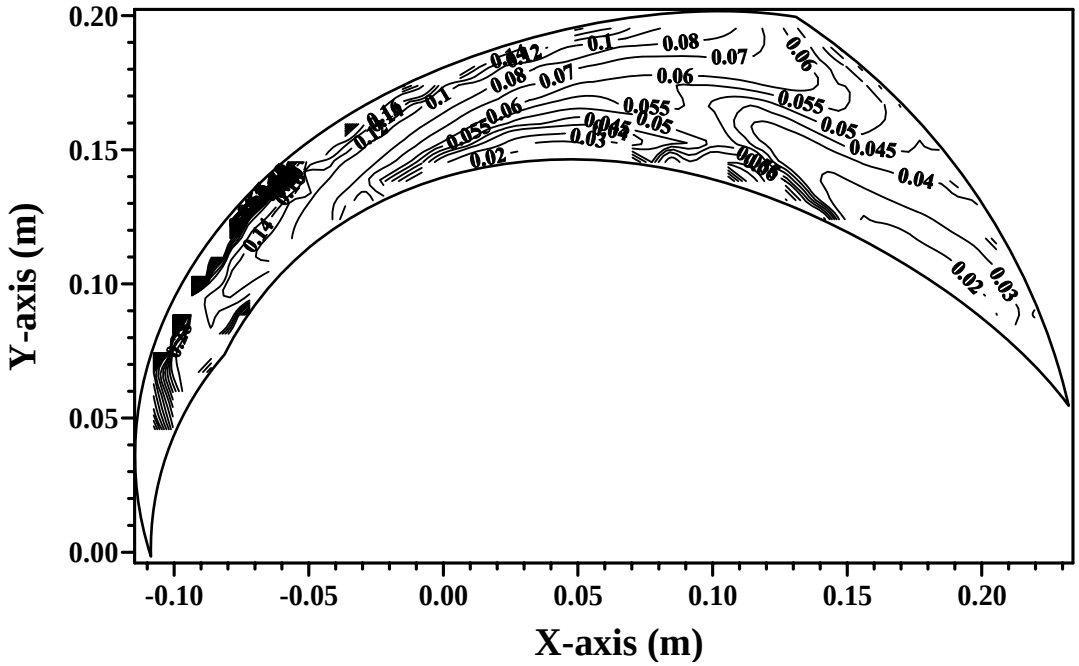


**Fig.(4.32) Two dimension couture plot of dissipation rate of turbulent kinetic energy (IMPELLER (2))**

# Chapter Five

# Conclusions and Recommendation

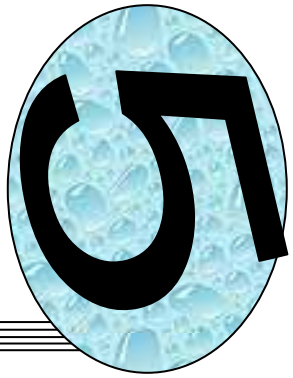


## 5.1 Conclusions: -

The main concluding remarks that have been achieved in this study may be summarized as follows:-

**1)** The relative rotating coordinate system introduced two additional terms, the first one is coriolies acceleration and second centripetal acceleration the direction of coriolies acceleration is approximately in tangential direction for centrifugal pump and the direction of centripetal acceleration in the radial direction.

**2)** The absolute velocity is increased through radial direction and relative velocity is decreased (velocity triangle).

**3)** The value of static pressure is increased through the radial direction in the impeller.

**4)** The values of pressure in **PS** are higher than the pressure at SS and the pressure difference between them depend on the angular velocity and delivered head.

**5)** The values of relative velocity in **PS** are lower than the relative velocity in **SS**.

**6)** The shape of impeller affects on the losses in the impeller, and the point by point method is relevant for blade formation.

**7)** The blade angle affects on the head that means as the blade angle increases the value of pressure delivered is high (high head).

**8)** The blade length affect on the losses that means as the blade angle increases the losses also increases (area of friction, circulation) and the

**9)** value of the head is small hence, it is relevant for pump of a high flow rate and low head, and vise versa.

**10)** In the (**CFD**) it is wrong to assume the flow to be laminar (if it is actually turbulent) because this leads to divergent in the solution or close the error to one.

**11)** For complex geometry always the flow is to be turbulent.

## 5.2 Recommendation for further works: -

**1)** Study the solution of **2D** by taking in to account the interface between intake, impeller& volute.

**2)** Study and Simulation of **3D** invicid analysis between all blades with interaction between impellers &volute.

**3)** Study and Simulation of **3D** turbulent fluid flow with different types of centrifugal pumps.

## References


**1.** Shepherd, D.G., “Principles of Turbo Machinery”, Macmillan Publishing CO., 1956.

**2.** Stephen, Lazrkiewicz & Trocklnsk,”Impeller Pumps”, Pergamon Press, 1965.

**3.** Versteeg, H.K., Malasevera, W., “AN Introduction to Computational Fluid Dynamics The Finite Volume Method”, Longman Group Ltd., 1995.

**4.** Patancar, S.V., “Numerical Heat Transfer and Fluid Flow”, Hemisphere Publishing Corporation, Taylor & Francis Group, New York, 1980.

**5.** J. H. Ferziger & M. Peric, “Computational Methods for Fluid Dynamics”, Springier – Verlage Berlin Heidelberg Newark 1996.

**6.** Stepanoff, A. J., “Centrifugal and Axial Flow Pumps”, John Whily & Sons, Inc., 1957.

**7.** Lobanoff, S., Vo1 & Ross, Robert, “Centrifugal Pump Design & Applications”, Gulf Publishing Company, 1985.

**8.** Reddy, Y.P., KAR, S,” Optimum Vane Number and Angle of Centrifugal Pumps with Logarithmic Vanes”, Journal of Basic Engineering, Transaction of ASME September, vol.(2) 1971, 411-425.

**9.** Pollard, D.,” A Method Of Hydraulic Design And Analysis Of Pump And Fans Using Computer Techniques and Comparison With Some Experimental Results”, I Mech., F, 1982, C242173.

**10.** Salisbury, A.G., “Current Concepts In centrifugal Pump Hydraulic Design “, I. Mech.Vol(1) F ,C 177/82., 1982,

**11.** Nobert, O., Stockman & John L. Kramer, “Method For Design Of Pump Impellers Using High Speed Digital Computer”, NASA TNA,Vol(2), 1536, 1963.

**12.** Martell & Matchless, “Using Viscous Calculation in Pump Design”. , Journal of Fluid Mechanics. 1991.

**13.** Tuzson, J. “Interpretation of Impeller Flow Calculations Journal of Fluid Mechanics, 1990.

**14.** Miner, R.Flak. "Two. Dimensional Flow Analysis of Centrifugal Pump", International Gas Turbine Institute, 1992.

**15.** Marigorta, M.F. Fernandez," Numerical Flow simulation pump with Impeller–volute interaction", ASME Fluids Engineering Davison Boston, (2000).

**16.** Van Esch, B.P.M..," Simulation of Three-Dimensional Unsteady Flow in Hydraulic Pumps", volgens het besluit van het College voor Promoties in het openbaar te verdedigen, 1997.

**17.** Alberto, T. & L. Gerhard," Numerical, Experimental and Theoretical Analysis of the Individual Efficiencies of a Centrifugal Pump", Darmstadt University of Technology, 2001.

**18.** Lomax, H. Pulliam, T.H., and David, W.Z., "Fundamentals of Computational Fluid Dynamics", NASA Ames Research Center, 1999.

**19.** Atta, Z.W., "Quasi-Three Dimensional Low Speeds Viscous Flow Between Axial Compression Cascade Blades", M.Sc. Thesis, Mech. Eng. ET. Uni. of Baghdad, 2000.

**20.** Gogzeh, M.M., "Three Dimensional Turbulent Flow between Two Axial Compressor Using Body Fitted Coordinate", Ph.D. Thesis, Mech. Eng. Dept., Univ. Of Baghdad. 2000.

**21.** Budugur Lakshminarayana, ". Fluid Dynamics and Heat Transfer of Turbomachines", John Willy & Sons, Inc. 1996.

**22.** Salisbury. A.G. " An introduction to the Principles of Rotodymic Pump Design ", Grandfield Institute of Technology .1985.

**23.** Shakir. S. M., "An experimental Study of the Effect of Blade Curvature and Tip Clearance on Centrifugal Pump Performance", M.Sc, Thesis Mech. Eng. Dept, Univ. of Babylon, 1999.

**24.** Anderson, D.A. Tenne Hill, J.C. And Pletcher, R.H., "Computational Fluid Mechanics and Heat Transfer", McGraw- Hill Book Company, 1984.

**25.** "The Finite Volume Method." Lyle Long, Email:Lnl@Psu.Edu, 2001.

**26.** Vavra. M.H.," Aero-Thermodynamics and Flow in Turbomachines", JOHN WILEY & SONS, INC. 1960.

**27.** Awbi, H. B. "Ventilation of Buildings ".E&FN SPON, London and New York, 1991.

**28.** Steven C. Chapra & Raymond P.Canale "Numerical Method for Engineers", the MCGRAW Hill Coupons with Programming and Software Application, 1998.

**29.** Abramian, M. & J.H.G.Howard" Experimental Investigation of the Steady and Unsteady Relative Flow in a Model Centrifugal Impeller Passage". Intern Gas Turbine Institute.1993.

**30.** George B. Thomas, Ross L. Finney" Calculus "Addison-Wesley Publishing Company. 1998.

**31.** Yuan, S. W. "Foundation of fluid mechanism "Prentice hall of India, 1976.

# Appendix [A]

## Point By Point Method.

This method of determining blade shape is based on the assumption that the transition $\sphericalangle \beta_1$ in to $\sphericalangle \beta_2$ depends on the radius **r** and on determining the control angle $\theta$ for given **r** and $\sphericalangle \beta$ .

The values of r and $\theta$ constitute polar coordinate for a given point on the blade.

Let us consider the elementary triangle $\mathbf{P\bar{P}T}$ as shown in Fig.(A.1), whose side PT lies between the two radii of an infinitely small central angle $\mathbf{d\theta}$, so that

$$\mathbf{PT = r\,d\theta} \qquad \text{…(A.1)}$$

And at the same time

$$\mathbf{PT = \frac{\bar{P}T}{\tan\beta}} \qquad \text{…(A.2)}$$

Since $\bar{P}T$ denotes and infinitely small increment in radius $\mathbf{dr}$, These equations yields

$$\mathbf{r\,d\theta = \frac{dr}{\tan\beta}} \qquad \text{…(A.3)}$$

$$\mathbf{d\theta = \frac{dr}{r\tan\beta}} \qquad \text{…(A.4)}$$

Integrating this equation is taken numerically by tabular method; this equation is multiplied by $\frac{180}{\Pi}$ to express the angle in degree.

$$\mathbf{d\theta = \frac{180}{\Pi}\int_{r_1}^{r}\frac{d\theta}{r\tan\beta}} \qquad \text{…(A.5)}$$

For blade of variable thickness it is more rational to assume some relation for the change in the relative velocity W and the meridonal component $W_m$ after finding $\measuredangle \beta$

$$\mathbf{SIN}\beta = \frac{\mathbf{W_r}}{\mathbf{W}} \qquad \textbf{…(A.6)}$$

$$\beta = \mathbf{SIN}^{-1}\frac{\mathbf{W_r}}{\mathbf{W}} \qquad \textbf{…(A.7)}$$

The value of $\mathbf{W_m}$ **&** **W** are assumed along the stream line as shown in Fig.(A.1) below.

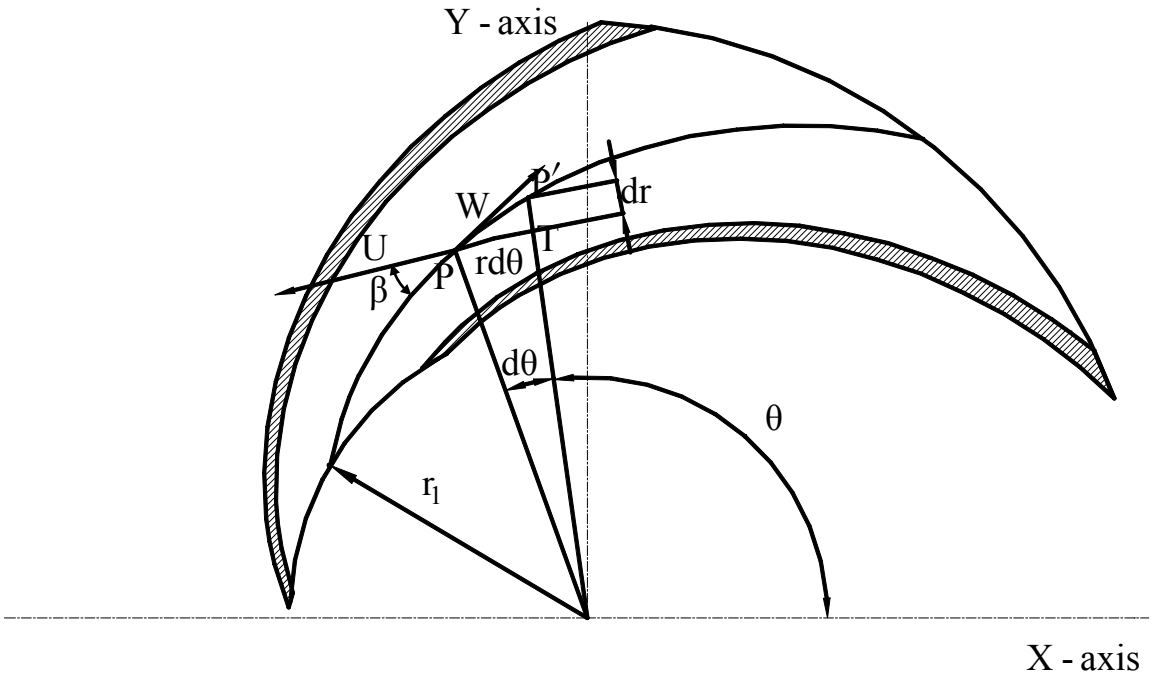


Fig.(A.1) shows the stream line between two blades.

# Appendix [B]

## Equation of Motion.

The fundamentals equation for incompressible flow is

Continuity equation

$$\frac{\partial \rho}{\partial t} + \nabla \cdot (\rho \vec{V}) = 0 \qquad \ldots(B.1)$$

Momentum equation

$$\rho \frac{D\vec{V}}{Dt} = -\nabla P + \mu \nabla^2 \vec{V} \qquad \ldots(B.2)$$

Energy equation is conceding with momentum equation for incompressible isothermal flow [31].

Its advantage to treat a flow with reference called relative system of coordinate which under goes a certain motion with respect to a fixed or absolute system.

The motion of relative system can in general, consists of a translation and a rotation about a momentary axis.

In turbomachin the relative systems rotate about fixed point, the derivation of relation between relative velocity and absolute velocity is derive by (vavra)[26] And produce the relation in vector form.

$$\vec{V} = \underbrace{\vec{W}}_{\text{relative velocity}} + \underbrace{\vec{\omega} \times \vec{r}}_{\text{peripheral velocity}} \qquad \ldots(B.3)$$

$$\vec{a} = \vec{a}_r + \underbrace{2\,\vec{\omega} \times \vec{W}}_{\text{coriolis accelerati on}} + \underbrace{\vec{\omega} \times (\vec{\omega} \times \vec{r})}_{\text{centripeta l accelerati on}} \qquad \ldots(B.4)$$

If we substitute equations (B.3) & (B.4) in equation (B.1) & (B.2) yields

$$\frac{D\vec{V}}{Dt}=\frac{D\vec{W}}{Dt}+2\vec{\omega}\times\vec{W}+\vec{\omega}\times(\vec{\omega}\times\vec{r})\Rightarrow=\frac{\partial\vec{W}}{\partial t}+\vec{W}\cdot\nabla\vec{W}+2\vec{\omega}\times\vec{W}+\vec{\omega}\times(\vec{\omega}\times\vec{r})$$

Continuity equation become

$\frac{\partial\rho}{\partial t}+\vec{W}\cdot\nabla\rho+\rho\nabla\cdot\vec{W}=0$ for steady flow the term $\frac{\partial\rho}{\partial t}$ is neglecting then

$$\nabla\cdot(\rho\vec{W})=0 \qquad \text{...(A.5)}$$

Momentum equation become

$$\rho\vec{W}\cdot\nabla\vec{W}=\rho(-2\vec{\omega}\times\vec{W}-\vec{\omega}\times(\vec{\omega}\times\vec{r}))-\nabla P+\mu\nabla^2(\vec{W}+\vec{\omega}\times\vec{r}) \qquad \text{…(B.6)}$$

The properties of cross product is

$$\vec{\omega}\times\vec{W}=-\vec{W}\times\vec{\omega}$$

$$\vec{\omega}\times\vec{r}=-\vec{r}\times\vec{\omega}$$

$$\rho\vec{W}\cdot\nabla\vec{W}=-\nabla P+\rho 2\vec{W}\times\vec{\omega}+\rho\vec{\omega}\times(\vec{r}\times\vec{\omega})+\mu\nabla^2(\vec{W}+\vec{\omega}\times\vec{r})$$

If a turbulent flow is considered .The velocities in equation above are replaced by the sum of time mean average component and fluctuating component as follows:

$$W=w+w' \qquad \text{…(B.7)}$$

If we substitute this equation and simplified the momentum equation we obtain the two dimensions.

$$\rho\vec{w}\cdot\nabla w_x = 2\rho w_y \omega_z + \rho x \omega_z^2 - \frac{\partial p}{\partial x} + \mu\nabla^2 w_x + \frac{\partial}{\partial x}(-\rho\overline{w'_x w'_x}) + \frac{\partial}{\partial y}(-\rho\overline{w'_x w'_y}) \quad \text{...(B.8)}$$

$$\rho\vec{w}\cdot\nabla w_y = -2\rho w_x \omega_z + \rho y \omega_z^2 - \frac{\partial p}{\partial y} + \mu\nabla^2 w_y + \frac{\partial}{\partial x}(-\rho\overline{w'_x w'_y} + \frac{\partial}{\partial y}(-\rho\overline{w'_y w'_y}) \quad \text{...(B.9)}$$

these values $(-\rho\overline{w'_y w'_y}, -\rho\overline{w'_x w'_y})$ are turbulent Reynolds stresses these terms (i.e.) closure equation (awbi) before momentum equation solved these terms can be represented by expression of the time mean variable already in the equations or by means of other variable are not given in the above equation in the later case additional PDE'S of the new variable must be also solved as well as the other transport equation given earlier.

The task of turbulence model is to express Reynolds stress in equation $(\rho\overline{w'_x w'_y})$ by set of auxiliary equation (differentiation and or algebraic) quantities time mean quantities of flow the majority of turbulence model used in solving practical fluid flow problems are based on the eddy or turbulent viscosity

The turbulence viscosity was suggested by Posen's Equation in 1877 if an isotropic turbulence is used (i.e. at any point in the flow the mean – square values of three fluctuating velocity component are equal $\overline{w'^2_x} = \overline{w'^2_y}$ the Reynolds stress can be represented by the following equation :-

$$-\rho\overline{w_x' w_y'} = 2\mu_t \frac{\partial w_x}{\partial x} - \frac{2}{3}\rho k \qquad \text{...(B.10)}$$

$$-\rho\overline{w_y' w_y'} = 2\mu_t \frac{\partial w_y}{\partial y} - \frac{2}{3}\rho k \qquad \text{...(B.11)}$$

$$-\rho\overline{w_x' w_y'} = \mu_t \left(\frac{\partial w_x}{\partial y} + \frac{\partial w_y}{\partial x}\right) \qquad \text{...(B.12)}$$

$\mu_t$ = turbulent or eddy viscosity

$$k = \frac{1}{2}\left(\overline{w_x'^2} + \overline{w_y'^2}\right) \qquad \text{...(B.13)}$$

$k$ Is the turbulent kinetic energy

In the transport equations for turbulent flows the turbulent stress term are added to the laminar stress by using the concept of effective viscosity $\mu_e$.

$$\mu_e = \mu_l + \mu_t$$

For turbulent flow the term $\frac{2}{3}\rho k$ is neglected $\mu_l << \mu_t$

Then equation of motion can be written for incompressible turbulent fluid flow in two dimensions in vector form

$$\rho\vec{w}\cdot\nabla\vec{w} = 2\rho\vec{w}\times\vec{\omega} + \rho\vec{\omega}\times(\vec{r}\times\vec{\omega}) - \nabla p + \nabla\mu_e\nabla\vec{w} \qquad \text{...(B.14)}$$

$$\rho\nabla\cdot\vec{w} = 0 \qquad \text{...(B.15)}$$

To solve the above equation the mathematical expression of effective viscosity $\mu_e$ will be required.

In a recalculating flow a two – equation turbulence model which describes the turbulence velocity by transport equation will be more appropriate .This model uses the turbulence kinetic energy $k$ and kinetic dissipation $\varepsilon$ . this is usually know as $k-\varepsilon$ turbulence model and currently it is the most widely used because of it's applicability to wide ranging flow problem and it's lower

computational demand than more complex model that are available ,the two equation are.

**k – Eq**

$$\nabla\cdot(\rho w k)=\nabla(\frac{\mu_e}{\sigma_k}\nabla k)+\mu_t\left[2\left[\left(\frac{\partial w_x}{\partial x}\right)^2+\left(\frac{\partial w_y}{\partial y}\right)^2\right]+\left[\frac{\partial w_x}{\partial y}+\frac{\partial w_y}{\partial x}\right]^2\right]$$

$$-C_\mu\rho\frac{k^{1.5}}{L} \qquad \text{...(B.16)}$$

$\sigma_k=1$ , $C_\mu$ is constant equal 0.09 , $\beta$ volumetric expansion

$$\nabla\cdot(\rho w \varepsilon)=\nabla(\frac{\mu_e}{\sigma_\varepsilon}\nabla \varepsilon)+\frac{C_1\varepsilon\mu_t}{k}\left[2\left[\left(\frac{\partial w_x}{\partial x}\right)^2+\left(\frac{\partial w_y}{\partial y}\right)^2\right]+\left[\frac{\partial w_x}{\partial y}+\frac{\partial w_y}{\partial x}\right]^2\right]$$

$$-C_2\rho\frac{\varepsilon^2}{K} \qquad \text{...(B.17)}$$

Now we return to the continuity & momentum equation to find the descretized equation.

In FV it is more convenient to working in X & Y coordinate in integral form.

We have five equations to solve ($w_x, w_y, p, k, \varepsilon$) equation the general conservative form in **FV** is written as follows**: -**

$$\int_s \rho\Phi\, v\cdot n\, ds=\int_s \Gamma\nabla\Phi.n ds+\int_\Omega q_\Phi\, d\Omega$$

We shall use the mid point rule approximation of the surface and volume integral .we look first at mass fluxes. only the east side of **2D CV** shown Fig. (A) Will be considered; the same approach applies to other faces. only the indices need be changed ,the mid point rule approximation of convective term leads to : -

$$\int_s \rho\Phi\, v\cdot n\, ds = \int_{s_e} (\rho\Phi\, v\cdot n\, ds)_e + \int_{s_n} (\rho\Phi\, v\cdot n\, ds)_n + \int_{s_w} (\rho\Phi\, v\cdot n\, ds)_w + \int_{s_s} (\rho\Phi\, v\cdot n\, ds)_s$$

For east side only.

$$\int_{s_e} \rho\Phi\, v\cdot n\, ds_e = \rho\Phi_e\,(v_x\cdot n_x + v_y\cdot n_y)_e\, ds_e = \rho\Phi_e\,(v_{xe}\cdot(y_{ne}-y_{se}) - v_{ye}\cdot(x_{ne}-x_{se})) = \dot{m}_e\,\Phi_e$$

The approximation of convective flux is for CV face but we want the nodal value of the quantity $\Phi$ we use the deferred correction.

The up wind scheme (UDS)

$$\Phi_e = \begin{cases} \Phi_E & \dot{m}_e < 0 \\ \Phi_P & \dot{m}_e > 0 \end{cases}$$

$$F_e^c = \max(\dot{m}_e,0)\,\Phi_p + \min(\dot{m}_e,0)\,\Phi_e$$

$$F^c = F_e^c + F_n^c + F_w^c + F_s^c$$

The central difference scheme **(CDS)**.

$$F_e^c = \dot{m}_e\left[(1-\frac{L_{Pe}}{L_{PE}})\,\Phi_P + \frac{L_{Pe}}{L_{PE}}\Phi_E\right]$$

then the differed correction interpolation for east side become

$$F_e^{C,DEFF} = F_e^{C,UDS} + \left(F_e^{C,CDS} - F_e^{C,UDS}\right)^{old}$$

the convective coefficient for east side is

$$A_E^C = \min(\dot{m}_e,0)$$

and the other coefficient for old iteration are represent the source term.

The approximation of diffusive term for east side is

$$F_e^{d,expl} = \int_s \Gamma\,\nabla\Phi.n\,ds = \int_s \Gamma\,(\frac{\partial\Phi}{\partial X}.n_x\,ds + \frac{\partial\Phi}{\partial X}.n_y\,ds)$$

we can find the value of derivative by using gauss divergence theorem.

$$\frac{\partial \Phi}{\partial X} = \frac{\int_{\Omega} \frac{\partial \Phi}{\partial X} d\Omega}{\Delta\Omega} = \frac{\sum_{i} \Phi_i \cdot n_x s_i}{\Delta\Omega} = \frac{\Phi_e (n_x s)_e + \Phi_n (n_x s)_n + \Phi_w (n_x s)_w + \Phi_s (n_x s)_s}{\Delta A}$$

$$\Delta A = \frac{1}{2}(r_{ne} - r_{sw}) \times (r_{nw} - r_{se}) = \frac{1}{2}\left[(x_{ne} - x_{sw}) \times (y_{nw} - y_{se}) - (y_{ne} - y_{sw}) \times (x_{nw} - x_{se})\right]$$

the value of derivative is in the center of **CV** center hence the interpolation is used.

$$(\frac{\partial \Phi}{\partial X})_e = (1 - \frac{L_{Pe}}{L_{PE}})(\frac{\partial \Phi}{\partial X})_P + \frac{L_{Pe}}{L_{PE}}(\frac{\partial \Phi}{\partial X})_E$$

$$(\frac{\partial \Phi}{\partial Y})_e = (1 - \frac{L_{Pe}}{L_{PE}})(\frac{\partial \Phi}{\partial Y})_P + \frac{L_{Pe}}{L_{PE}}(\frac{\partial \Phi}{\partial Y})_E$$

This interpolation represents the explicit part in the differed interpolation, a good approximation for the implicit part of the method is easily used if if we use local (n , t ) orthogonal coordinate system.

$$F_e^{d,impl} = \Gamma_e (\frac{\partial \Phi}{\partial n})_e s_e = \Gamma_e (\frac{\Phi_E - \Phi_P}{L_{PE}})_e s_e = \Gamma_e \frac{s_e}{L_{PE}} (\Phi_E - \Phi_P)$$

the deferred correction interpolation for east side is

$$F_e^{d,DEFF} = F_e^{d,impl} + \left(F_e^{d,expl} - F_e^{d,impl}\right)^{old}$$

$$F_e^{d,DEFF} = \Gamma_e \frac{s_e}{L_{PE}} (\Phi_E - \Phi_P) + \left(F_e^{d,expl} - F_e^{d,impl}\right)^{old}$$

$A_E^d = -\Gamma_e \frac{s_e}{L_{PE}}$ then the coefficient of east side only is

$$A_E = A_E^c + A_E^d = \min(\dot{m}_e, 0) - \Gamma_e \frac{s_e}{L_{PE}}$$

with same procedure for all sides.

$$A_N = A_N^c + A_N^d = \min(\dot{m}_n, 0) - \Gamma_n \frac{s_n}{L_{PN}}$$

$$A_W = A_W^c + A_W^d = \min(\dot{m}_w, 0) - \Gamma_w \frac{s_w}{L_{PE}}$$

$$A_S = A_S^c + A_S^d = \min(\dot{m}_s, 0) - \Gamma_s \frac{s_e}{L_{PE}}$$

$$A_E = A_P^c + A_P^d = \max(\dot{m}_e, 0) + \max(\dot{m}_n, 0) + \max(\dot{m}_w, 0) + \max(\dot{m}_s, 0)$$
$$- (A_E^d + A_N^d + A_W^d + A_S^d)$$

$$Q_P = \sum_i \left(F_i^{d,expl} - F_i^{d,impl}\right) + \left(F_i^{d,expl} - F_i^{d,impl}\right) + q_{\Phi P}\, d\Omega, i = e, w, n, s$$

hence the equation for one **CV** is written as follows :-

$$A_W \Phi_W + A_S \Phi_S + A_P \Phi_P + A_N \Phi_N + A_E \Phi_E = Q_P$$

all the procedure is done to the conservative quantities.

$$ds_1 = \sqrt{(x_a - x_b)^2 + (y_a - y_b)^2}$$

$$n_y = -\frac{x_a - x_b}{d_{s1}}$$

$$n_x = \frac{y_a - y_b}{d_{s1}}$$

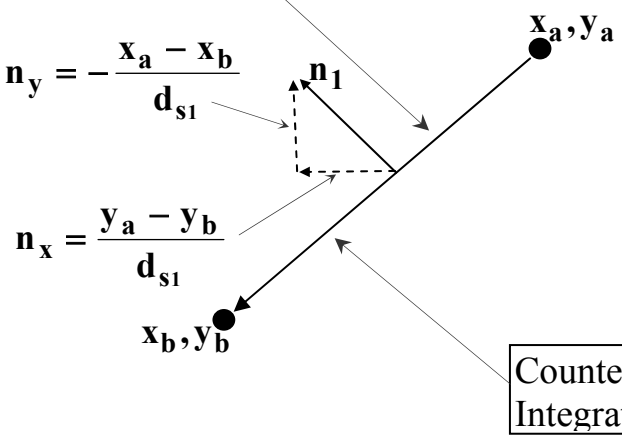


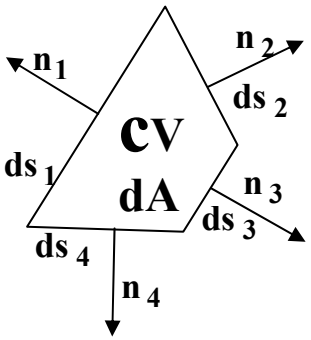


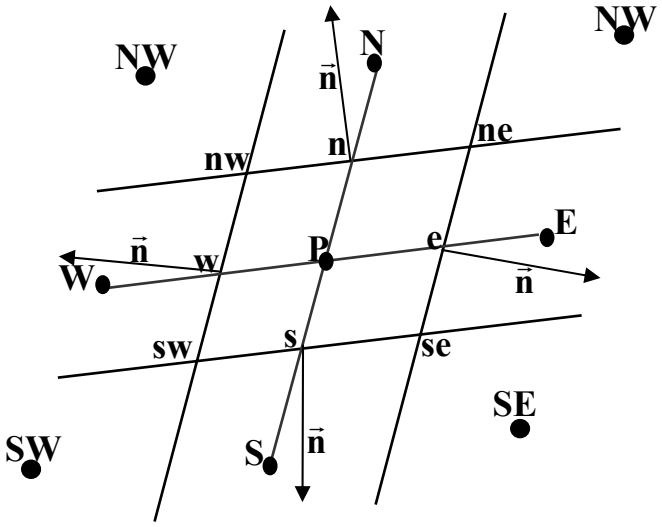


$$\mathbf{n} = n_x\,\mathbf{i} + n_y\,\mathbf{j}$$

$$\mathbf{n} = \frac{y_a - y_b}{d_{s1}}\,\mathbf{i} - \frac{x_a - x_b}{d_{s1}}\,\mathbf{j}$$

$$n_x\,ds = \quad dy = \quad (x_a - x_b)$$

$$n_y\,ds = -dx = -(y_a - y_b)$$

$$\mathbf{n}\,ds = -dy\,\mathbf{i} + dx\,\mathbf{j}$$

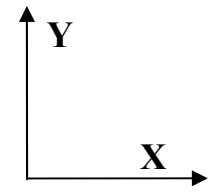


**Fig. (A) Figure shows 2D Finite volume (area) and normal vector.**

# APPENDIX [C]

## The Divergence Theorem

The divergence theorem says that under suitable condition the out ward flux of a vector field across a closed surface equals the triple of divergence of the field over the region enclosed by region enclosed by surface [31].

$$\iint_{s} F.n\ ds = \iiint_{\Omega} \nabla.F\, d\Omega$$